RADIOGRAPHIC DETERMINATION OF THE LAY-UP INFLUENCE ON FATIGUE DAMAGE DEVELOPMENT UNDER BEARING/BYPASS CONDITIONS

A Thesis
Presented to
The Academic Faculty

by

Carl G. Tompson

In Partial Fulfillment
of the Requirements for the Degree
Master of Science in Mechanical Engineering in the
School of Mechanical Engineering

Georgia Institute of Technology
May 2009

RADIOGRAPHIC DETERMINATION OF THE LAY-UP INFLUENCE ON FATIGUE DAMAGE DEVELOPMENT UNDER BEARING/BYPASS CONDITIONS

Approved by:

Dr. W. Steven Johnson, Advisor
School of Materials Science and Engineering
Georgia Institute of Technology

Dr. Andrew Makeev
School of Aerospace Engineering
Georgia Institute of Technology

Dr. Kyriaki Kalaitzidou
School of Mechanical Engineering
Georgia Institute of Technology

Date Approved: 1 May 2009

ACKNOWLEDGEMENTS

I would like to thank my advisor, Dr. Steve Johnson, for his continual guidance throughout the course of this project. I would also like to thank Rick Brown for his invaluable assistance in test setup and equipment maintenance. I would like to express my appreciation to Amar Atre for his assistance with ABAQUS. I would especially like to thank my family and friend for their unconditional support.

TABLE OF CONTENTS

Page

LIST OF TABLES

Page

LIST OF FIGURES

Page

LIST OF SYMBOLS AND ABBREVIATIONS

K_{tn}	Stress Concentration Factor
L/w	Ratio of length to width
d/w	Ratio of hole diameter to width
e/d	Ratio of edge distance to hole diameter
R	Stress or Load ratio

SUMMARY

The goal of this academic project was to study the effects of different variables on the damage initiation and progression around four bolt holes of a joint in carbon fiber/graphite epoxy composite coupons. The tracked variables included the type of layup, R values, stress levels, and damage mechanisms observed in each specimen. In-situ x-ray of the individual coupons recorded the extent of damage, mostly longitudinal splitting and bearing failure, as a function of the cycle count. The following lay-ups were included: [45/90/-45/0_2/45/0_2/-45/0]s, [0_4/45/0_3/90/0]s, [±5/65/$(\pm5)_2$/-65/±5]s, and [±5/65/$(\pm5)_2$/-65/5/65]s,

In particular, the objective was to determine the stress levels at which detectable damage starts developing by applying 50,000 cycles at incremental stress levels. Once damage was initially detected, we typically raised the stress level 2.5 ksi and cycled another 50,000 cycles until damage reached a point where the bolt holes had elongated 10% of the original diameter of 0.25 inches. This type of testing was be continued for several different R ratios and comparisons were be made between the performances of different lay-ups at varying load levels. A finite element model was created in ABAQUS to help understand the stress fields within the laminates.

CHAPTER 1: INTRODUCTION

Advanced composite materials have been in use now for many decades. The structural applications of these materials seem to be nearly limitless since they can be molded to fit almost any shape. However, even with all the advances in the world of composites, there is still a lack of understanding of the fatigue properties of these materials. Unlike traditional metal structures, composites exhibit various competing damage modes which drastically complicate analysis. These are delamination, fiber matrix debonding, fiber breakage, fiber pull-out, and matrix cracking. The failure begins with matrix cracking. The saturation of matrix cracking opens the door to the more serious forms of damage [1].

Composite materials are being used in structural applications in a wide variety of industries. The most common two are the aerospace and sports equipment industry. Composites are also beginning to be used more in the field of civil and structural engineering. As in most structures, there is a need to place holes in aircraft for a variety of purposes. Holes are needed for anything from fasteners and joints to access panels and windows. Because of this, it is important to know how composites behave with the introduction of stress concentrations, especially in mechanically fastened joints.

This research focused on the fatigue of bolted joints in non-traditional laminates, in which the longitudinal 0º plies were replaced by off-axis plies. The substitution of these off-axis plies can result in entirely new laminates without any 0º, 45º, or 90º plies. This was shown by P.J. Treasurer at Georgia Institute of Technology in 2006 [2]. In 1964 Davis, McCarthy and Schrub showed that non-woven laminates with fibers biased

at ±5º performed better under fatigue than unidirectional laminates [3]. In 1999 P. Berbinau proposed that a minimal reduction in strength would hopefully be offset by a marked increase in a structures resistance to crack propogation, or damage resistance [4]. During the testing phase, each specimen was monitored for several damage modes including longitudinal splitting and bear damage/hole elongation. Damage was measured through the use of in-situ X-ray in conjunction with a dye penetrant.

CHAPTER 2: BACKGROUND

There have been many advances made in the realm of joining advanced composite materials. However, the most common way to join them is with mechanical fasteners. The following is a review of previous studies relevant to mechanically fastened joints in composite materials.

2.1. Open Hole Considerations

When circular holes are placed in a composite material a stress concentration is produced. However, unlike metals, stress concentrations around holes in composites vary as a function of lay-up. These varying stress concentration factors were investigated by C. S. Hong and John H. Crews, Jr. [5] at NASA in 1979. They found that factors affecting stress concentration factors included length to width ratios as well as diameter to width ratios. Different boundary conditions such as uniform stress and uniform displacement were also investigated. It was discovered that, for a semi-infinite sheet, the stress concentration factor varied between $K_{tn} = 6.43$ for 0º laminates and $K_{tn} = 2.3$ for 90º laminates. The quasi-isotropic lay-ups showed a stress concentration factor of $K_{tn} = 3$, which is similar to metals. A graphical presentation of these results can be seen in Figure 1. Approximate solutions for stress concentrations were also developed by Fung-En Harn [6].

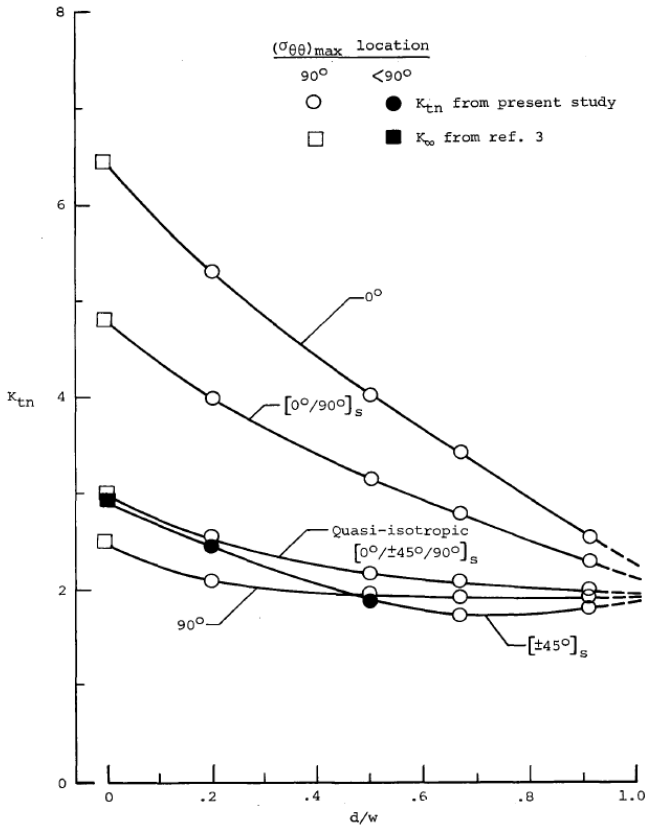

Figure 1: Stress-concentration factors for orthotropic laminates with a circular hole and uniform stress boundary condition; L/w = 10 [5]

The mechanical properties of the material around the hole can also influence the stress concentration. An examination of the effect of composite constituent properties on notched strength performance of composite materials [7] was performed by M. F. Pinnell at the University of Dayton in 1997. Under tensile conditions, the strength of the material is based on its ability to dissipate energy around a notch. Fiber modulus and matrix toughness are the properties that govern this ability. Pinnell found that composites containing fibers with a higher modulus had lower stress concentrations under tensile loading.

2.2. Filled Hole Considerations

These holes often behave differently depending on whether or not the hole is filled. When the hole is open the full potential of the stress concentration is realized. However, when the hole is filled with a fastener, it can behave differently.

2.2.1. Effects of Clamp-up

Yan, Wen, Chang and Shyprykevich studied the clamping effects on the tensile strength of composite plates with a bolt filled hole [8] at Stanford University in 1999. They showed that the strength of a notched specimen will be reduced by inserting a fastener. Furthermore, the more clamping force applied to the fastener, the lower the strength of the composite plate. This is attributed to the fastener suppressing the longitudinal splitting that is said to reduce the stress concentration at the hole. This can be seen graphically in Figure 2.

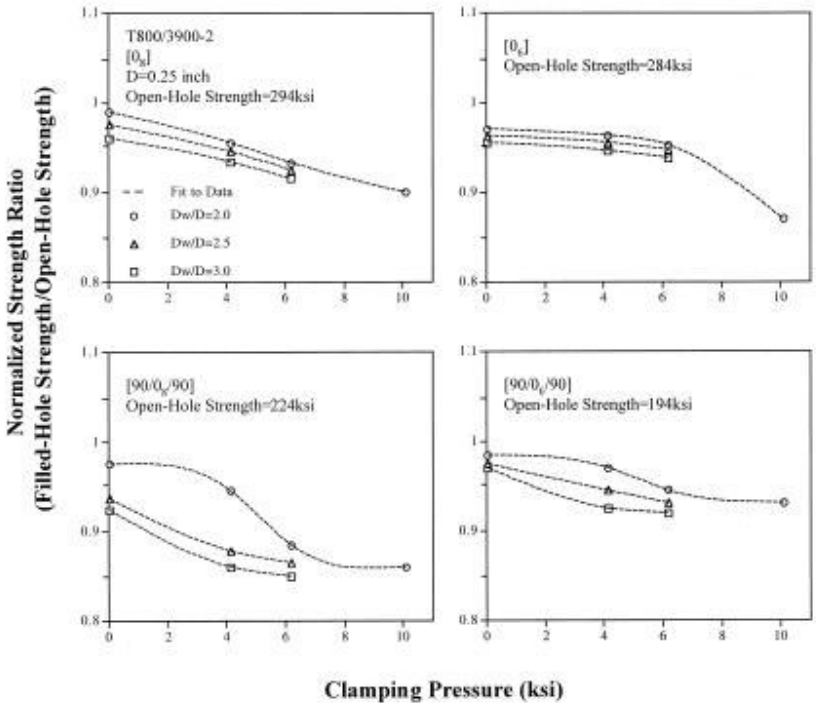

Figure 2: Effect of clamping pressure on tensile strength of filled-hole laminates. [8]

Yan et al. also investigated the effect of clamping force with respect to washer size. They found that for washer to hole diameter ratios less than 3, net tensile strength is reduced. However, as the washer size continues to increase, the strength returns to normal and is sometimes improved. This increase in tensile strength is attributed to the washer sharing the load through friction. These results can be seen graphically in Figure 3. The effects of washer size and clamping force were found to be inverted for bolted joint applications.

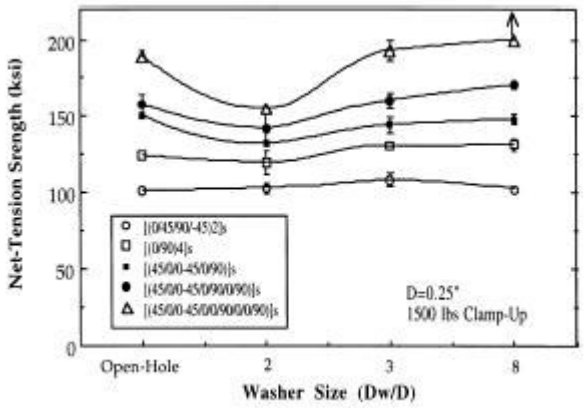

Figure 3: Effect of washer size on notch strength of filled-hole laminates (constant clamping load) [8]

2.2.2. Pin Loaded Holes

Another change in behavior comes when the pin-filled hole is loaded. Crews, Hong and Raju studied the effects of a pin-loaded hole on stress concentrations in finite orthotropic laminates [9]. This work was performed at NASA in 1981. They found that the stress concentration factors were inversely proportional to the *W/D* ratio. This says that with a constant hole diameter, as width decreases the concentration of bearing stress increases. The results can be seen graphically in Figure 4.

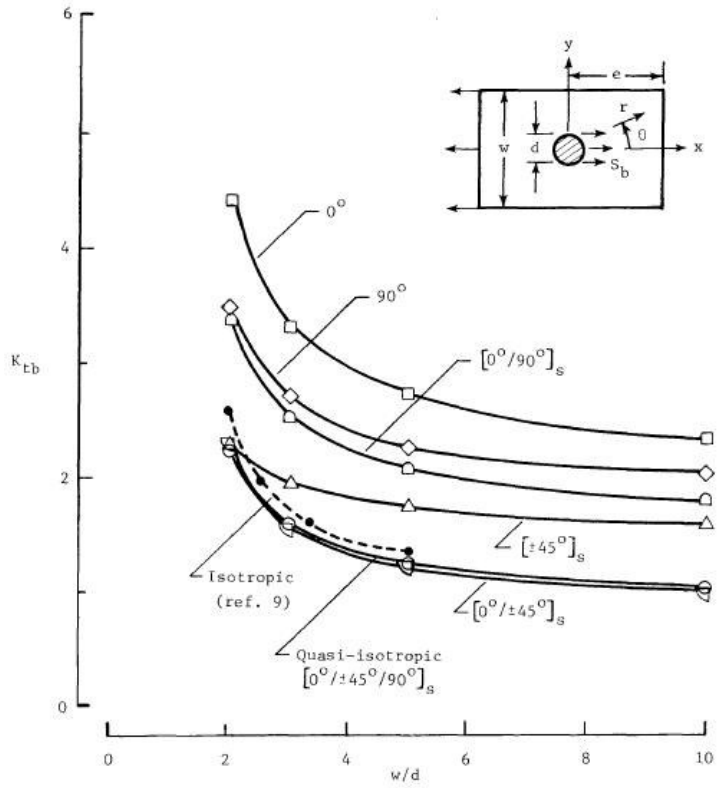

Figure 4: Stress concentration factors for pin-loaded holes as a function of w/d; e/d=10 [9]

2.3. Mechanically Fastened Joints

More often than not, composite structures have joints. There are several types of connections used for joining two composite members in a structure. These include interlocking connections, bolted, bonded, and a combination of bolted and bonded. However, for most applications the simplest, easiest to maintain, and most cost-effective connections are mechanically fastened. Mechanically fastened joints are also used primarily in structures that need to be disassembled for repair or inspection. The behavior of these mechanical joints is governed by several parameters including width, edge distance, material thickness and fiber orientation. This behavior involves a much higher level of complexity than metals, due to the seeming unlimited combinations

between composite materials and fiber pattern [10]. This is aggravated by the fact that the loads that cause failure in these joints can not be predicted by perfectly elastic or perfectly plastic models. The influence of the previously mentioned parameters was investigated by Rosner and Rizkalla [10] at the University of Manitoba in 1995. It was found that the predominant factor, influencing the capacity of a connection, is the width of the connected members. The bearing strength of a joint increases as the width to hole diameter ratio is increased. However the strength increase begins to level off around $w/d = 5$. The effect of edge distance showed a similar trend with the bearing strength increasing with the increase of the edge distance to diameter ratio. These curves also leveled off around $e/d = 5$. They also found that material thickness had little effect on the overall behavior of the connection.

It was also been shown that the ratios of *w/d* and *e/d* have an effect on the failure mode of the laminate. Images of these different failure modes can be seen in Figure 5. At small values of *w/d*, tension is a prevalent mode of failure, while small values of *e/d* result in the shear mode of failure. As both of these ratios increase the failure mode transitions to bearing.

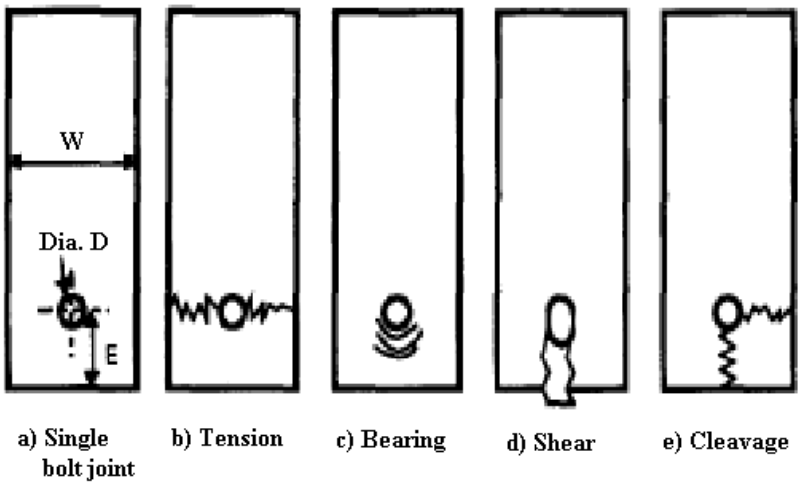

Figure 5: Failure modes of a single bolt tension joint [10]

2.3.1. Effects of Clamp-up

Khashaba, Sallam, Al-Shorbagy and Seif investigated the effect of washer size on bearing stresses [11] at Zagazig University, Egypt in 2005. This study showed that when load was plotted against displacement, the slope of the curve decreased as washer diameter was decreased for a constant torque. They found that for a set tightening torque of 15 Nm, an optimal washer size can be found by plotting washer size vs. bearing strength. The bearing strength of the joint increases with washer size until 18mm and then begins to decrease. Although the smaller washers had minimum contact area and thus maximum contact pressure, the bearing strength is still less than the 18mm washer. Khashaba et al. hypothesized that this behavior is due to the lateral compressive stresses under the washer causing microcracks and resulting in premature failure. Although the laterally constrained area increases with washer sizes above 18mm, the contact pressure also decreases resulting in a lower bearing strength for the joint. Once an optimum washer diameter was determined, the effects of tightening torque could be investigated.

Using the optimum washer size of 18mm, the tightening torque was varied from 0 Nm to 15 Nm. Over the range of torques tested, it was shown that the bearing strength increases with increasing tightening torque.

Crews studied the effects of clamp-up on bearing stresses [12] at NASA in 1980. He found that a pin loaded hole (no clamp-up) will cause abrupt failure and unstable hole elongation. However, even at "finger tight" clamp-up levels the bearing strength is improved. As the torque on the bolt is increased the bearing strength of the joint continues to rise. More clamp-up force also helps to stabilize the hole elongation after initial bearing failure. Because of this, the ultimate joint strength is significantly higher than initial failure load. These results can be seen graphically in Figure 6.

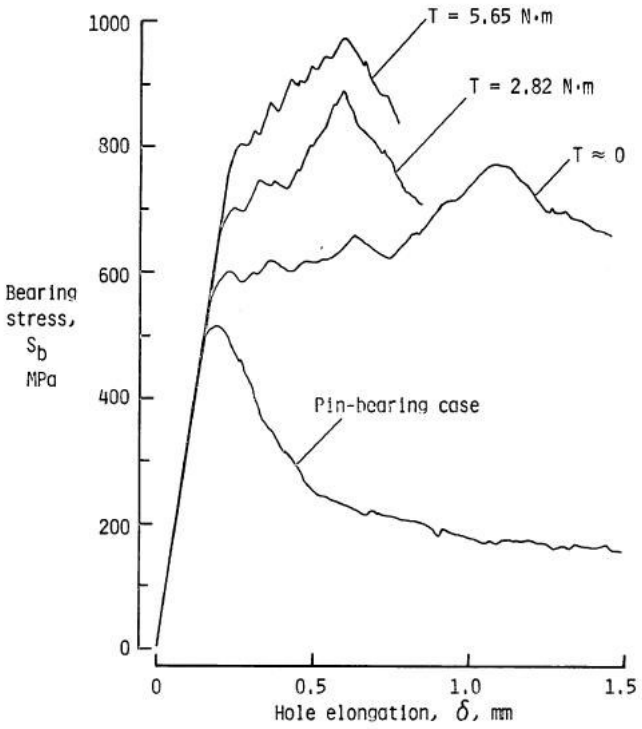

Figure 6: Static hole elongation for several clamp-up conditions [12]

Crews also found that bolt clamp-up altered the failure mode of the joint. The common failure mode for a pin loaded hole is bearing with "brooming" exhibited at the hole. However, under small clamp-up loads, joints failed in a combination of shearout under the washer and bearing failure beyond the washer. As clamp-up increased, some joints even failed in a mixture of shearout, bearing, and tension. The 50 percent improvement in ultimate strength for finger tight torque levels, compared to the pin bearing case, shows the effects of suppressing the bearing mode.

Marshall, Arnold, Wood and Mousley also observed the effect of clamping force [13] at Paisley College of Technology in 1989. They saw that the introduction of a clamping load generally improves the stress state in a joint. They also showed that a higher clamping action can be generated by a stiffer washer. These higher clamping forces also increase friction in the joint which has been shown to reduce bearing stresses in joints. However, it was found that high clamping ratios stresses tend towards that of a pinned joint, which can only be detrimental to joint performance.

Cooper and Turvey studied the effects of joint geometry and bolt torque on structural performance [14] at Lancaster University in 1995. They found that at low edge distance to diameter ratios (*E/D*) and width to diameter ratios (*W/D*) the effect of bolt torque was negligible. However, as these ratios were increased, critical values of *E/D* and *W/D* emerged from the data. This can be seen for *W/D* in Figure 7. These critical ratios are the dimensions that ensure a bearing failure for a given bolt torque. Increasing the *E/D* and *W/D* ratios was also found to increase the joint stiffness. Cooper and Turvey also found that joints that failed in bearing exhibited significant post failure load carrying

capacity. This was attributed to the double shear set-up, which constrained the failed material from deforming out of plane.

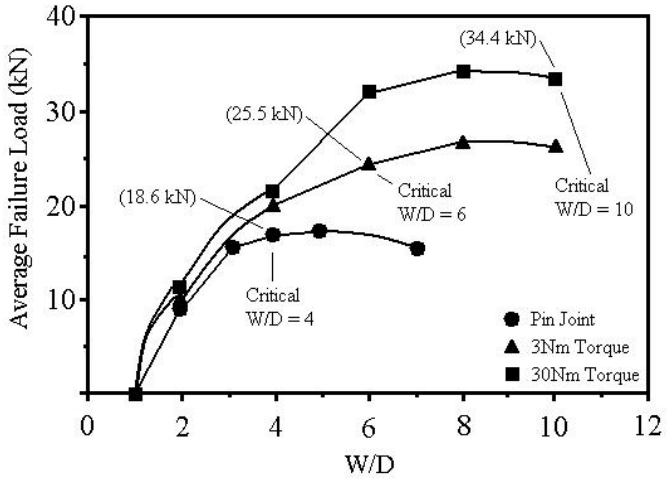

Figure 7: Average joint load capacities for varying bolt clamping torques. [14]

Nassar, Virupaksha and Ganeshmurthy also investigated the effects of bolt tightness on the behavior of composite joints [15] at Oakland University in 2007. They found that increasing bolt tightness increases the strength of the joint as well as reduces the potential for delamination around the bolt hole under tensile loading. However, bolt tightness can not be increased beyond the joint strength. Bolt tightness can also have negative effects. Tightening only one bolt in a joint with multiple fasteners can initiate the bearing failure in a composite plate. It was found that only when both bolts are sufficiently tightened does the joint gain stiffness. Both the configuration of the bolt tightening and the material of the joint were found to have negligible effect on the strength of the joint.

Studies have shown that bolt clamp-up improves the strength of composite joints. However, resin based composites are viscoelastic at room temperature, and this behavior is more pronounced at elevated temperature and moisture levels. This viscoelasticity can cause relaxation of clamp-up forces. Shivakumar and Crews investigated bolt clamp-up relaxation in a graphite/epoxy laminate [16] at NASA in 1982. They found that clamp-up forces relax even at room temperature. The rate of relaxation was found to increase with time and moisture content of the composite. They also showed that the combined effects of temperature and moisture are additive. Clamp-up forces were shown to relax as much as 71% at elevated temperature and moisture conditions over a 20 year period. These results can be seen graphically in Figure 8.

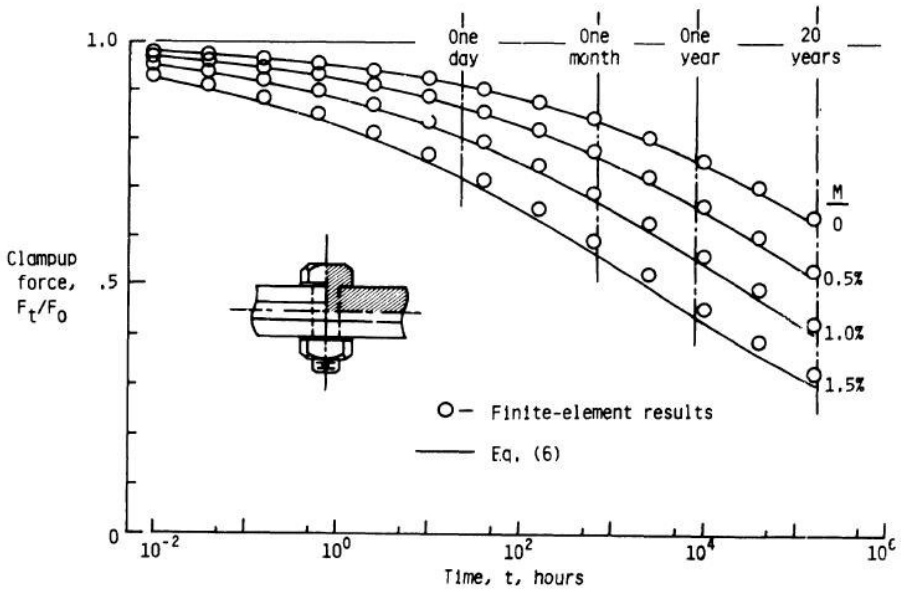

Figure 8: Clamp-up relaxation for several moisture levels at 66ºC [16]

2.3.2. Effects of Fiber Orientation

The effects of fiber orientation were investigated by Rosner [17] in his thesis at the University of Manitoba in 1992. It was found that bearing strength of a composite is still extremely dependent on the ratios of specimen width and edge distance to hole diameter. However, when fiber orientation was also considered, Rosner showed that there is a decline in bearing strength as fibers move away from the 0º orientation. Thus, when unidirectional laminates are considered, the highest bearing stress is achieved by 0º fibers and 90º fibers having the lowest bearing stress. These results can be seen graphically in Figure 9.

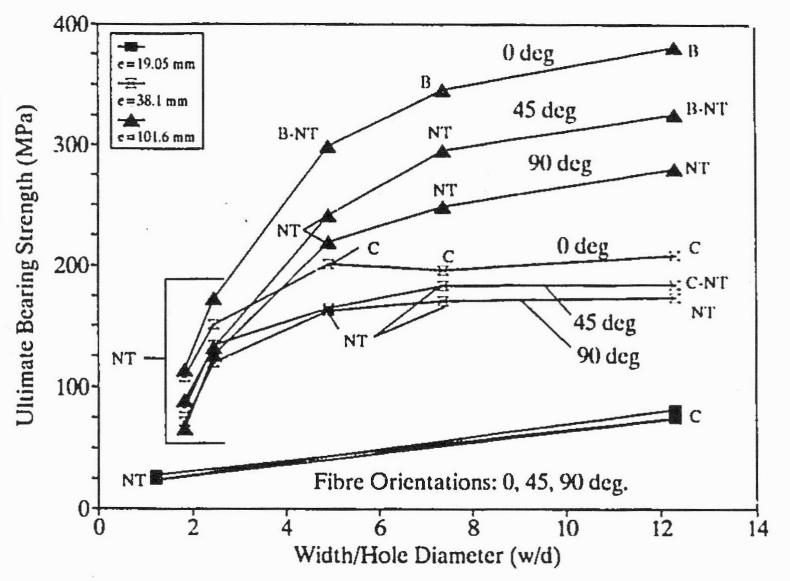

Figure 9: Bearing strength vs *w/d* ratio for varying fiber orientations in unidirectional laminates [17]

2.3.3. Effects of Bolt-Hole Clearance

Bearing stresses, within a composite joint, can also be directly affected by the fastener itself. The clearance between the fastener and the surrounding material, the

amount of contact area under the washer or bolt head and the amount of torque used to tighten the fastener can all play a large role in the stiffness and bearing capacity of a composite joint.

Stress is traditionally calculated as the ratio of load to area. In the case of bearing stress, this area is the contact area between the bolt and the composite. As the clearance between the fastener and the surrounding hole increases, the contact area will decrease. This will cause the bearing stress at the hole to increase without changing the load. Thus, the tighter the bolt fits the better. Lawlor, Stanley and McCarthy investigated this effect in single shear, single bolt joints [18] at the University of Limerick in 2002. They found that in near fit holes, the contact angle between the bolt and the hole is typically 160-170º, and is fairly consistent through the thickness. For larger clearance holes, Lawlor et al. determined that the angle of contact was 130-140º at the shear plane and reduced significantly through the thickness. This smaller contact area and thus greater bearing stress was said to be the cause of higher clearance joints having lower strength.

However, even with a near fit clearance, the initial bolt-hole contact area is small. Crews and Naik analyzed the effects of bolt-hole contact at NASA Langley in 1993 [19]. They found that as bearing stress increases in the connection, the contact angle or area will also increase. This is illustrated in Figure 10.

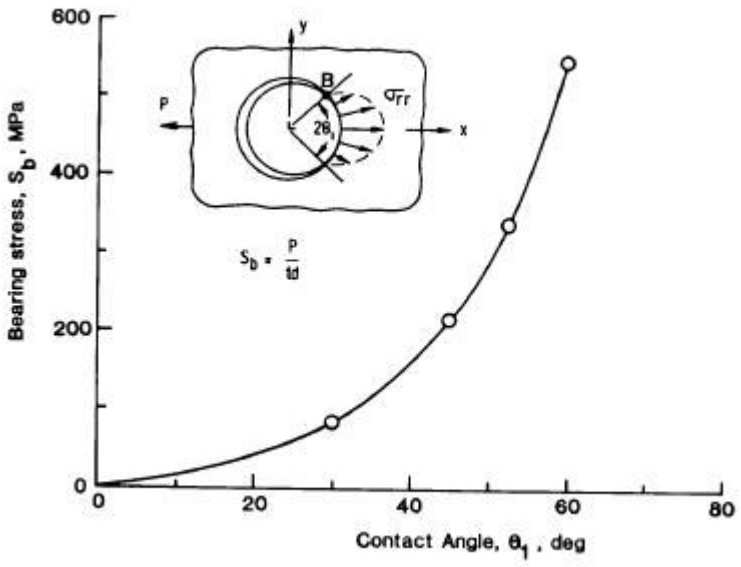

Figure 10: Contact Angle vs. Bearing Stress by Crews and Naik [19]

The contact area between the bolt and hole is not only affected by the bolt diameter but also the thickness of the laminate. The Composite Materials Handbook [20] provides a bearing strength reduction curve for diameter to thickness ratio. This curve, shown in Figure 11, was taken from test data and can be recreated for any test setup.

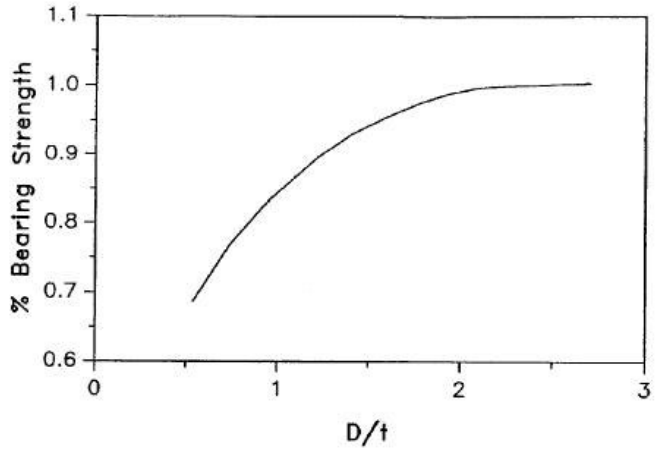

Figure 11: Bearing stregth reduction vs. Diameter to thickness ratio [20]

Lawlor, McCarthy, and Stanley studied the effects of clearance on single bolt, single shear, composite bolted joints [21] at the University of Limerick in 2002. They felt that a vital aspect in realizing the full potential of composites to reduce the weight of structures is in the efficient design of joints. This is because joints represent potential weak points in a structure. Thus the design of a structure tends to be controlled by its joints. Poorly designed joints can lead to heavier structures, in service structural problems and high life cycle costs. This is a significant problem because composites have lower maximum joint efficiencies than metals.

Lawlor et al. varied not only the clearance between the bolt and the hole, but also the level of torque applied to the fastener. They mainly investigated the worst-case scenarios of finger tight or 0.5 Nm vs. full torque or 16 Nm and clearances within f7 ISO tolerances (near fit to 80 μm) along with clearances outside f7 ISO tolerance (160 μm to 240 μm). The f7 tolerance is one of the bolt hole clearance standards instituted by the ISO and widely used within the aircraft industry. Quasi-isotropic as well as zero dominated layups were also studied along with protruding and countersunk bolts.

A drop in joint stiffness was seen as clearance was increased in all of the configurations tested by Lawlor et al. This can be seen graphically in Figure 12. It was also found that regardless of the amount of clearance and torque, the maximum load did not change much between configurations. Even though for protruding bolts the effect of clearance on ultimate strength was almost negligible, the ultimate strain showed a strong dependency on clearance. Lawlor et al. believed this is because larger clearances result in more concentrated loads on the laminate and thus causing more extensive laminate

damage. Because of this the laminate absorbs more energy and delays final failure, which is by bolt failure in these configurations.

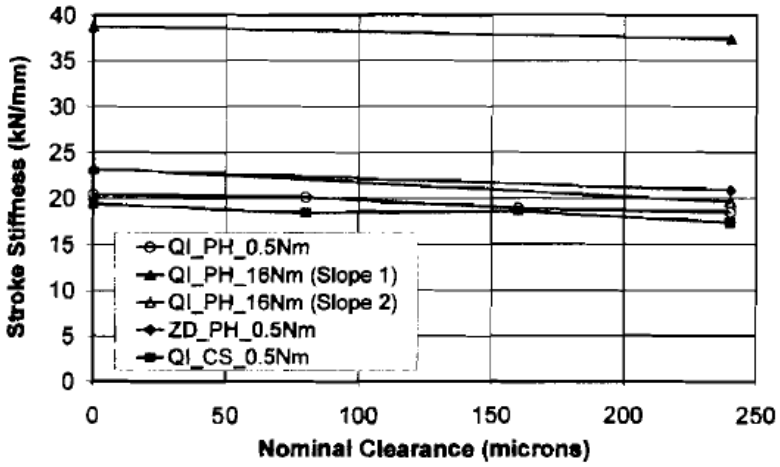

Figure 12: Clearance vs. Stiffness for tests performed by Lawlor et al. [21]

Further examination on the effects of clearance was performed on single lap, multi-fastener composite joints by Lawlor et al. [22] at the University of Limerick in 2004. The specimens tested had three bolts arranged linearly in the loading direction. The clearance in the first two holes was near fit and the clearance in the third hole was varied between values within f7 ISO tolerance (near fit to 80 μm) and values outside of f7 ISO tolerance (160μm to 240 μm). These configurations were all tested for load distribution under quasi-static conditions [23]. It was found that as the clearance of one bolt increased, the other two bolts would see an increased percentage of the load. After this, the near fit and worst case setups were tested to failure under both quasi-static conditions and fully reversed cyclic fatigue.

The results from the load distribution testing, for the near fit specimen, held true to the usual assumptions with the outer two bolts carrying approximately 35% of the load in each bolt. However, as the clearance in the third hole was increased, the load distribution began to change. With an increase in clearance, the third bolt began to carry less and less of the load. In the worst case scenario, the third bolt was just beginning to take up load as the maximum applied load was reached.

Next the specimens were tested quasi-statically to failure. Initially there was a large difference in stiffness between the near fit and worst case joints. However, as the displacement increases, the two joints reach the same stiffness. It was found that clearance had no significant impact on the ultimate failure load. Under current joint design rules, the middle bolt is not considered to be a failure threat. However, the results of this experiment have shown that when clearance variation is considered, the first and middle bolts share a larger portion of the load. This can cause the first and middle bolts to fail simultaneously.

The data from the quasi-static failure tests showed that the stiffness of both joints decreased with increased loading past 20 kN. However, in the near fit joint, the largest drop in stiffness occurs at a 5% greater load than in the joint with the maximum clearance. Even thought the ultimate failure load is the same regardless of variation in clearance, significant failure events occur at lower loads in joints with greater clearance. These results seem to be aligned with those from the single-bolt joints.

The fatigue testing for the multi-bolted joints was performed by Lawlor et al. at a number of different stress levels to achieve a large variation in life. One of the failure

criteria used was 10% hole elongation. This criterion proved to indicator of the imminence of catastrophic failure for the joints. This was shown by plotting the peak to peak displacement against number of cycles. A sharp increase was seen in the peak to peak displacement as the joint reaches 10% elongation. This curve also shows that the peak to peak displacement rises sooner for the maximum clearance joint than for the near fit joint. The data shows that clearance has more of an effect on failure initiation and this effect diminishes as the failure progressed. Because of this earlier onset of damage the joints with greater clearance exhibited shorter fatigue lives.

Lawlor et al. also examined the bolt-hole clearance effects in double-lap, multi-bolt composite joints [24] at the University of Limerick in 2004. The results from these experiments were in-line with the finding from their work with single-lap, multi-bolt composite joints. Clearance was not found to have a significant effect on the quasi-static strength. However, it was found to affect the failure mode, more specifically at which bolt the failure occurred. The initial failure load also decreased up to 25% with the increase of clearance in two of the three bolts. It was also found that hole elongation initiated sooner in joints with more clearance.

Vangrimde and Boukhili investigated the use of flexibility formulae as simple tools to predict the behavior of a joint [25] in 2002 at Katholieke Universiteit Leuven. The flexibility formulae are used to predict the load carried by each bolt in a multi-bolt joint. These formulae take into account all of the properties of the composite laminates as well as the fasteners and washers used in the joint. Their results showed a strong correlation between theoretical models, using these formulae, and the experimental data.

Their data showed that the applied torque did not alter the bearing stiffness but increased bolt-hole clearance significantly lowers bearing stiffness. However these formulae are only valid for the linear portion of the bearing stress - bearing strain curve. Initially the bearing stress-strain curve is approximately linear and thus the stiffness is constant. This holds true until about 80% of the ultimate bearing strength where there is a clear knee point in the data which marks the first perceptible damage and results in a reduction in stiffness. This knee point is where the curve becomes non-linear and the flexibility formulae become invalid. This damage load shows independence from specimen geometry but increases with bolt torque. Washers also proved to play an important role in maintaining linearity before reaching the damage load.

2.3.4. Effects of Bearing and Bypass Loading

In joints with multiple fasteners, holes may be exposed to bearing loads as well as loads that bypass the hole. The ratio of the bearing load to the bypass load depends on the stiffness and configuration of the joint. This bearing-bypass ratio remains nearly constant at each fastener, as the joint is loaded, until damage begins to develop. Different bearing-bypass ratios tend to produce different modes of failure and strengths in each fastener hole. The effects of bearing-bypass loading on a composite laminate were investigated by Crews and Naik [26] at NASA in 1987. They used a single fastener specimen and induced bearing and bypass loading using a specially designed test setup. By varying the bearing-bypass ratio and testing specimens to failure a Bearing-Bypass Diagram was created. This diagram can be seen in Figure 13. It shows results for tension and compression reacted bearing for damage onset strength. The data shows that

the failure mode can be altered by changing the bearing/bypass ratio for a constant geometry. It should be noted that this data is for statically loaded specimens and not fatigue. S. P. Garbo provided strength data and failure prediction under bearing-bypass loading for composite laminates [27]. Naik and Crews provide similar predictions [28].

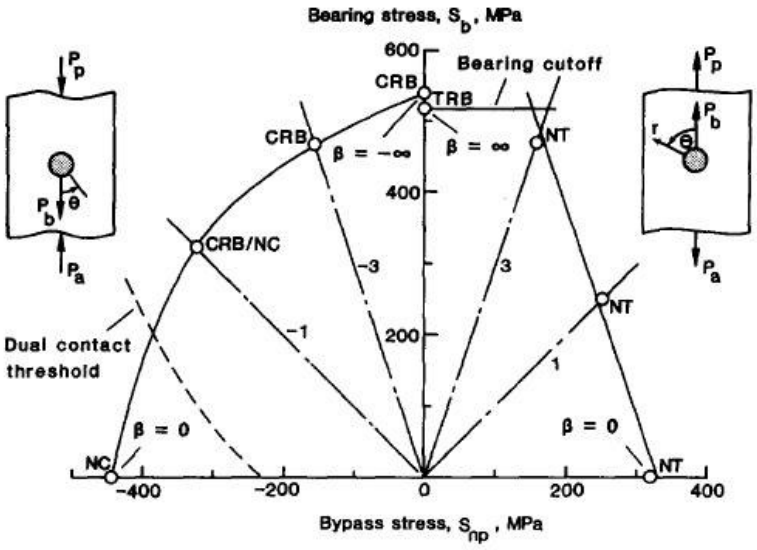

Figure 13: Bearing-bypass diagram for damage-onset strength [26]

2.3.5 Fatigue Considerations

Some of the same factors that influence the behavior of bolted joints under static and quasi-static loading conditions also affect joint behavior in fatigue conditions. Lim, Kim and Lee researched the fatigue characteristics of bolted joints for composite laminates [29] at the Korea Advanced Institute of Science and Technology in 2004. Using knowledge obtained from previous static and quasi-static testing, they selected the geometry of the joint to induce bearing failure. It was found from the fatigue tests on quasi-isotropic laminates that the fatigue life decreased linearly with respect to the applied load. Lim et al. also showed that the fatigue life of quasi-isotropic laminates

increased with increasing levels of bolt torque. However, increasing bolt torque showed now effect when the stress levels were normalized to the static joint strength.

In the same work, Lim et al. also investigated cross ply laminates with the majority of the plies in the load bearing direction. When the joints were not preloaded with bolt torque, they showed similar trends to the quasi-isotropic laminates. Both laminates showed a fatigue strength at one million cycles that was 50% of the static strength. However, when torque was applied to the bolts, the fatigue strength at three million cycles was more than 90% of the static strength for the joint. This showed that the quasi-isotropic laminates have superior bearing strength but, the cross-ply laminates exhibit greater strength retention in fatigue. This can be seen graphically in Figure 14. They also showed that the angle of the outer most ply had no effect on the fatigue life of the joints.

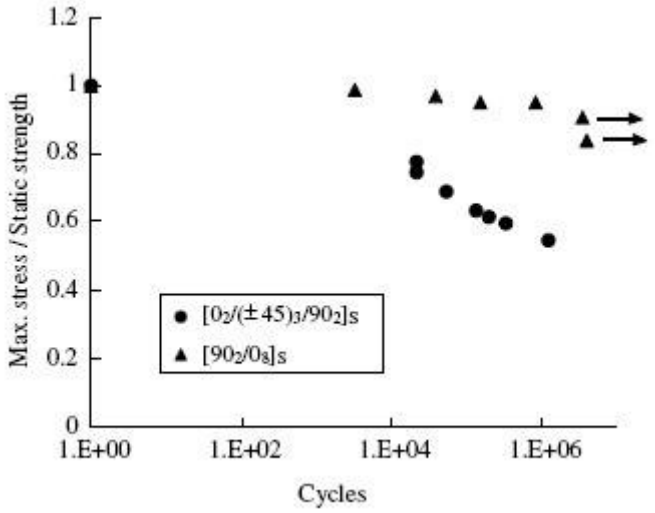

Figure 14: Normalized stress vs cycle curves with bolt torque of 35 MPa for various laminates [29]

In his work on bolt-bearing fatigue of graphite epoxy laminates [12], Crews showed that bolt clamp-up also effects hole elongation under fatigue loading. He

demonstrated that as clamping toque is increased, the amount of permanent hole deformation under fatigue loading will be reduced. These trends can be seen in Figure 15.

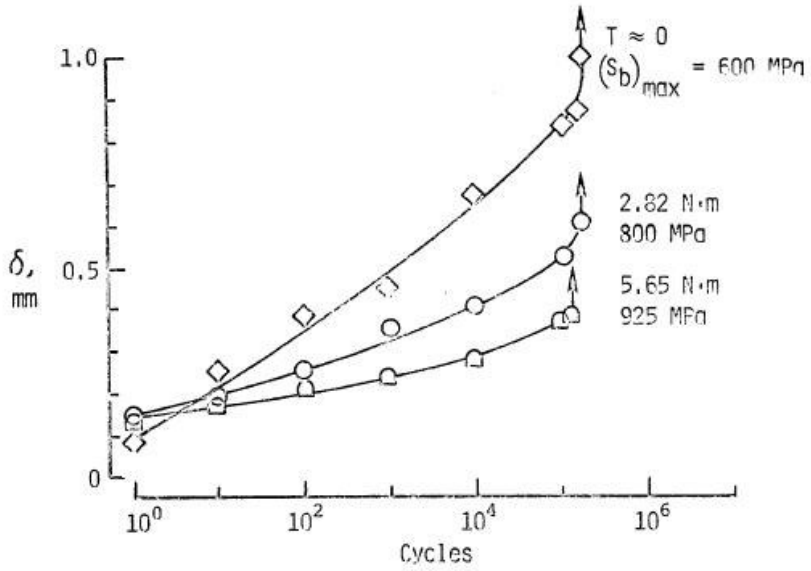

Figure 15: Hole elongation curves for several clamp-up cases [12]

The bolt hole clearance is also an issue under fatigue loading. Kam investigated the fatigue characteristics of bolt hole growth in graphite epoxy laminates for clearance and interference fit bolts [30] at Douglas Aircraft Company in 1981. He found that when bolts are interference fit, the hole does not elongate anymore than the initial hole expansion due to the interference fit. Kam also determined that when the bolt is clearance fit, the hole will elongate linearly over the tested range of five hundred thousand cylces. In one case, drastic hole elongation was noticed when the bolt began to slip in the hole. This produces cyclic impulse loads at diametrically opposite hole locations. Ramkumar and Tossavainen found, in their work on strength and lifetime of bolted laminates [31] at Northrop Corporation, that these impulse loads result in a

dramatic increase in the rate of hole elongation. This dramatic rate increase usually occurs after 1 – 2% hole elongation.

Several statistical analyses of the factors affecting strength and fatigue life of composite bolted joints have been performed. Person and Eriksson attempted to create a ranking of a number of factors [32] at the Royal Institute of Technology in Stockholm. They considered design factors such as joint geometry. They also investigated material and environmental factors as well as fastening factors such as clearance and clamping torque. Herrington and Sabbaghian also performed an analysis considering stress level, clamping torque and outer ply angle [33] at the University of New Orleans. They found that the dominating factor is the ratio of applied stress to ultimate strength.

CHAPTER 3: EXPERIMENTAL PROCEDURES

Following is a description of the experimental equipment, techniques and procedures used of the course of this research. The prepreg material, lay-ups, and specimen configurations are described. This is followed by the description of the equipment and methods used for the tests. Finally, the use of the X-ray radiography equipment is detailed.

3.1. Materials, Lay-ups, and Specimen Geometry

The material tested was a carbon fiber toughened epoxy resin prepreg. The specimens used in this study were fabricated in the following manner. 7.62 cm (3 in.) prepreg tape was laid up into panels by hand, and the panels were cured at 177ºC (350°F) according to manufacturer specifications. The panels were then cut into 7.62 cm (3 in.) x 19.37 cm (7.625 in.) coupons using a diamond saw. Four holes were then drilled using a 6.35 mm (0.25 in.) diamond-impregnated drill bit. Specimens were then labeled with a specimen number and the corresponding lay-up. Specimen geometries are shown in Figure 16, Figure 17 and Figure 18.

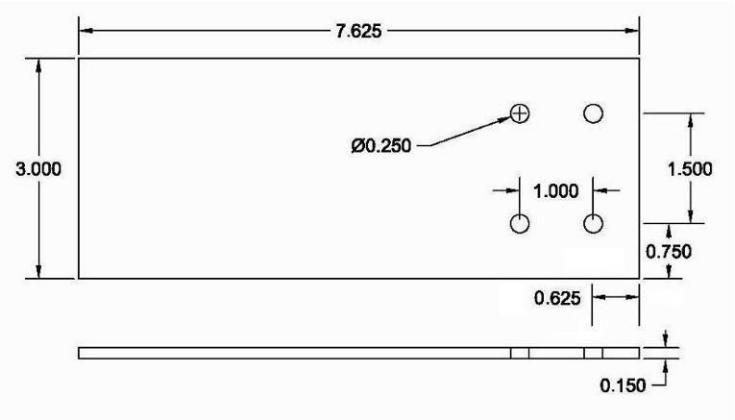

Figure 16: Specimen Configuration

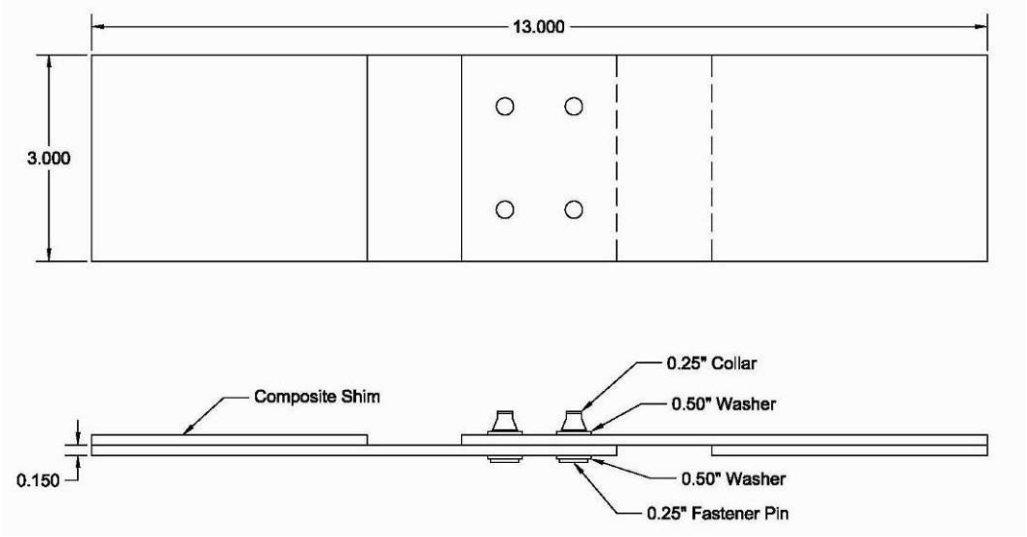

Figure 17: Single Shear Configuration

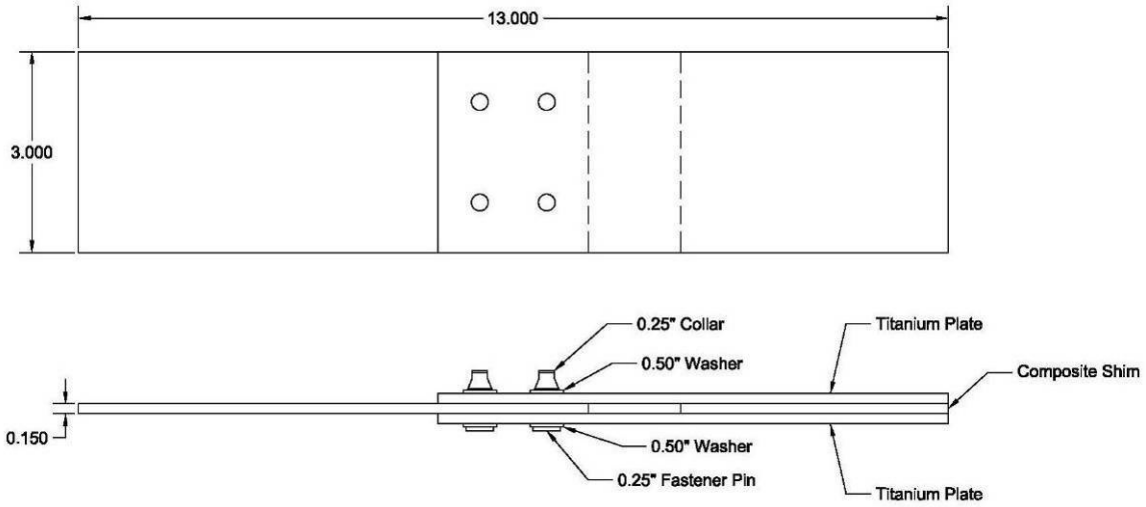

Figure 18: Double Shear Configuration

Four different lay-ups were considered in the current research: two traditional "hard" lay-ups, and two non-traditional "hard" lay-ups. The two traditional lay-ups are commonly used in current aircraft structures, and the stacking sequences are $[45/90/-45/0_2/45/0_2/-45/0]_s$ and $[0_4/45/0_3/90/0]_s$. In the non-traditional lay-ups the 0° plies were replaced with off-axis 5° plies and the 45° and 90° plies were replace with 65° plies. This was done in an attempt to improve the damage tolerance and bearing capabilities

while maintaining the overall laminate stiffness. The stacking sequences of the non-traditional lay-ups were $[\pm5/65/(\pm5)_2/-65/\pm5]_s$ and $[\pm5/65/(\pm5)_2/-65/5/65]_s$.

Hereafter, these laminates will be referred to by the percentage of certain plies. $[45/90/-45/0_2/45/0_2/-45/0]_s$ and $[0_4/45/0_3/90/0]_s$ will be known as 50/40/10 and 80/10/10, respectively– the percentage of 0°/45°/90° plies. Similarly, $[\pm5/65/(\pm5)_2/-65/\pm5]_s$ becomes 80/20 (80% of ±5° plies, 20% of ±65° plies) and $[\pm5/65/(\pm5)_2/-65/5/65]_s$ becomes 70/30 (70% of ±5° plies, 30% of ±65° plies). These laminates are all considered to be "hard" laminates, because the longitudinal stiffness is significantly higher than the transverse stiffness. These laminates layups and their corresponding identifiers have been listed in Table 1. Also included in this table are the longitudinal stiffness values normalized to the longitudinal stiffness of the 80/20 laminate.

Table 1: Laminates, Identifiers and Normalized Stiffness Values

Layup	Identifier	Normalized Stiffness
$[0_4/45/0_3/90/0]_s$	80/10/10	1
$[\pm5/65/(\pm5)_2/-65/\pm5]_s$	80/20	0.97
$[\pm5/65/(\pm5)_2/-65/5/65]_s$	70/30	0.86
$[45/90/-45/0_2/45/0_2/-45/0]_s$	50/40/10	0.75

Fastener consisted of close tolerance Hi-Shear threaded titanium pins, frangible collars, and washers, shown in Figure 19. The collars are designed such that the hexagonal head shears off at a predetermined torque level of 7.9 N-m (70 in-lb), ensuring consistent clamping force. Half clamp-up was used in the current research. This was done because a torque level of 4.29 N-m (38 in-lb) was determined to be an approximate representation of the clamping force after relaxation. Half clamp-up also left the hexagonal head in place which made fastener removal easier during radiographic investigation.

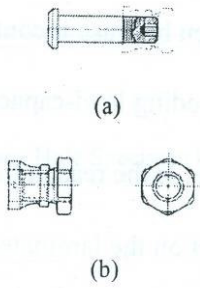

Figure 19: Mechanical fastener used (a) pin and (b) collar

3.2. Testing Apparatus

The following sections describe the load frames, test accessories, and stabilization fixtures utilized in this research.

3.2.1. Hydraulic Test Frame

The fatigue testing was performed on a 245 kN (55 kip) MTS servo-hydraulic test frame with 98 kN (22 kip) hydraulic Surfalloy-coated grips. The machine, shown in Figure 20, was equipped with a TestStar IIs data acquisition and control system, and the MTS Basic TestWare software package was utilized. The test frame was equipped with a lead enclosure for radiographic purposes.

Figure 20: 245 kN (55 Kip) MTS servo-hydraulic test frame with lead lined enclosure

During a maintenance period on the 98 kN (22 kip) test frame, a 98 kN (22 kip) MTS servo-hydrolic test frame with hydraulic Surfalloy-coated grips was used. The machine, shown in Figure 21, was equipped with a TestStar IIs data acquisition and control system, and the MTS Basic TestWare software package was utilized.

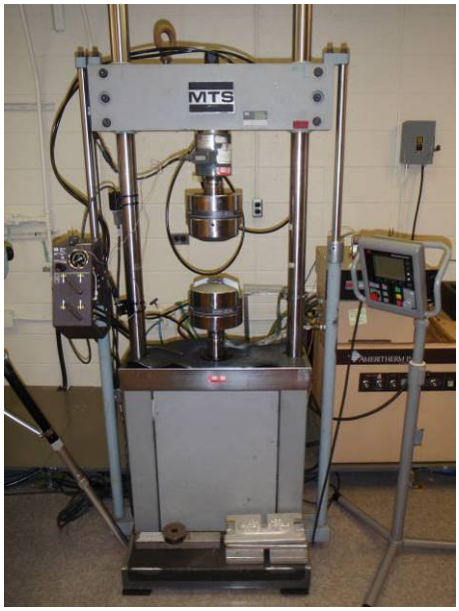

Figure 21: 98 kN (22 kip) MTS servo-hydraulic test frame

3.2.2. Test Fixtures

Initially, test specimens were arranged in a single shear configuration as seen in Figure 17. All attempts were made to make the loading as symmetric as possible. However, because of the configuration, there is some inherent eccentricity in the loading. This eccentricity causes a bending moment about the center of the specimen. This bending moment in turn causes out of plane deflection. This causes the stress states and damage mechanisms to be much more complicated than simple bearing loading found in a double shear configuration shown in Figure 18. Because of this complex stress state, specimens experienced failure by bolt pull through and shear out at much lower loads than expected. Some images of these failures can be seen in Figure 22 and Figure 23. There was also very little documentable damage progression under the single shear configuration. This was the motivation to switch to the double shear configuration.

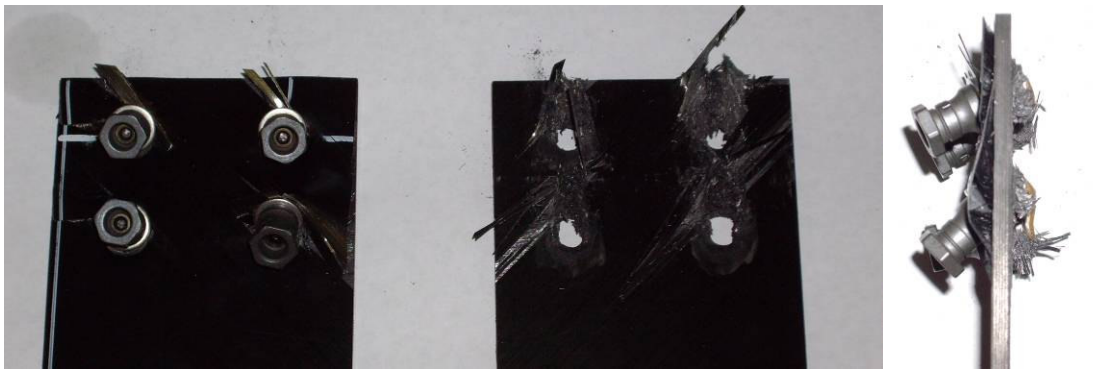

Figure 22: Single shear specimen failure by bolt pull through

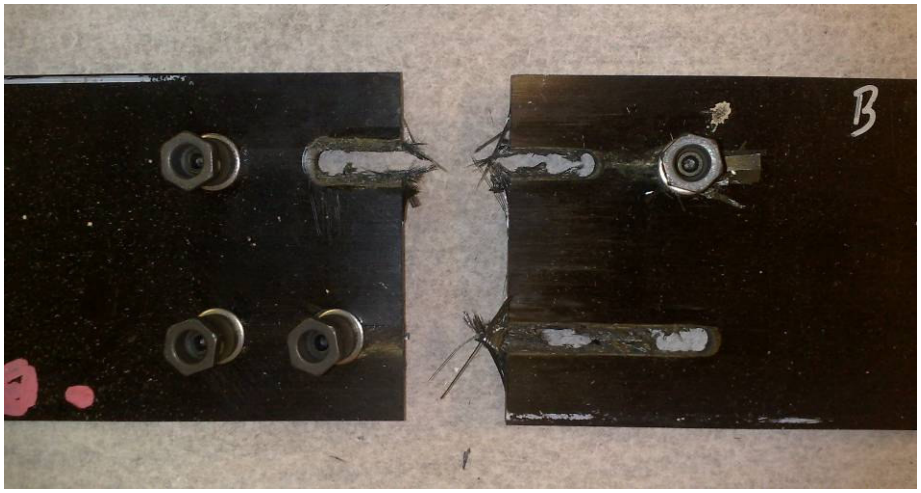

Figure 23: Single shear specimen failure by shear out

In an attempt to prevent out of plane deformation in the single shear specimen and the compression dominated tests in the double shear specimen, fixtures were utilized. A single fixture was designed and fabricated for both cases with shims and Teflon being used as needed. The fixture was machined by the Georgia Institute of Technology Mechanical Engineering Machine Shop out of 6061-T6 Aluminum. The resulting fixture and subsequent assemblies are shown in Figure 24, Figure 25 and Figure 26.

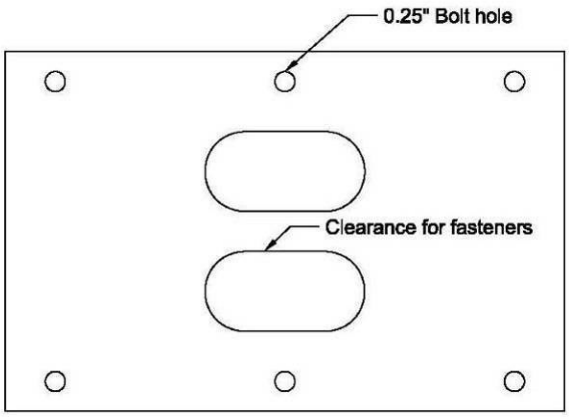

Figure 24: Bearing support fixture

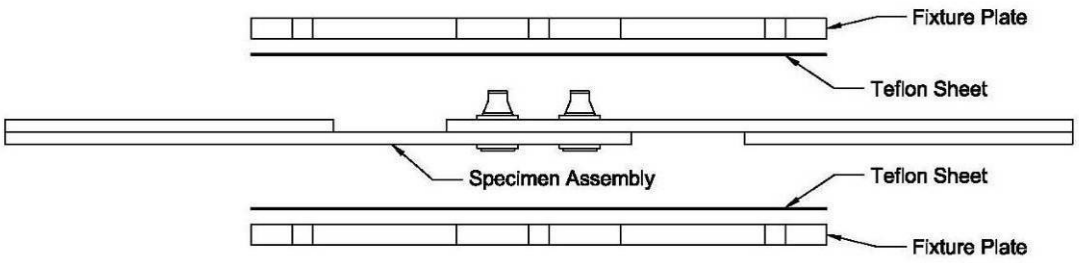

Figure 25: Fixture assembly for single shear specimen

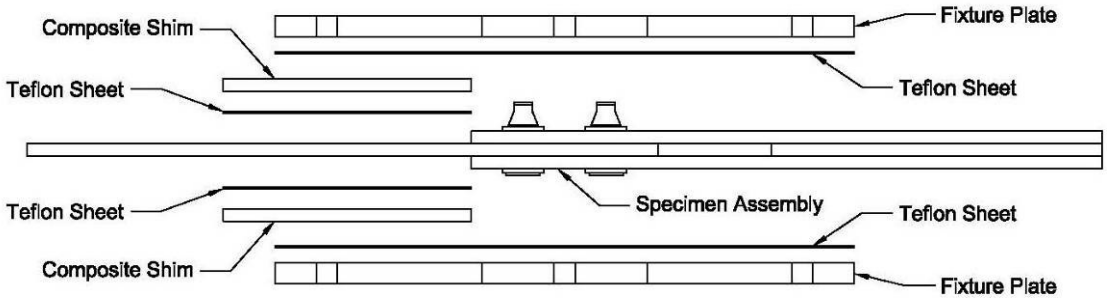

Figure 26: Fixture assembly for double shear specimen

3.3. Testing Procedures and Justification

The following sections describe the various procedures used for the different test types, as well as the justification for these procedures. Only one of each specimen was tested at each stress ratio.

3.3.1. Tensile Testing Procedures

Prior to tensile testing, specimens were visually inspected for nicks, surface irregularities, warpage, and asymmetry. The width and thickness of each specimen was measured with a dial caliper at the midpoint and both ends to ensure consistent dimensions. The diameter of each of the four holes was also measured.

Following visual inspection, one coupon was placed between two titanium plates such that the four holes aligned. A pin, with a small notch in the head, was then inserted through a washer on one side with a washer and a collar on the other. The collars were tightened to finger-tight. A small flat head screwdriver in a vise was used to secure the pin, while a torque wrench set to 4.29 N-m (38 in-lb) was used to tighten the collar. This was repeated for each fastener. This is the same assembly seen in Figure 18. Once assembled, the specimen was inserted into the grips. Alignment was ensured by the centering guides, and confirmed with visual inspection. A clamping force of 13.8 MPa (2000 psi) was applied using the hydraulic grips. After alignment and gripping occurred, testing was ready to begin. The target load and amplitude of oscillation were set and the test ran for 50,000 cycles or a predetermined critical damage criteria. Critical damage was defined as a 10% elongation of the hole beyond its original, nominal diameter of 6.35 mm (0.25 inches). This process was repeated in increments of 17.24 MPa (2.5 ksi) from 103.4 MPa (15 ksi) until failure.

After each load increment, the specimen was inspected radiographically as described in 3.4.1. From the resulting X-ray images the longitudinal splitting was measured at each hole as a method for comparing the damage tolerance of the different laminates.

3.3.2. Compression Testing Procedures

Before compression testing, specimens were inspected visually and assembled as described in 3.3.1. Once assembled, the specimen was placed in the fixture with shims in

place. The center of the bolt pattern with visually aligned with the center bold in the fixture. The fixture was then assembled and bolts were finger tightened with wingnuts.

Once assembled, the specimen was inserted into the grips. Alignment was ensured by the centering guides, and confirmed with visual inspection. A clamping force of 13.8 MPa (2000 psi) was applied using the hydraulic grips. After alignment and gripping occurred, testing was ready to begin. The target load and amplitude of oscillation were set and the test ran for 50,000 cycles or a predetermined failure criteria. Failure was, once again, defined as a 10% elongation of the hole beyond its original, nominal diameter of 6.35 mm (0.25 inches). This process was repeated in increments of 17.24 MPa (2.5 ksi) from 103.4 MPa (15 ksi) until failure.

After each load increment, the specimen was inspected radiographically as described in 3.4.1. From the resulting X-ray images, the longitudinal splitting was measured at each hole as a method for comparing the damage tolerance of the different laminates.

3.3.3. Critical Damage Determination

The critical damage criterion was defined as 10% elongation of the original, nominal hole diameter of 6.35 mm (0.25 inches). Once this criterion was reached the cycling was halted. The elongation was measured by the actuator displacement in the servo-hydraulic test frame. The hole diameter was measured at the beginning of each test to determine the amount of elongation needed to reach critical damage. At the initiation of testing, an interlock was set to halt the test when critical damage was reached. This method of measurement was verified with calipers at the end of each test.

3.3.4. Testing Procedure Justification

The motivation for using this "Damage Initiation Method" of testing came from previous research by Joshua Rast. In his work on characterizing the fatigue damage in non-traditional laminates of carbon fiber composites [34], it was noticed that 60-80% of the total damage occurred before 50k cycles in a 10^6 cycle test. For this reason, 50k was chosen as an ideal cycle count to determine the effects of each variable.

3.3.5. Damage Measurement Justification

For each in-situ radiographic image, the longitudinal split length was measured and recorded. This split length was defined as the distance from the center of the hole to the farthest crack tip.

Previous work has shown the difference between damage states in layups with a varying amount of longitudinal fibers. The more longitudinal fibers there are in a layup, the "harder" the laminate. Using an IM-7 carbon fiber system, A. Etheridge showed that longitudinal splitting was the predominant form of damage in "hard" layups [35] [36]. Based on this work, longitudinal splitting was chosen as the parameter on which to base damage progression.

3.4. Radiographic Procedures

Radiographic inspection of damaged specimens was performed with a Faxitron 110 kV portable X-ray unit used in conjunction with the 245 kN (55 kip) MTS test frame. A lead-lined plywood enclosure, fabricated for radiation safety, was mounted on the test frame as seen in Figure 27. Radiation safety training was attended, and the x-ray room

was certified by the Georgia Tech Office of Radiation Safety to meet applicable state and federal safety requirements.

Figure 27: MTS test frame and lead lined enclosure without X-ray unit in place

3.4.1. Radiographic Inspection

X-rays were taken at increasing load levels to determine if damage had occurred. Because the graphite fiber and epoxy resin provide limited contrast for the x-ray, zinc iodide die penetrant was used. The die penetrant leaches into the cracks in the specimen and helps to distinguish the damaged areas. The solution consists of 60 g Zinc Iodide (ZnI_2) 98% pure, 8 mL distilled water, 10 mL Isopropyl alcohol, and 3 mL Kodak photo flow 200. This solution was prepared during prior research.

Preparation of the specimen prior to x-ray consisted of removing the compression fixture when necessary, as well as the bolts and titanium plates. This was accomplished by unloading the specimen and removing it from the test frame. After disassembly, the zinc iodide was applied to the hole diameter using a 250 µL Hamilton luer tip syringe. Extreme care was taken to avoid surface contamination, since residual zinc iodide

solution on the front or back surface of the specimen could obscure damage. Once the zinc iodide was applied the surfaces of the specimen were wiped thoroughly with a clean paper towel to further prevent surface contamination.

Once specimen preparation was complete, the specimen was secured in the grip and the x-ray film was placed directly behind the hole pattern. Initially, Polaroid Type 55 blank and white instant sheet film was used. This film was place in a holder and then aligned behind the hole pattern in the specimen. Unfortunately, during the research, Polaroid discontinued their instant film line. When the Polaroid Type 55 film supply was depleted, Kodak Industrex MX125 Ready Pack standard x-ray film was utilized. A lead blocker was used, with the Kodak film, to insure that only half of the film was exposed so that each piece of film could be used for two exposures.

The portable x-ray unit, shown in Figure 28, was positioned as seen in Figure 29. Alignment was guaranteed by a riser arm equipped with a safety interlock, aligning marks on the floor, and visual cues on the radiation enclosure. The parameters for the Faxitron 110 kV x-ray unit were set differently for the two film types. The initial parameters for the Polaroid film were a voltage of 33 kV, current 3 mA, and time of 73 seconds, based on previous research [35] [36]. The parameters had to be changed for the new Kodak film. These parameters were optimized through trial and error. The parameters for the Kodak film were a voltage of 25 kV, current 3 mA, and a time of 35 seconds. After the room was cleared, the door was closed, enabling the final safety interlock. The specimen was then irradiated to determine the existing damage within the hole pattern. The image would then be processed in accordance with 3.4.2.

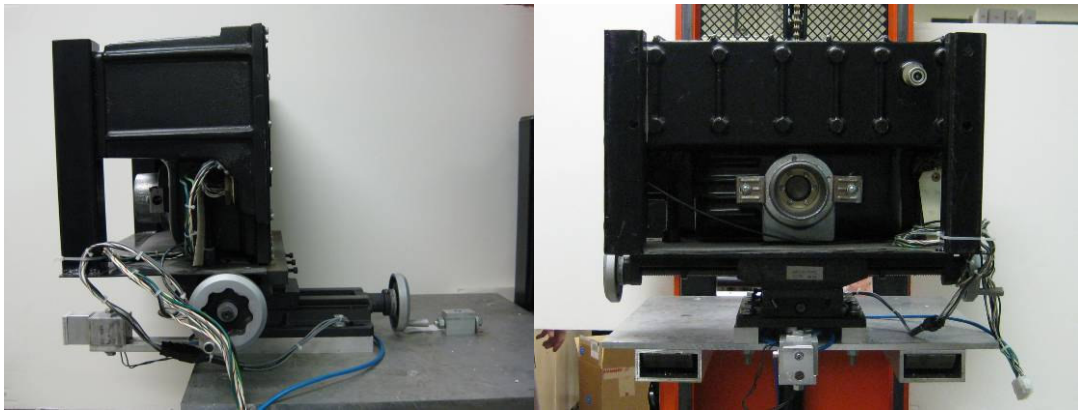

Figure 28: Faxitron X-ray unit

Figure 29: Faxitron unit positioned for X-ray

3.4.2. Film Processing and Imaging

Following X-ray exposure, the two different film types were both processed in different ways. The following sections explain the procedures used in film processing.

3.4.2.1. Polaroid Film Processing and Imaging

Following X-ray exposure, the Polaroid Type 55 sheet film was processed. The Polaroid type 545i film holder was switched from load to process mode and the film was

removed from the holder. This action spread the developing agent on both the positive and negative films. Per manufacturer specification, thirty seconds were allowed to ensure film development. The positive and negative were then separated. The positive image was inspected to determine image quality, and if deemed acceptable, the negative was placed in a fixing agent of 18% sodium sulfite solution made from Kodak anhydrous sodium sulfite. The negative remained in the fixing solution for at least 30 minutes. After removal from the fixing solution, the negative was rinsed in warm tap water for 5 minutes to remove any residual developing and fixing agents. Finally the negative was air dried.

The negatives were then scanned to obtain a digital image. The scanning was done using a HP Scanjet G4050 with negative scanning capabilities. The extent of damage was determined by visually inspecting the digital image. Any further enhancements or analysis could be performed using the HP Photosmart Essential software.

3.4.2.2. Kodak Film Processing and Imaging

Following X-ray exposure, the Kodak Industrx MX125 Ready Pack film was processed. The film was first taken to a dark room and processed under dim red lights to prevent light from contaminating the image. First a corner of the film was cut to ensure that the images remained distinct from one another, because there were two exposures per piece of film. The film was then removed from the ready pack and placed in a solution of Kodak Single Part Developer. All chemical solutions were prepared per the manufacturers specifications. The film remained in the developer solution for 5 minutes

and was agitated once every minute. The film was then removed from the developer and placed in the Kodak Stop Bath solution using rubber tipped bamboo tongs. A different set of film handling tongs was used for each solution. The film remained in the stop bath for 30 seconds. Next, the film was placed in a fixing solution prepared exactly like that used with the Polaroid film as described in 3.4.2.1. The film stayed in the fixing solution for 15 minutes and was agitated every 3 minutes. After the fixing solution the film was then washed under running water for 15 minutes to remove any residual chemicals. Once the film had been washed, it was dipped in a solution of Kodak Photo Flo to aid in the drying process and to prevent water spots. Finally, the film was air dried.

The film was then scanned to obtain a digital image. The scanning was done using a HP Scanjet G4050 with negative scanning capabilities. The extent of damage was determined by visually inspecting the digital image. Any further enhancements or analysis could be performed using the HP Photosmart Essential software.

CHAPTER 4: EXPERIMENTAL RESULTS AND DISCUSSION

This section will present the experimental results from the bolted joint testing. All data in this section has been normalized to the ultimate strength of the un-notched 50/40/10 laminate. This section also offers comparison organized by test parameter. Comparisons have been made based on the relative stiffness of each laminate. The table of the relative stiffness values can be seen in **Error! Reference source not found.** in section 3.1.

4.1. Cyclic Tension (R = -0.1)

The first set of fatigue tests were dominated by tension loading. The loading ratio was set at R = -0.1, which indicates a load reversal of 10% in compression. These tests were performed according to the procedure outlined in 3.3.1. Figure 30 shows the sharp contrast between the damage in laminates with 0º fibers versus laminates with slightly off axis 5º fibers. It can be seen that damage in the 80/10/10 laminate initiates and propagates much more rapidly than the 80/20 laminate. The 80/10/10 laminate also exceeds the critical damage criterion before the 80/20 laminate. Because the amount of damage that occurs in the 80/10/10 laminate is so much greater than the rest of the laminates tested at R = -0.1, it has been omitted from the rest of the cyclic tension comparison.

The stress at which damage initiated as well as where the critical damage criterion was exceeded can be seen in Figure 31. This data has been normalized to the static ultimate tensile strength of the 50/40/10 composite laminate. It can be seen from this

figure that the initiation of damage occurred at the same stress level for each laminate. For each test at R = -0.1, the damage developed in the form of longitudinal splitting. This is the common form of damage for "hard" laminates. This type of damage is caused by large concentrations of shear stress at the holes. In these tests the 50/40/10 laminate withstood the highest absolute stress, while the 70/30 laminate exhibited the most resistance to damage. The 80/20 laminate exhibited the least damage resistance, and also withstood the lowest absolute stress. Both the 80/20 and 70/30 laminates showed relatively steady rates of damage progression, while the 50/40/10 was more varied. Figure 32 shows the end damage state of each of the three laminates after the final damage criterion, of 10% hole elongation, was reached. In the non traditional laminates, the split crack tips in different longitudinal (±5º) plies diverge as the crack propagates. In all of the laminates it can be seen that the final damage state was a crushing caused by bearing failure. However, in the non traditional laminates there was also some delamination caused by the elongation of the holes. A comprehensive set of damage X-rays can be seen in the Appendix.

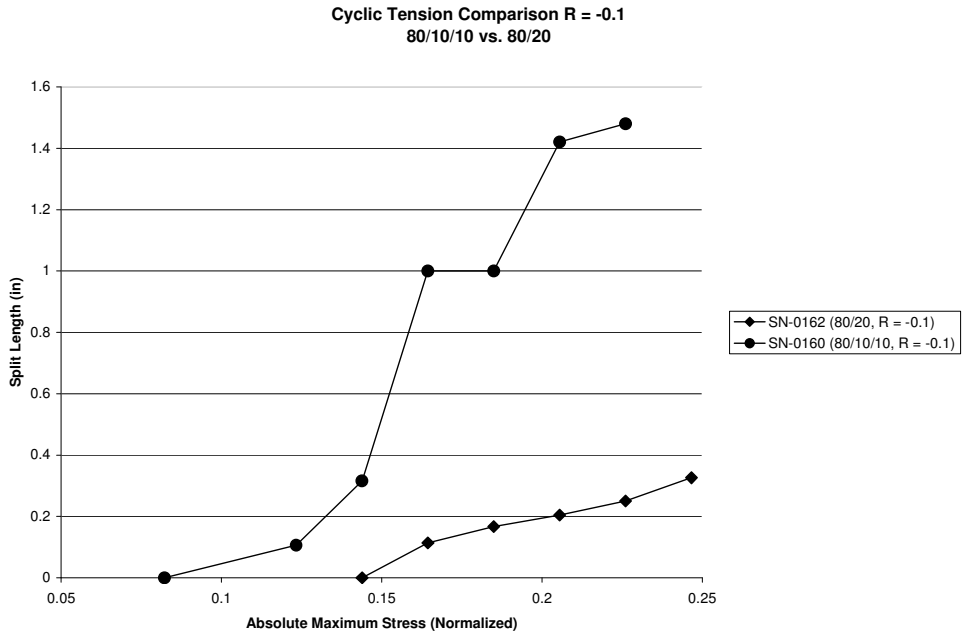

Figure 30: Cyclic tension comparison of damage in 80/10/10 and 80/20 laminates at R = -0.1

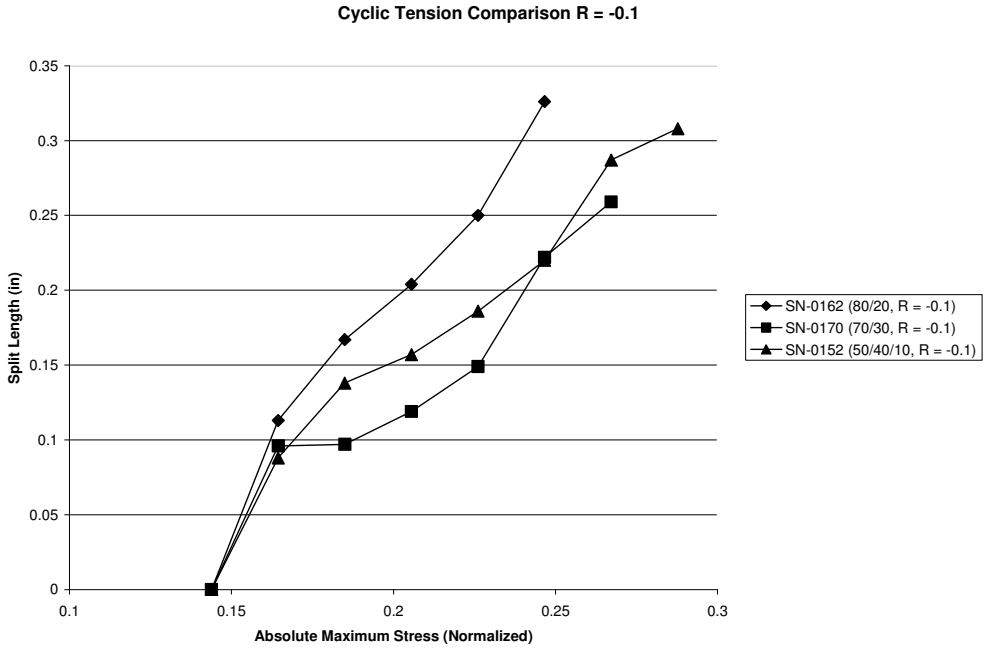

Figure 31: Cyclic Tension Data (Specimen, Layup, R ratio)

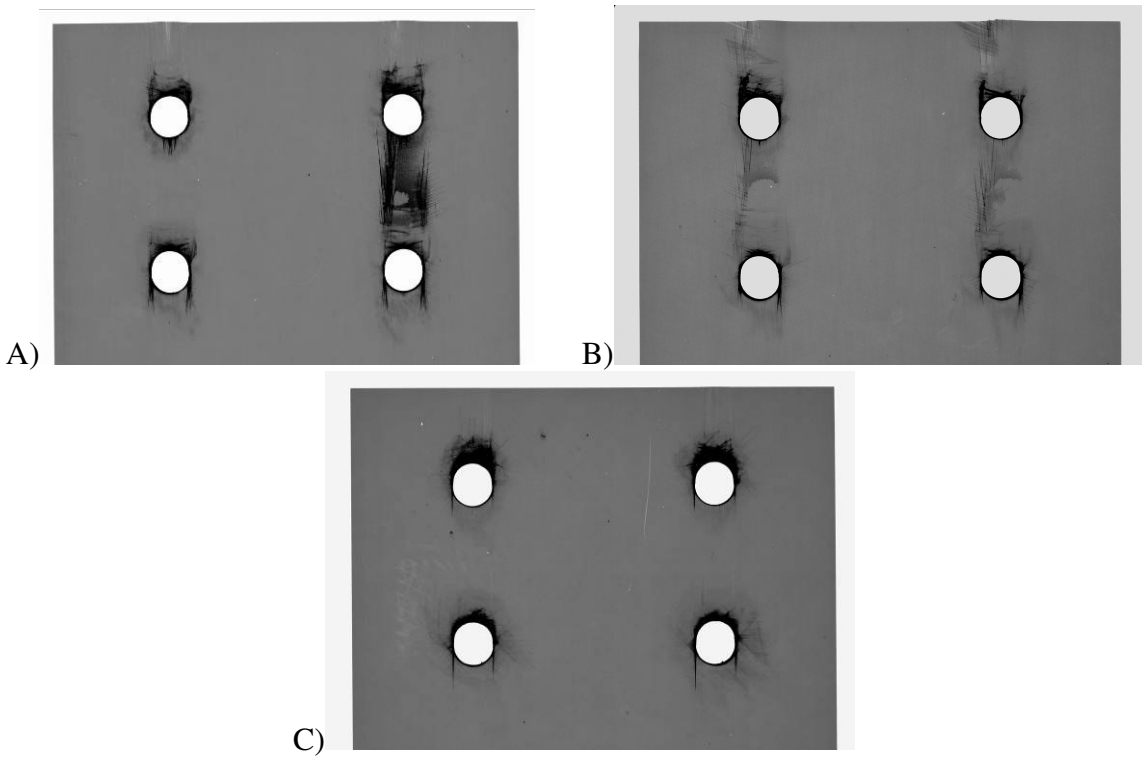

Figure 32: Radiographic images of the final damage state for tests at R = -0.1
A) 80/20 laminate B) 70/30 laminate C) 50/40/10 laminate

4.2. Cyclic Mostly Tension (R = -0.35)

The next set of fatigue tests were also dominated by tension loading. The loading ratio was set at R = -0.35, which indicates a load reversal of 35% in compression. These tests were performed according to the procedure outlined in 3.3.1. Figure 33 shows the sharp contrast between the damage in laminates with 0º fibers versus laminates with slightly off axis 5º fibers. It can be seen that damage in the 80/10/10 laminate initiates and propagates much more rapidly than the 80/20 laminate. The 80/10/10 laminate also exceeds the critical damage criterion before the 80/20 laminate. Because the amount of damage that occurs in the 80/10/10 laminate is so much greater than the rest of the

laminates tested at R = -0.35, it has been omitted from the rest of the cyclic tension comparison.

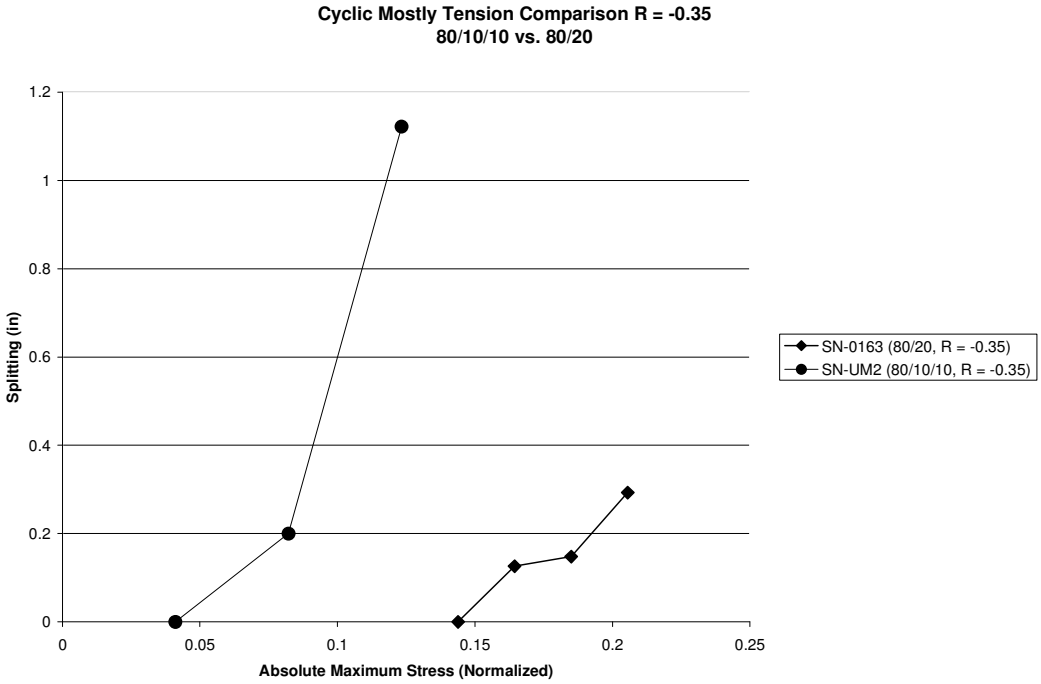

Figure 33: Cyclic mostly tension comparison of damage in 80/10/10 and 80/20 laminates at R = -0.35

Figure 34 shows the various levels of damage initiation as well as where the final damage criterion was met. The data has been normalized to the ultimate strength of the 50/40/10 laminate. In these tests, as in the tests at R = -0.1, the 50/40/10 laminate withstood the largest absolute stress. Although the 80/20 and 70/30 laminates withstood the same absolute stress, the 70/30 laminate exhibited superior damage resistance. However, it should be noted that the stress at which damage initiated was higher for the 80/20 laminate. Figure 35 shows the extent of the damage that occurred in each of the three laminates at R = -0.35. The 15% increase in reversal load caused all of these specimens to withstand a lower absolute stress when compared with R = -0.1. The

absolute stress is tensile in this comparison. The average reduction in strength was 20%. This decrease in final stress also caused a decrease in total damage seen in each specimen. In the non traditional laminates, the split crack tips diverge due to the off axis plies as the crack propagates. In all of the laminates it can be seen that the final damage state was crushing caused by bearing. A comprehensive set of damage X-rays can be seen in the Appendix.

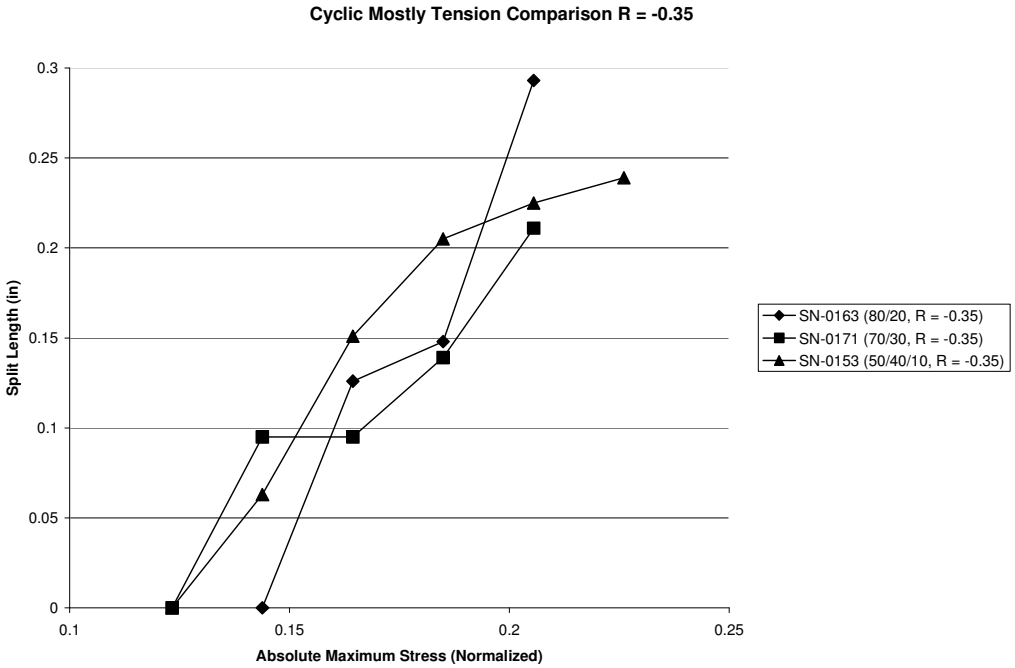

Figure 34: Cyclic Mostly Tension Data (Specimen, Layup, R ratio)

A) 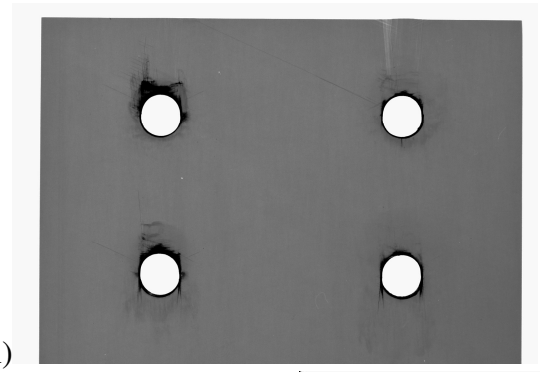 B) 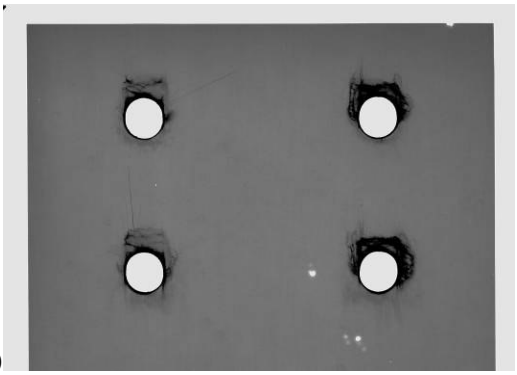

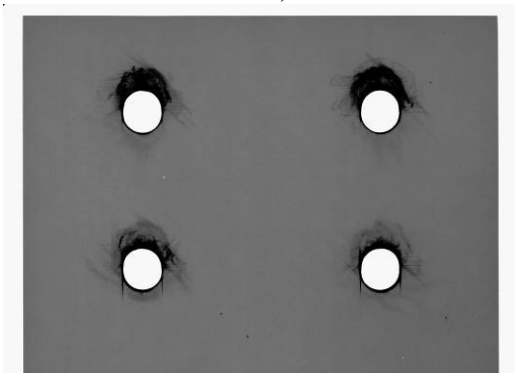

Figure 35: Radiographic images of the final damage state for tests at R = -0.35
A) 80/20 laminate B) 70/30 laminate C) 50/40/10 laminate

4.3. Cyclic Compression (R = -10)

This set of fatigue tests were dominated by compressive loading. The loading ratio was set at R = -10, which indicates a load reversal of 10% in tension. These tests were performed according to the procedure outlined in 3.3.2. Figure 36 shows the stress at which damage initiated and the stress at which the final damage criterion is reached. The data has been normalized to the ultimate strength of the 50/40/10 laminate. The damage in these tests did not follow the same trend as in the previous tests. Because of the compression dominated loading, the main mode of damage was crushing due to bearing. The progression of this damage was much more difficult to document. For this reason, only the initiation and final damage states are recorded. It is interesting to not that, unlike in the tensile dominated tests, damage initiated at a different stress in each laminate. Damage in the 80/10/10 laminate initiated at the lowest absolute stress. This laminate

also withstood the lowest absolute stress. Unlike in previous tests, the 70/30 laminate withstood the largest absolute stress. The 80/20 and 80/10/10 withstood the same maximum stress, however, damage in the 80/20 laminate initiated significantly later. This illustrates the damage suppression resulting from the presence of the slightly off axis 5º plies. Figure 37 shows the final damage state of each specimen in these tests. It can be seen that the damage in these specimens is dominated by crushing unlike in the previous tests. The 80/20 specimen shows a significant amount of damage between the holes due to the elongation of the upper holes. The larger percentage of 65º plies in the 70/30 laminate prevented the damage between the holes. However, the damage showed up in more significant crushing under all holes. The 50/40/10 laminate seems to have experienced the least amount of damage. A comprehensive set of damage X-rays can be seen in the Appendix.

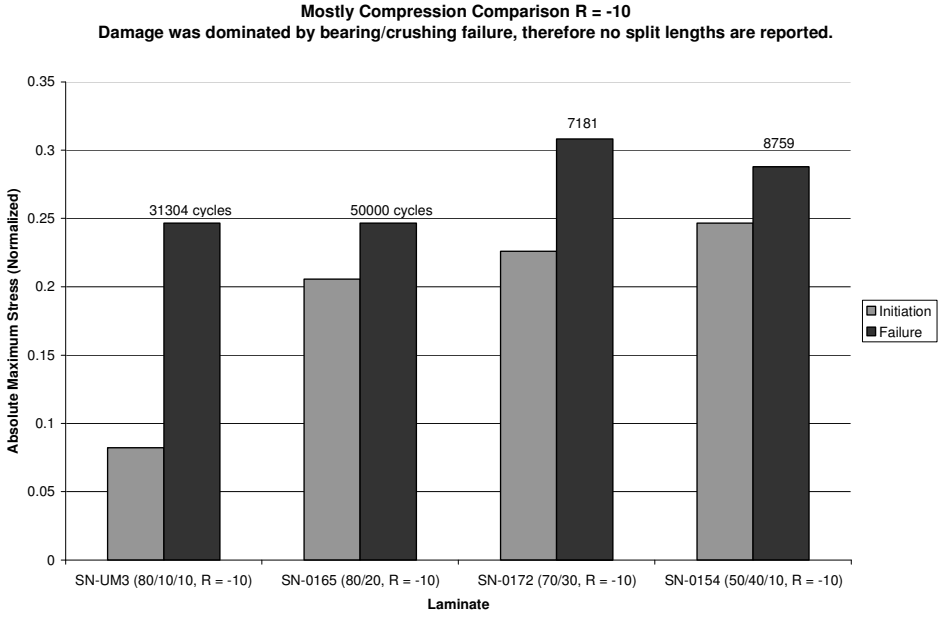

Figure 36: Mostly Compression Data (Specimen, Layup, R ratio)

A) 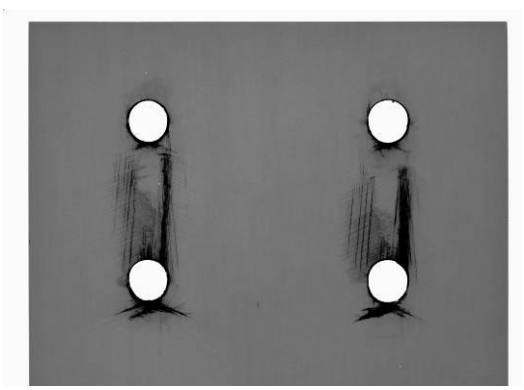 B) 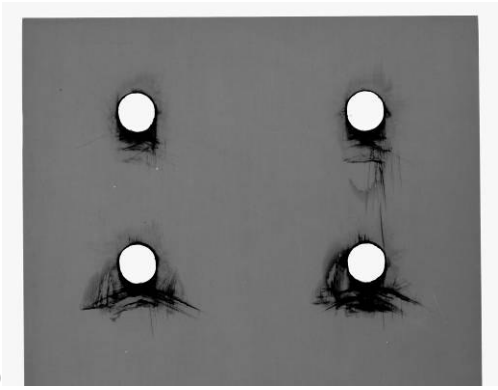

C) 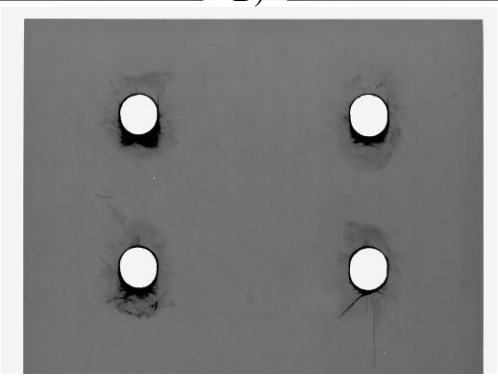

Figure 37: Radiographic images of the final damage state for tests at R = -10
A) 80/20 laminate B) 70/30 laminate C) 50/40/10 laminate

4.4. Residual and Undamaged Strengths

After each laminate reached the critical damage criterion in fatigue, they were then pulled to determine the residual strength left in the laminate. This was done for the specimens at R = -0.1 and R = -0.35. Undamaged specimens were also tested to determine ultimate strength.

4.4.1. Residual Strengths

Each specimen was pulled at a rate of 1.27 mm (0.05 inches) per minute. During the test, load and displacement data were collected. The maximum strength was determined from this data and recorded as the residual strength of the specimen. These

residual strengths are reported in Table 2. The stress values in the table are normalized to the maximum reported ultimate strength of the un-notched 80/20 laminate.

Table 2: Residual strengths for laminates at R = -0.1 and R = -0.35

Specimen	Layup	R	Normalized Critical Damage Stress	Normalized Residual Strength
SN-0160	80/10/10	-0.1	0.138	0.112
SN-0162	80/20	-0.1	0.150	0.158
SN-0170	70/30	-0.1	0.163	0.183
SN-0152	50/40/10	-0.1	0.175	0.221
SN-UM2	80/10/10	-0.35	0.075	0.104
SN-0163	80/20	-0.35	0.125	0.178
SN-0171	70/30	-0.35	0.125	0.207
SN-0153	50/40/10	-0.35	0.138	0.229

It can be seen that the residual strengths for the laminates tested at R = -0.35 are higher than those tested at R = -0.1, with the exception of the 80/10/10 laminate. From an inspection of the final damage states, shown in section 4.1 and 4.2, the cyclic mostly tension specimens seem to have less overall damage than the cyclic tension specimens when the critical damage state is reached. The specimens have comparable amounts of crushing or bearing damage, but the mostly tension specimens have less splitting. This decrease in splitting causes the cyclic mostly tension specimens to have higher strengths after reaching the critical damage state. The residual strength data is plotted in Figure 38. It can be seen that as the amount of cross-plies increase, the bearing resistance increases and thus the residual strength increases.

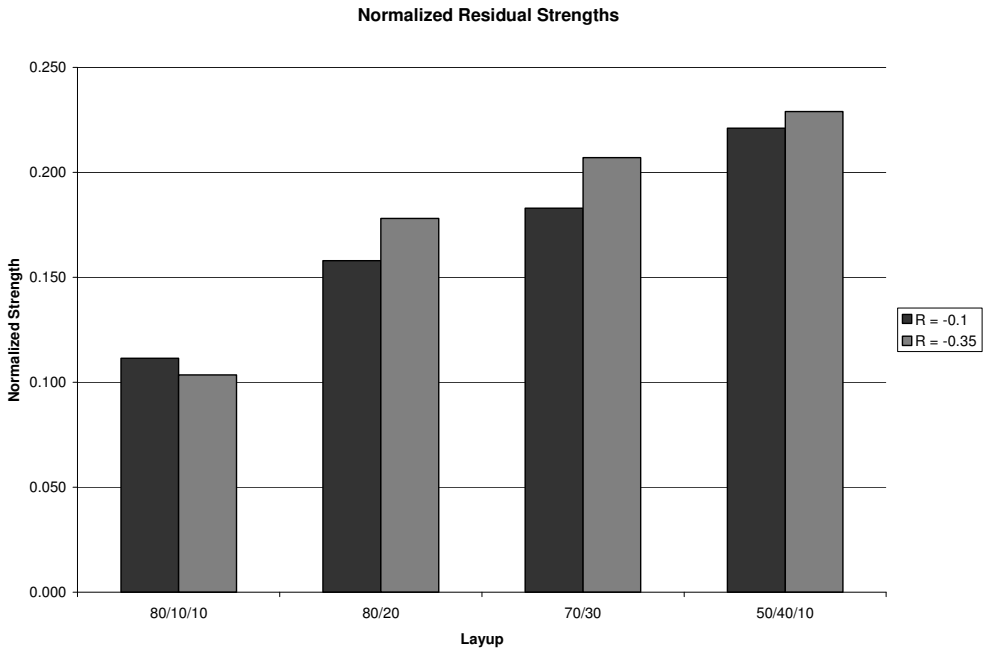

Figure 38: Normalized residual strength data

4.4.2. Undamaged Strengths

An undamaged specimen of each laminate was tested to determine the ultimate strength. These laminates were pulled at a rate of 0.05 inches per minute. During the test, load and displacement data were collected. The ultimate strength for each laminate was determined from this data. The ultimate strengths are reported in Table 3. The ultimate strength values are normalized to the reported maximum tensile strength of the un-notched 80/20 laminate. This table also contains the residual strengths reported as a percentage of the respective ultimate strength of each laminate.

Table 3: Undamaged strengths and normalized residual strengths

Layup	Normalized Stiffness	Normalized Ultimate Strength	Residual Strengths	
			R = -0.1	R = -0.35
80/10/10	1	0.14	78.80%	73.14%
80/20	0.97	0.20	78.02%	87.90%
70/30	0.86	0.21	86.52%	97.87%
50/40/10	0.75	0.25	89.29%	92.53%

It can be seen from Table 3 that as the amount of cross-plies increases strength increases. The effect of loading ratio or percent reversal can also be seen. With the exception of the 80/10/10 laminate, the laminates tested at R = -0.1 have less strength remaining after reaching the critical damage criteria than those tested at R = -0.35. This is attributed to greater impact as the hole elongates under a larger amount of load reversal. This causes the hole to elongate more rapidly without significant splitting thus limiting the strength reduction. The residual strength data from the table has been plotted in Figure 39. It can be seen that for the same critical damage state, all the laminates lose approximately 20% of their strength. The 70/30 laminate retains slightly more strength then the rest and the 80/10/10 laminate retains the least.

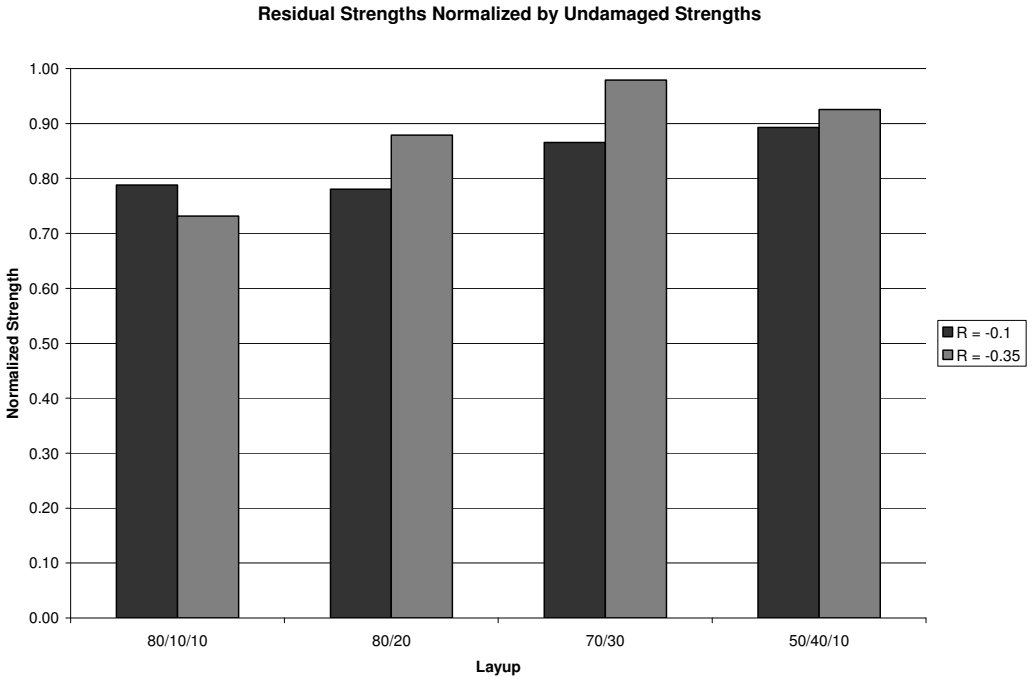

Figure 39: Residual strengths normalized by undamaged strengths

CHAPTER 5: FINITE ELEMENT ANALYSIS

This section will discuss the model that was developed to better understand the internal stresses that resulted in damage.

5.1. Development

The specimens were modeled in ABAQUS using the C3D8R element. This is an 8-node linear brick with reduced integration and hourglass control. The entire double shear configuration, seen in Figure 18, was modeled for accuracy; including the bolts, washers, collars, and titanium plates. All components were modeled as 3-D solids, and given isotropic properties with the exception of the composite coupon. The composite laminate properties were derived from the ply properties using classical lamination theory. Bearing constraints were assigned to the surfaces between the bolt and the titanium and composite plates. Similarly, friction constraints were assigned to all other surfaces in contact. Boundary conditions constrained translation and rotation in the grip area on the titanium plates. Appropriate loading was applied at the composite plate. A load level was chosen in the middle of the test spectrum. It was important to choose a load high enough to cause significant deformation and yield desirable stress data, and still be sufficiently below the stress where the maximum damage criterion was exceeded. The stress level chosen was 138 MPa (20 ksi). The mesh was refined until an acceptable level of accuracy was attained. Once the model was complete, sensitivity studies were performed to determine the effects of friction, as well as the effects of hole size variation within the model.

5.1.1. Mesh Refinement

The first step in assuring the accuracy of the finite element model was to insure the accuracy of the mesh. To do this the number of meshing elements was varied with increasing refinement until a suitable convergence was attained. The number of elements was a function of the global element size as well as the number of nodes through the thickness and around the holes. In order to accuracy and stability within an individual element it is best to maintain a near 1:1 ratio of the side dimensions. Therefore, as the number of through thickness elements was increased, the global element size had to be decreased accordingly. Figure 40 shows the progression of the mesh refinement process in graphical form.

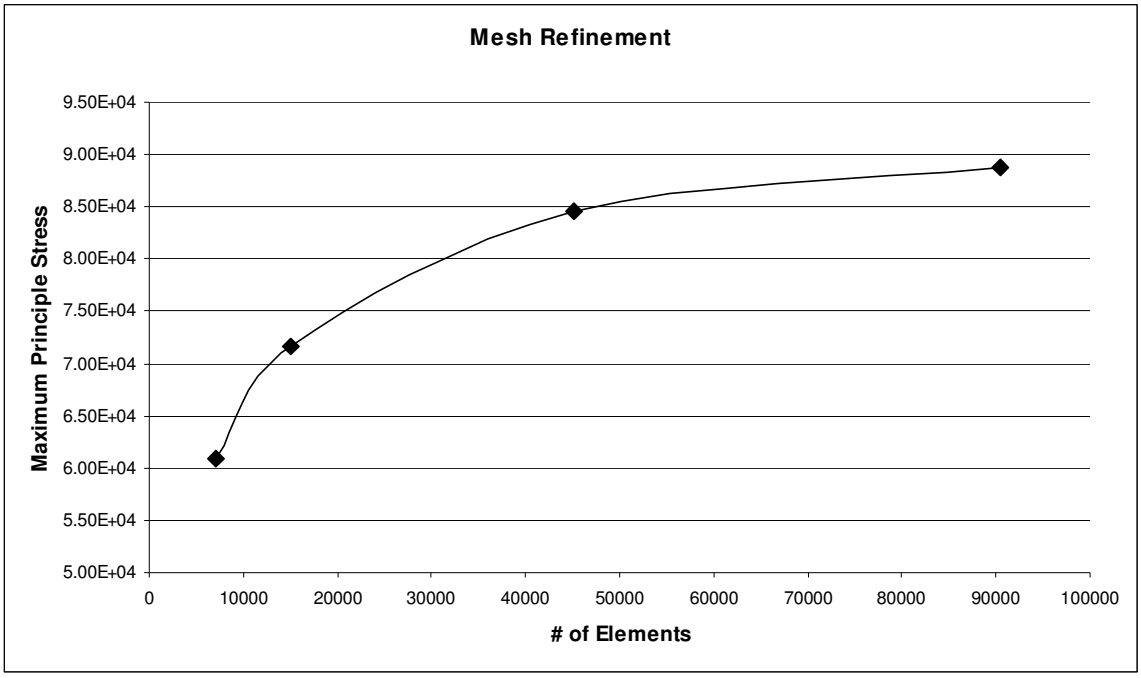

Figure 40: Mesh refinement vs. maximum principle stress

The figure shows that the number of elements was plotted against the maximum principle stress to show convergence. Maximum principle stress was chosen because it

occurs at the holes, which is the area of interest. The mesh refinement process was stopped at approximately 90,000 elements. This step showed a 4.9% change from the previous mesh and was deemed adequate for the current analysis.

5.1.2. Friction Sensitivity

It is clear that friction exists between all the surfaces in contact within the test setup. The main area of interest is the friction between the titanium plates and the composite coupon. However, it is not known how significantly this friction affects the bearing and bypass loading seen by the composite coupon. To further investigate this, the model was run specifying a frictionless environment at the contact surfaces and comparing the output to a model with a normal friction parameter with a friction coefficient of 0.1, as reported by Ludema in 1991. [37]

Several parameters were collected for this comparison, maximum Von Mises stress, maximum longitudinal stress, maximum transverse stress and maximum shear stress. When these stresses were compared between the two cases, it was found that the frictionless case showed a 5% greater transverse stress. The rest of the stresses were separated by a fraction of a percent. These values can be seen in Table 4.

Table 4: Friction sensitivity comparison

Friction Sensitivity			
Stress	Friction	No Friction	% Difference
Maximum Von Mises	9.24E+04	9.25E+04	0.10%
Maximum S_{11}	2.40E+04	2.41E+04	0.38%
Maximum S_{22}	8.30E+04	8.70E+04	4.89%
Maximum S_{12}	5.00E+04	5.00E+04	0.00%

Based on the information provide by the comparison between the models with and without friction, it was decided that the friction has a negligible effect on the bearing and

bypass stresses within the model. However, to maintain an accurate representation of the physical specimens, the model will use friction.

5.1.3. Hole Diameter Variation

The specifications to which the composite coupons were fabricated specifies a hole diameter from 6.35 mm (0.250 in) to 6.4262 mm (0.253 in). Even with this minimal change in hole diameter, the amount of contact between the bolt and the surrounding hole is altered. This variation in clearance can effect the stress field around the hole as well as the stiffness of the overall joint [21]. Because of this the holes were modeled at 6.35 mm (0.250 in) as well as the 6.4262 mm (0.253 in). Several stress values from both models were then compared to determine the significance in the current analysis. Table 5 shows the stress values produced by each size hole.

Table 5: Sensitivity of hole size comparison

Hole Size Sensitivity			
Stress	Small Holes 0.25Ø	Large Holes 0.253Ø	% Difference
Maximum Von Mises	9.72E+04	9.24E+04	-4.96%
Maximum S_{11}	2.43E+04	2.40E+04	-1.23%
Maximum S_{22}	7.35E+04	8.30E+04	12.93%
Maximum S_{12}	5.18E+04	5.00E+04	-3.44%

It can be seen in Table 5 that the transverse stress exhibited an almost 13% increase with only a 0.0762 mm (0.003 in) increase in diameter. After measuring the holes, in the specimens tested, the trend seems to be toward the larger diameter holes. Therefore the model will have the worst case scenario 6.4262 mm (0.253 in) diameter hole.

5.2. Results

Once the model was constructed, it was run using the individual properties of each laminate in tension as well as compression. The results were then analyzed to determine the bearing and bypass loading within the specimen.

5.2.1. Bearing and Bypass Loading

The model was created to help understand the stress fields within each specimen. The main points of interest were the bearing and bypass stresses. The purpose was to determine how much of the far field stress was transferred by bearing through the first set of holes, and how much bypassed the first set and was transferred by bearing through the second set of holes. This was accomplished by comparing the far field stress to the stress between the hole sets. This comparison was performed for each of the four laminates.

The far field stress was taken from a section 7.62 cm (3.0 in) from the loaded end of the composite specimen. This far field stress was then compared with the stress from a section 16.51 cm (6.5 in) from the loaded end. This section was directly between the two hole sets. The stresses used in the comparison were calculated averages from each of the two sections. The section placement can be seen in Figure 41. The data collected from these two cross sections in each laminate is reported for tension and compression.

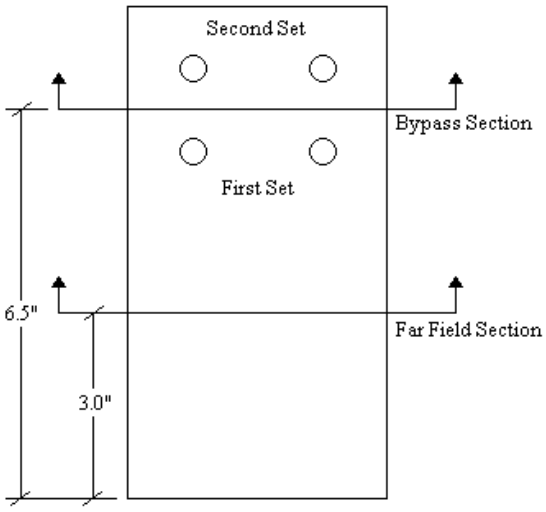

Figure 41: Far Field and Bypass Sections

Table 6: Bypass stress comparison in tension

Tension Bypass Stress Comparison (MPa/psi)			
Laminate	Far Field Stress	Bypass Stress	Percent Bypass
80/10/10	138 (20000)	65.16 (9450)	47.25%
80/20	138 (20000)	67.22 (9750)	48.75%
70/30	138 (20000)	74.12 (10750)	53.75%
50/40/10	138 (20000)	86.18 (12500)	62.50%

The data in Table 6 shows that the amount of stress that bypasses the first set of holes is related to the amount of off-axis plies contained in the laminate. As the amount of off-axis fibers increase the amount of bypass stress increases.

The amount of bearing stress in each set of holes was also collected from the model for each laminate. The maximum bearing stress was recorded for each hole set. The bearing stress in the second set of holes was then reported as a percent remaining from the first set of holes. The bearing stress data is reported in Table 7. When this data is compared to the bypass data, it can be noted that the two follow similar trends. There is a variation of a few percentage points between bearing and bypass. However, the bearing data seems to vary with the amount of off-axis plies contained in the laminate.

This says that the bearing and the bypass stress are closely related to one another for this hole configuration.

Table 7: Bearing stress comparison in tension

Tension Bearing Stress Comparison (MPa/psi)			
Laminate	First Hole Set	Second Hole Set	Percent Remaining
80/10/10	800 (116000)	390 (56500)	48.71%
80/20	758 (110000)	393 (57000)	51.82%
70/30	696 (101000)	403 (58500)	57.92%
50/40/10	696 (101000)	465 (67500)	66.83%

The same information was also collected in compression. The amount of bypass stress for each laminate can be seen in Table 8 and the bearing stress comparison is shown in Table 9.

Table 8: Bypass stress comparison in compression

Compression Bypass Stress Comparison (MPa/psi)			
Laminate	Far Field Stress	Bypass Stress	Percent Bypass
80/10/10	138 (20000)	60 (8675)	43.38%
80/20	138 (20000)	63 (9200)	46.00%
70/30	138 (20000)	69 (10025)	50.13%
50/40/10	138 (20000)	80 (11550)	57.75%

Table 9: Bearing stress comparison in compression

Compression Bearing Stress Comparison (MPa/psi)			
Laminate	First Hole Set	Second Hole Set	Percent Remaining
80/10/10	717 (104000)	396 (57500)	55.29%
80/20	717 (104000)	407 (59000)	56.73%
70/30	700 (101500)	427 (62000)	61.08%
50/40/10	765 (111000)	496 (72000)	64.86%

The data has been plotted to obtain a better comparison between bypass and bearing stresses as well as tensile and compressive loading. Figure 42 shows the trends within the bearing and bypass stresses under tensile loading. This can be compared with the trends within the bearing and bypass stresses under compressive loading, shown in Figure 43.

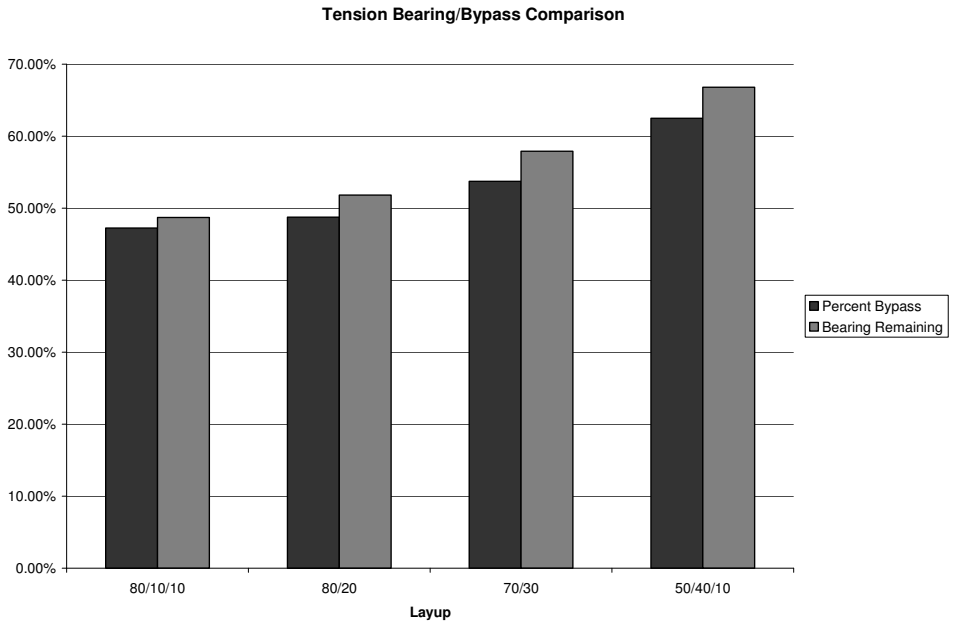

Figure 42: Comparison of bearing and bypass stresses under tension

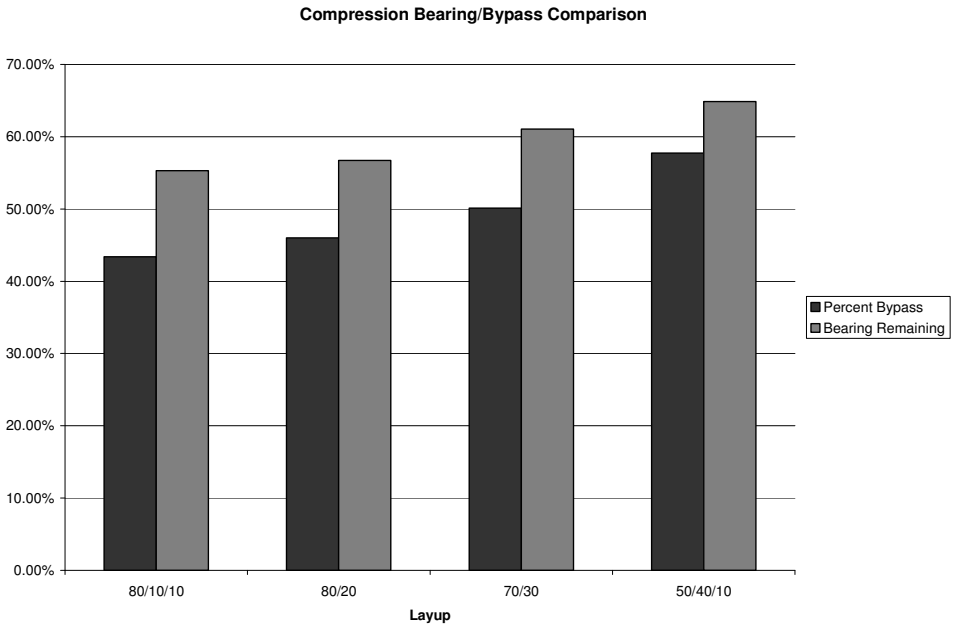

Figure 43: Comparison of bearing and bypass stresses under compression

It can be seen from the comparisons that as stiffness decreases, bearing and bypass stresses increase. This is true for both the tensile and compressive loading. In

both cases the percentage bearing stress, seen by the second set of holes, is greater than the percent of bypass stress. However, this difference is greater in compression where failure is bearing dominated. This is caused by the significant increase in the edge distance to diameter ratio from tension to compression. This increase in the e/d ratio causes more of the load to be transferred through bearing and thus decreases the bypass stress in compression.

It should also be noted that the stiffness of the 80/20 laminate is within a 5 percent of the titanium it is bolted to in the joint. In the tensile case, the bypass load is nearly 50 percent. This shows, for this configuration, that if two identical materials are joined, the bypass should be right at 50 percent. As the composite decreases in stiffness, with respect to the titanium, the bypass loading increases. This causes the stresses in the first set of holes to decrease which increase the ultimate joint strength.

CHAPTER 6: FINITE ELEMENT VERSUS EXPERIMENTAL COMPARISON

This section will discuss the correlations between the results from the finite element model and the experimental results.

6.1. Damage Development

In order to validate the finite element model as well as gain a better understanding of the experimental data, the two have been inspected for similarities. It is believed that the stress concentrations seen in the finite element model should correspond to the locations of damage in the experimental data. To further investigate this, the stress fields from ABAQUS were compared directly to X-ray images from the fatigue testing.

6.1.1. Maximum Stresses

It is obvious that the highest stresses in the laminate occur at the holes. This can be seen clearly in the model as well as in experimental damage locations. To better understand the stress filed around the hole, the greatest value for each of the principle stresses was measured at the hole. It should be noted, from the previous discussion of bearing and bypass in Section 5.2.1., that the highest stresses occur in the first set of holes. This data is presented for tension in Table 10 and for compression in Table 11. The locations of these maximum stresses can be seen in Figure 44 and Figure 45.

Table 10: Maximum principle stresses in tension for each layup

Maximum Stresses in Tension					
Layup	S_{xx}	S_{yy}	S_{xy}	Mises	Principle
80/10/10	-40730	84000	60690	119300	86270
80/20	-40170	86450	57000	114100	88640
70/30	-35550	89580	51000	104100	91620
50/40/10	-45000	102100	44000	102700	103700

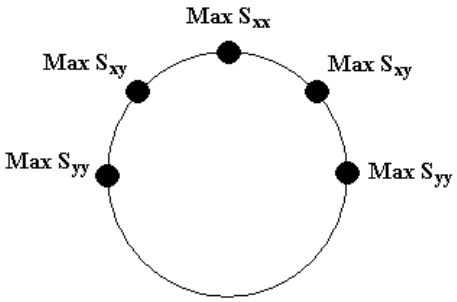

Figure 44: Maximum stress locations for tensile loading

Table 11: Maximum Principle stresses in compression for each layup

Maximum Stresses in Compression					
Layup	S_{xx}	S_{yy}	S_{xy}	Mises	Principle
80/10/10	33780	-78200	47600	104000	37380
80/20	32720	-79680	44280	104500	35950
70/30	29190	-80830	38640	101800	32230
50/40/10	40000	-83700	31000	111200	42690

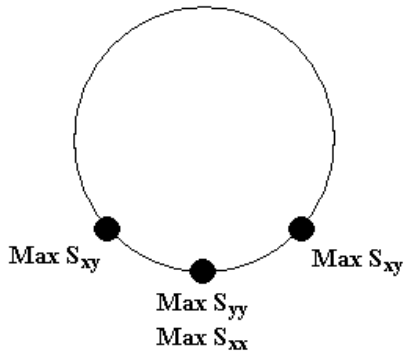

Figure 45: Maximum stress locations for compressive loading

It can be seen that the largest stress that occurs under tensile loading is in the transverse direction. This is also true under compression. However, the largest difference is the location of these maximum stresses. It can be seen in Figure 44 that each of the maximum stresses, due to tension, occur in a unique location. However, Figure 45 shows and the longitudinal and transverse stresses have compounding effects. Based on these findings, the transverse stress will be investigated for tensile loading. Similarly, longitudinal and transverse will be investigated for compressive loading.

6.1.2. Experimental Comparison in Tension

The transverse stress field was compared with the X-ray image of damage at the equivalent stress level in the 80/20 laminate. These images can be seen in Figure 46. Unfortunately, not much can be seen at this level of magnification. Therefore, a close-up was taken at the bottom left hole. These images can be seen in Figure 47.

A) 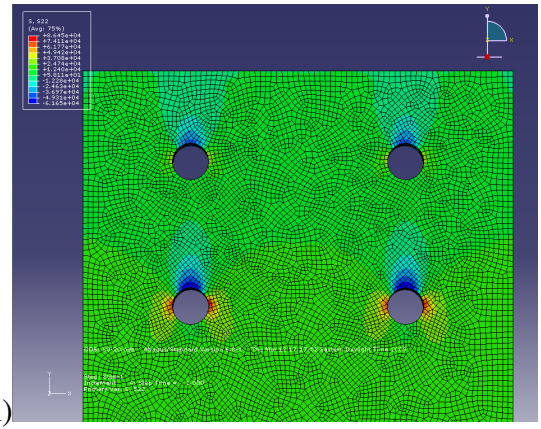 B) 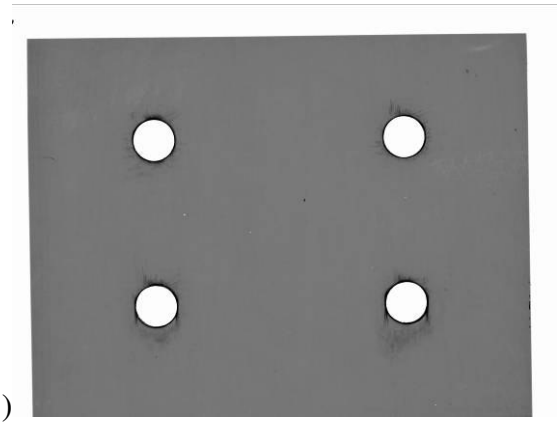

Figure 46: Model vs. Experimental comparison for 80/20 laminate under tension
A) ABAQUS transverse stress field B) In-situ X-ray image

A) 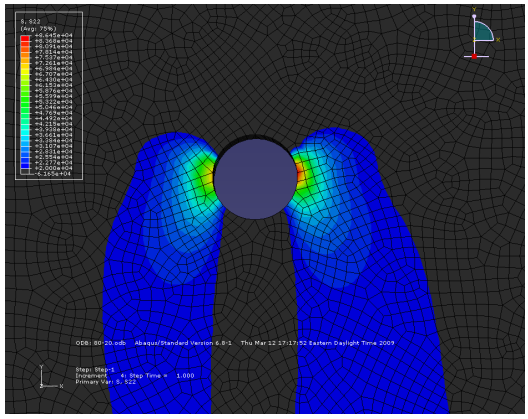 B) 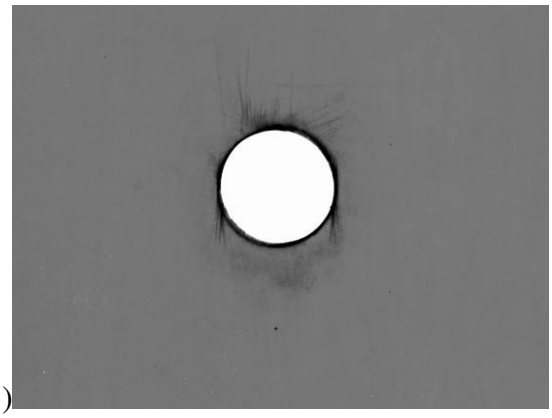

Figure 47: Model vs. Experimental comparison of single hole for 80/20 laminate under tension
A) ABAQUS transverse stress field B) In-situ X-ray image

The scale was modified in the ABAQUS stress field to show a clearer depiction of the transverse stress. It can be seen that the elevated transverse stress coincide with the location of the longitudinal splitting in the In-situ X-ray image. Thus, in tension

dominated cycling, the transverse stress concentration leads to initial damage occurring as splitting downward from the first set of holes.

Upon further inspection of the 80/10/10 laminate, it is apparent that more than the transverse stresses caused damage. The splitting in this specimen occurs above and below the holes. It was found that the shear stress field aligned with the damage state in the 80/10/10 laminate. Images of the transverse and shear stress fields as well as an In-situ X-ray image of damage can be seen in Figure 48. It can be seen that the stress fields are almost identical to that of the 80/20 laminate. However, the damage state is quite different at the same load level. This illustrates how the ±5º off axis plies help suppress damage. The 0º plies have only the matrix to resist shear, where as the 5º plies overlap and create a resistance to the shear stress. The longitudinal splitting is also dampened by the ±5º plies. Because the cracks must cross other plies, they require more energy to propagate.

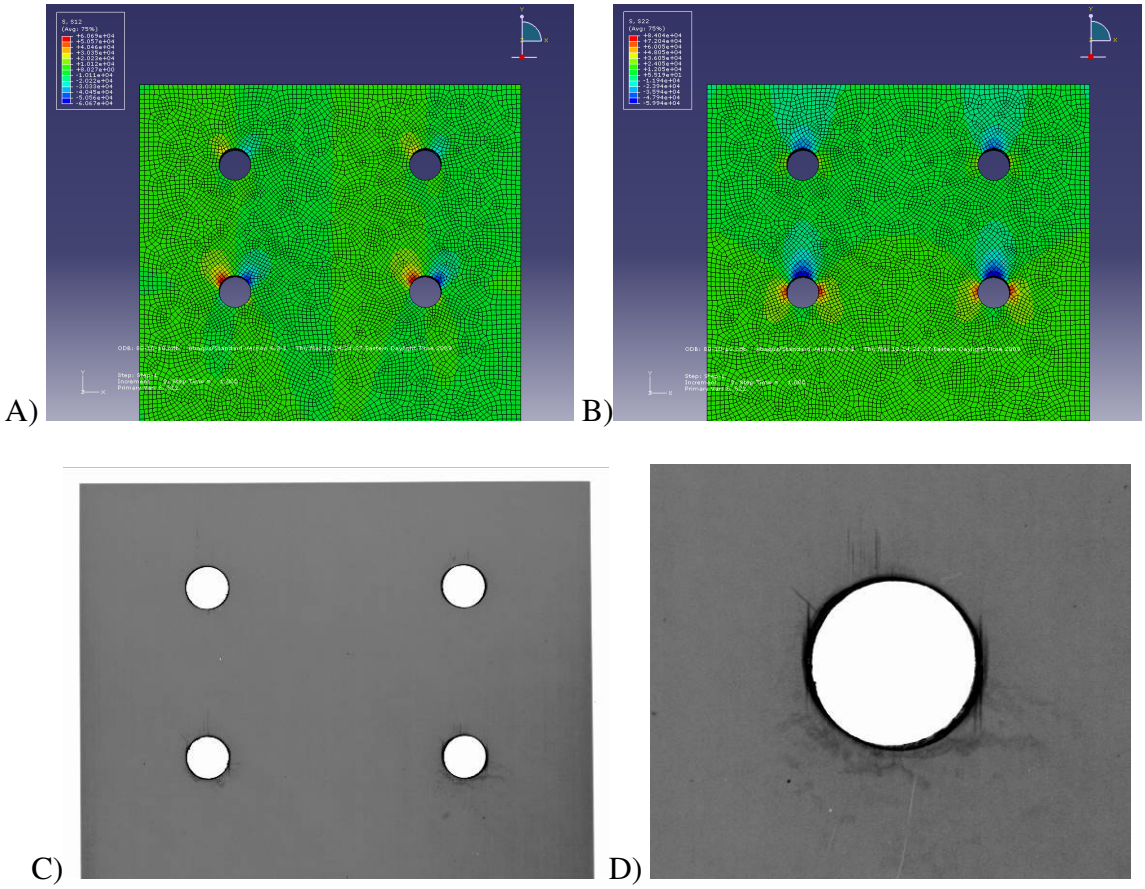

Figure 48: Model vs. Experimental comparison of 80/10/10 laminate under tension
A) ABAQUS shear stress field B) ABAQUS transverse stress field
C) In-situ X-ray image D) Hole Close-up

6.1.2. Experimental Comparison in Compression

When the loading becomes mostly tension the geometry of the joint is reversed with respect to the loading. This means the edge distance to diameter ratio increases from $e/d = 2.5$ in tension to $e/d = 24$ in compression. This increase in e/d causes the failure mode to change from shear dominated to bearing dominated. Because of the change in failure mode, the bearing stresses are the most applicable to damage. Shown in Figure 49 are the ABAQUS bearing stress filed and the In-situ X-ray image of damage in the 80/20 laminate.

A) 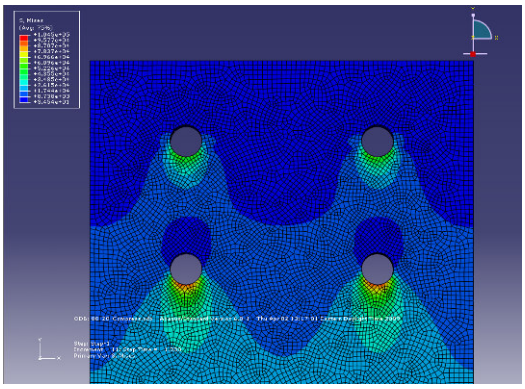 B) 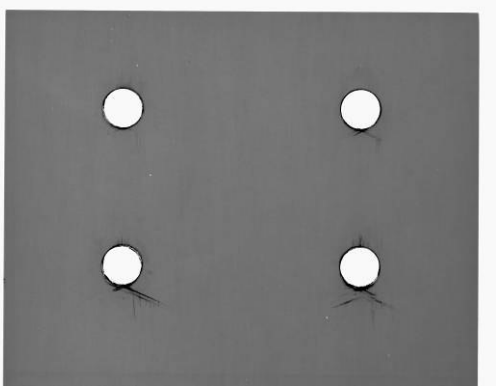

Figure 49: Model vs. Experimental comparison of 80/20 laminate under compression A) ABAQUS bearing stress field B) In-situ X-ray image

The figure shows that the damage state corresponds to the stress field. However, as the bearing failure is initiated, it causes matrix cracking to occur in the 65º degree plies. This splitting is along the fiber direction and appears below the bearing damage. This can was attributed to the compounding effects of the longitudinal and transverse stresses at the bottom of the holes.

CHAPTER 7: SUMMARY AND CONCLUSIONS

This section will summarize the test variables and conclusions will be drawn from the testing.

7.1. Summary of Test Variables

The following is a discussion of the effects of the variables considered in the testing; specifically the type of layup, stress ratio and stress levels.

7.1.1. Type of Layup

There was a distinct difference that could be seen between the performance of the different layups tested. This difference was even seen between the two non-traditional layups. At each stress ratio tested the 70/30 laminate outperformed the 80/20 laminate. The split lengths recorded for the 70/30 were shorter in all cases and the maximum absolute stress seen was higher. This is a clear effect of the trade off between stiffness and toughness. The 80/20 laminate is approximately 13% stiffer than the 70/30, which in turn makes the 70/30 laminate tougher and more damage resistant. This same trend was seen in the residual strengths as well. The ultimate strength of the 70/30 laminate is higher than that of the 80/20 laminate. At each of the stress ratios tested, the residual strengths of the 70/30 laminates reached a larger percentage of their ultimate load, than the 80/20 laminate.

When the non-traditional laminates are compared to the more traditional laminates, the distinction becomes even clearer. The comparison between the 80/10/10 laminate and the 80/20 laminate shows that the non-traditional laminate is far superior to the traditional. The damage sustained by the 80/10/10 laminate was, on average, 3 times

greater than that experienced by the 80/20 laminate. The maximum absolute stress seen by the 80/20 was greater at each stress ratio tested. The 0º fibers of the traditional 80/10/10 laminate only make it 3% stiffer than the 80/20 laminate. This superiority is clearly a function of the ±5º plies. These plies obviously create an increase in toughness, allowing the 80/20 to exceed the 80/10/10 in absolute maximum stress at all stress ratios while sustaining less overall damage.

This distinction between traditional and non-traditional is not quite as clear when the comparison is with the 50/40/10 laminate. In each of the tension dominated stress ratios, the 50/40/10 laminate achieved higher maximum stresses than each of the non-traditional laminates. However, the 70/30 laminate sustained less overall damage than the 50/40/10 laminate. In the compression dominated stress ratio, the 70/30 was the laminate that withstood the largest absolute stress, but the 50/40/10 laminate appeared to sustain the least overall damage. It is important to remember that the 80/20 and 70/30 laminates are 30% and 15% stiffer than the 50/40/10 laminate, respectively. In structures design, this increase in stiffness without a significant increase in damage, makes the non-traditional laminates clearly superior.

7.1.2. Stress Ratios and Stress Levels

There was also a distinct difference observed in laminate behavior with respect to stress ratios. The three stress ratios tested were R = -0.1, R = -0.35 and R = -10. The variation in stress level not only affected the final damage state, but also the maximum absolute stress level experienced in the laminates.

When the two tension dominated stress ratios were compared, it was found that an increase in load reversal lowered the stress levels achieved by the laminates. At the stress

ration R = -0.1, which is 10% load reversal, all laminates experienced longer split lengths at higher maximum absolute stresses before reaching the critical damage condition. This is attributed to the larger reversal load causing more impact at hole and thus elongating the hole more rapidly. This more rapid elongation of the hole decreased the overall damage in the laminates. It is thought that this decrease in overall damage is what caused the residual strengths to be higher at the stress ration of R = -0.35 than R = -0.1. The compression dominated stress ratio, R = -10, caused a slight increase in absolute maximum stress for some laminates with no change in others.

7.2. Conclusions

The fatigue performance of two non-traditional carbon fiber/epoxy, composite laminates, $[\pm5/65/\pm52/-65/\pm5]_s$ and $[\pm5/65/\pm5_2/-65/5/65]_s$, was compared with two more traditional laminates, $[45/90/-45/0_2/45/0_2/-45/0]_s$ and $[0_4/45/0_3/90/0]_s$. The internal damage state of each laminate was assessed through the use of in-situ radiography at predetermined intervals. The stress ratio and stress levels were varied to gain insight into damage initiation and critical damage states. The critical damage state was defined as a 10% elongation of the initial hole diameter.

The non-traditional laminates were slightly out performed, in terms of absolute maximum stress, in the tension dominated stress ratios by the 50/40/10 laminate. However, the 70/30 laminate showed the least overall damage, in each of the tension dominated stress ratios, when the critical damage criterion was reached. The 70/30 laminate also achieved the largest absolute stress in the compression dominated tests. When all of this is considered with the increased stiffness exhibited by the non-traditional laminates, the 70/30 appears to have superior fatigue performance. The judgment

between the 80/20 and the 50/40/10 would need to be case based. This is due to the 30% difference in stiffness between the laminates. However, the 80/20 laminate shows impressive damage resistance accompanied by the increased stiffness.

7.2. Recommendations for Future Work

This research has opened the door to understanding the layup dependency of damage initiation and progression in mechanically fastened composite joints. However, much more work is needed in this area.

To gain a better understanding of how layup affects damage, it would be necessary to test a broader range of layups. This would include non-traditional laminates that more closely resemble traditional laminates and have a larger variation in percentage of longitudinal plies.

In this research, a small sample of stress ratios was investigated. Testing a larger range of stress ratios would allow a better understanding of how different layups are affected by load reversal.

This increase in experimental data should be accompanied by a more detailed numerical model. The analysis in this research was created to better understand the stress fields and their effect on damage. However, a more detailed model could be created to more accurately depict the different layups and help predict damage within the joints. A modeling technique exists to create a mesh around a hole that is oriented to fiber direction. This meshing technique could be used to understand damage in each individual ply. It could even predict damage initiation by ply.

In addition to the items previously mentioned, all of the experiments in this research were performed in lab air. This is not an accurate depiction of the application

environment in which composites are utilized. To gain a full understanding of how joints perform in actual structures, many more variable would need to be considered. Aircraft structures experience temperature ranging from -51ºC (-60ºF) to 54ºC (130ºF) as well as locations ranging from dry desert to humid costal environments. Environmental aging is necessary to depict actual, in-service behavior. To accurately simulate these conditions, the composite materials would need to experience humidity and UV exposure. Tests would also need to be performed at elevated and reduced temperatures.

Once all of these factors have been considered, a true understanding of fatigue damage in composite joints can begin to form.

APPENDIX

IN-SITU X-RAY IMAGES

This appendix contains the full scope of X-ray images for the specimens tested.

Images of Laminates Tested at R = -0.1

80/10/10 Laminate

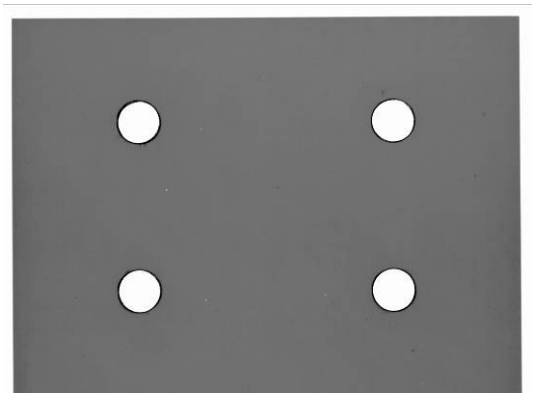

34.5 MPa (5 ksi) 50000 cycles

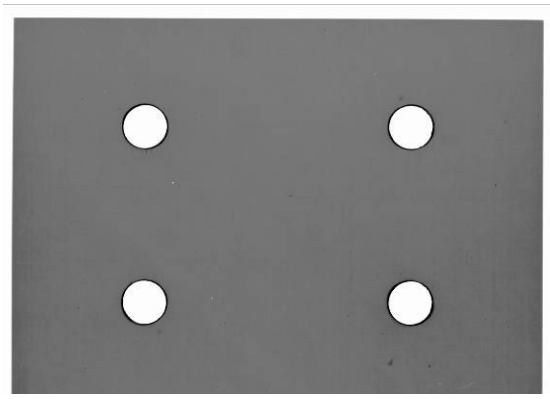

69 MPa (10 ksi) 50000 cycles

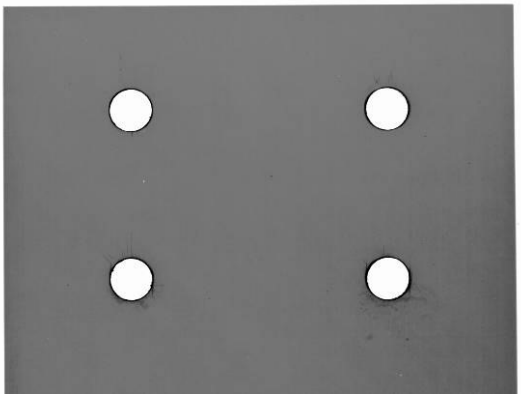

103 MPa (15 ksi) 50000 cycles

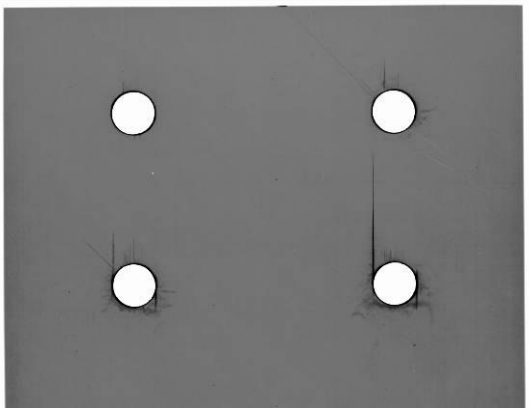

121 MPa (17.5 ksi) 50000 cycles

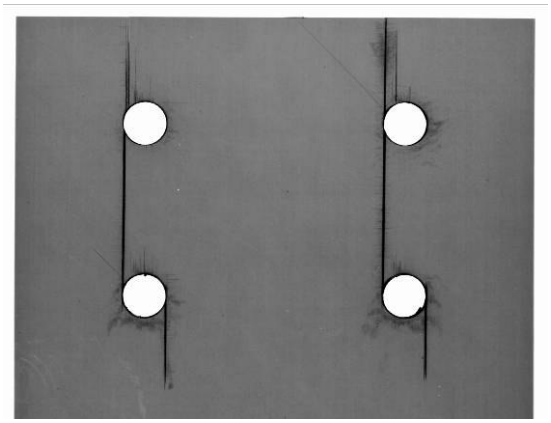

138 MPa (20 ksi) 50000 cycles

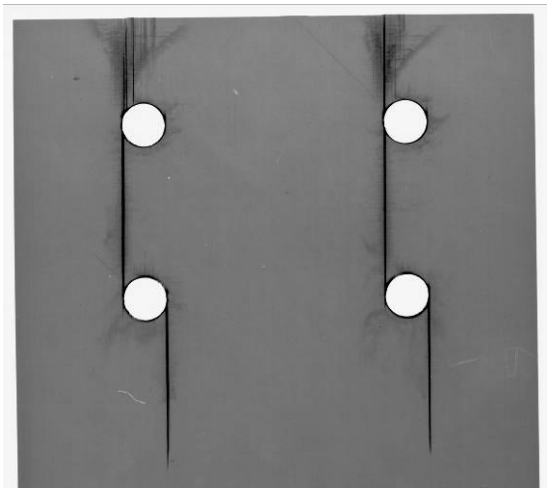

155 MPa (22.5 ksi) 50000 cycles

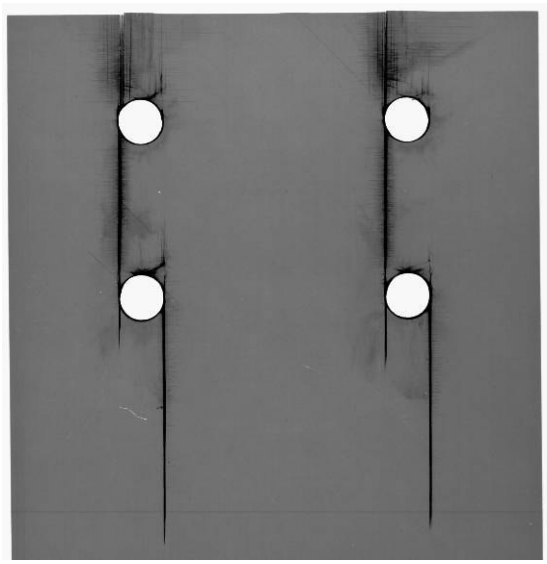

172 MPa (25 ksi) 50000 cycles

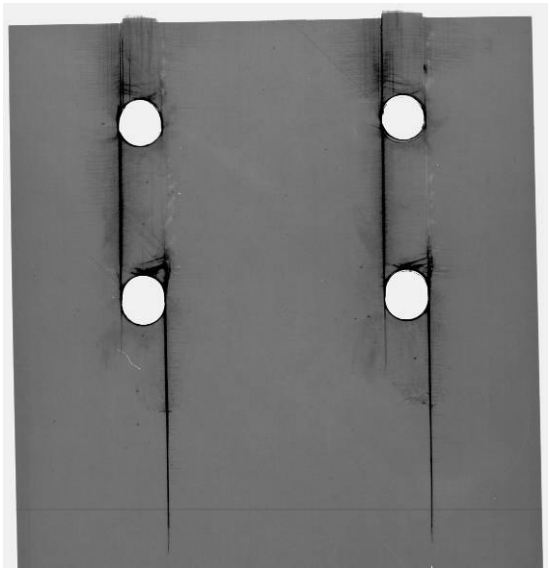

190 MPa (27.5 ksi) 33 cycles
Critical Damage Achieved

80/20 Laminate

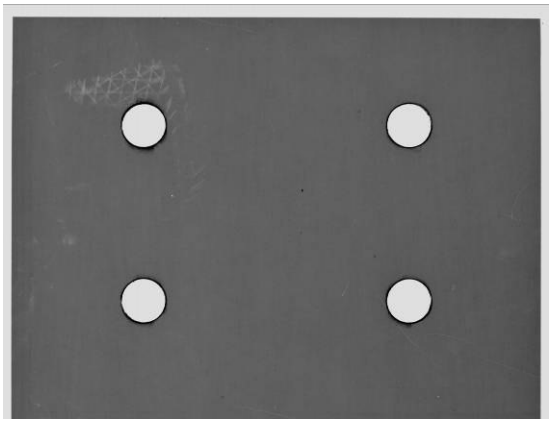

34.5 MPa (5 ksi) 50000 cycles

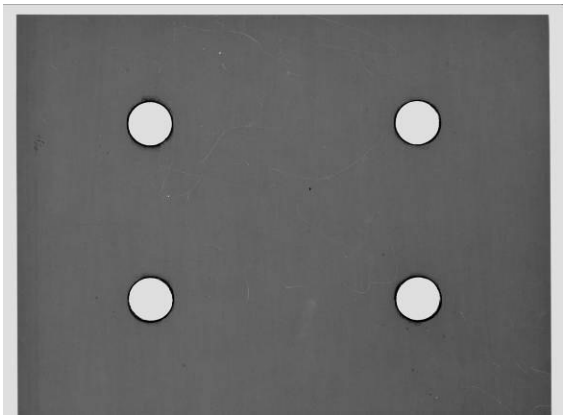

69 MPa (10 ksi) 50000 cycles

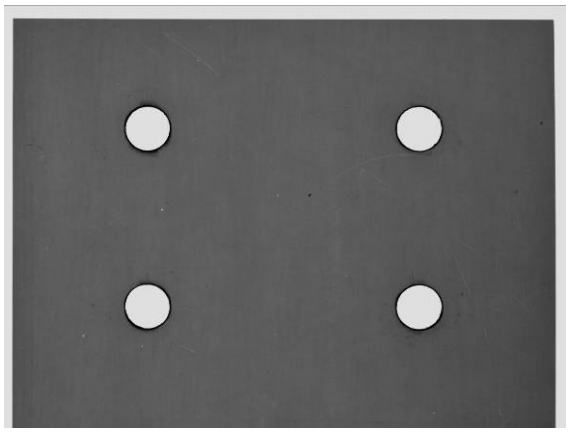

103 MPa (15 ksi) 50000 cycles

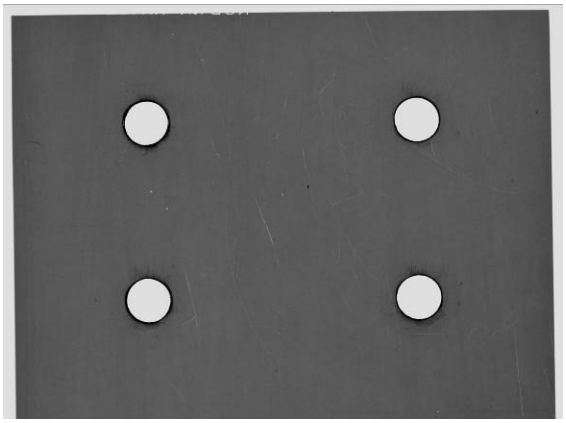

121 MPa (17.5 ksi) 50000 cycles

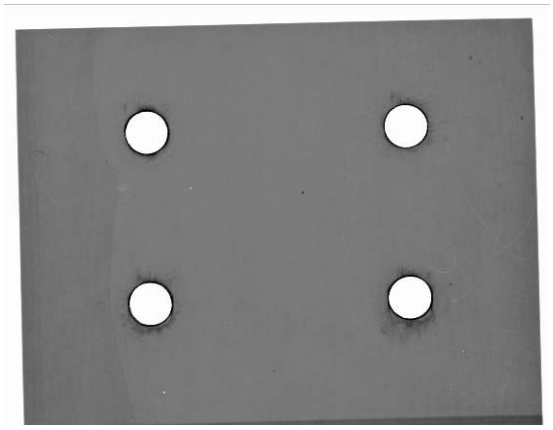

138 MPa (20 ksi) 50000 cycles

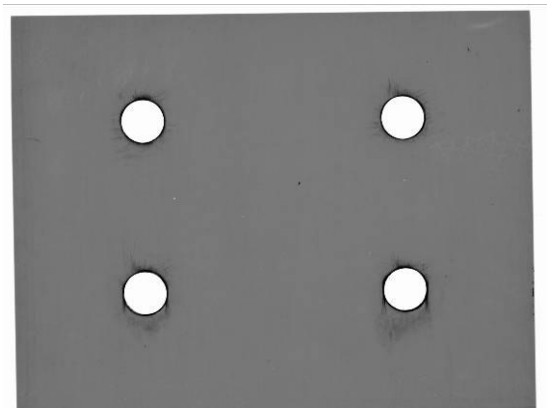

155 MPa (22.5 ksi) 50000 cycles

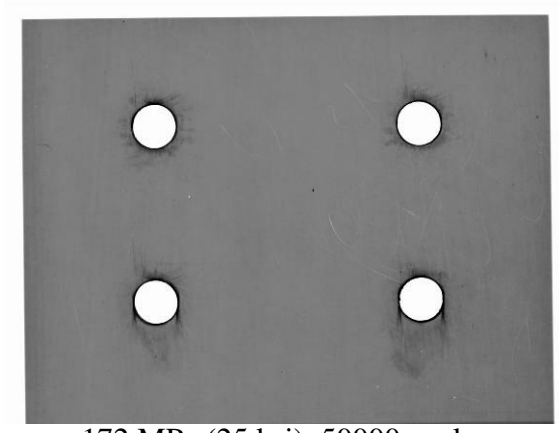

172 MPa (25 ksi) 50000 cycles

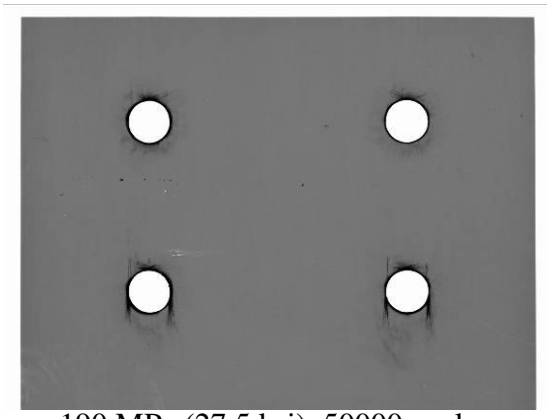

190 MPa (27.5 ksi) 50000 cycles

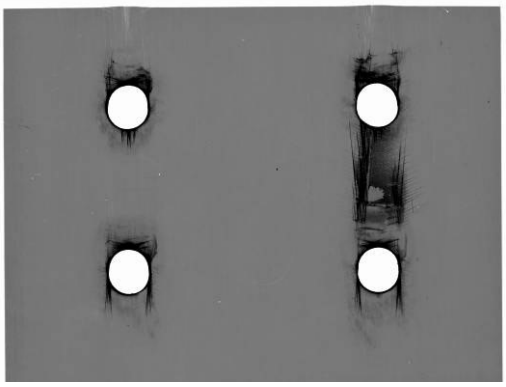

207 MPa (30 ksi) 7596 cycles
Critical Damage Achieved

70/30 Laminate

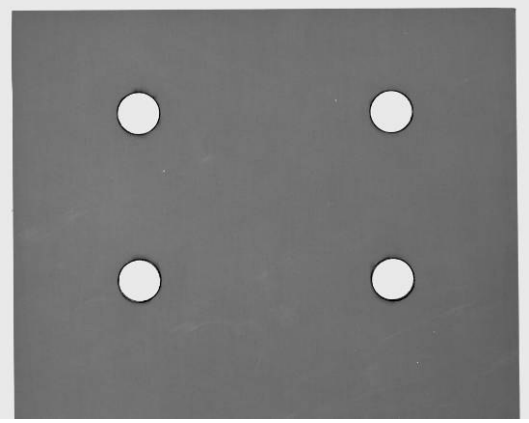

34.5 MPa (5 ksi) 50000 cycles

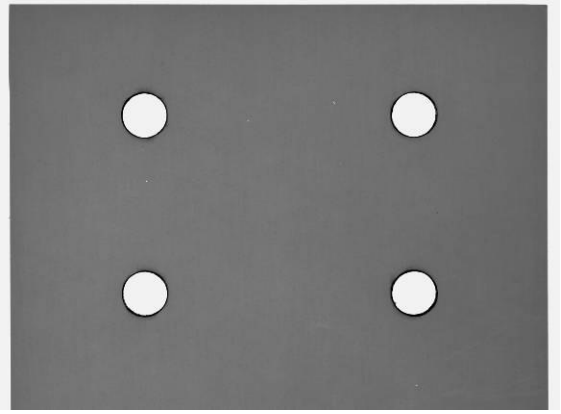

69 MPa (10 ksi) 50000 cycles

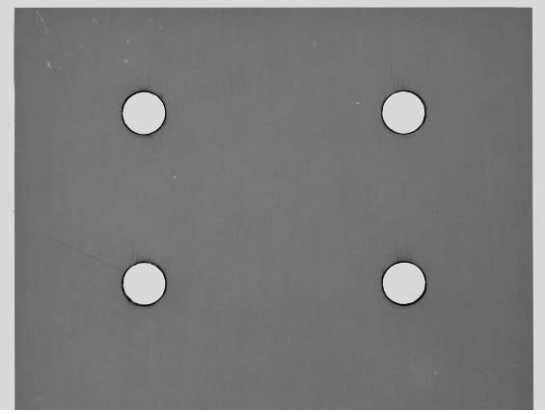

103 MPa (15 ksi) 50000 cycles

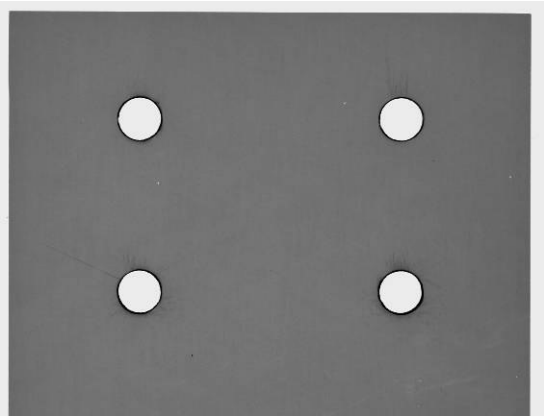

121 MPa (17.5 ksi) 50000 cycles

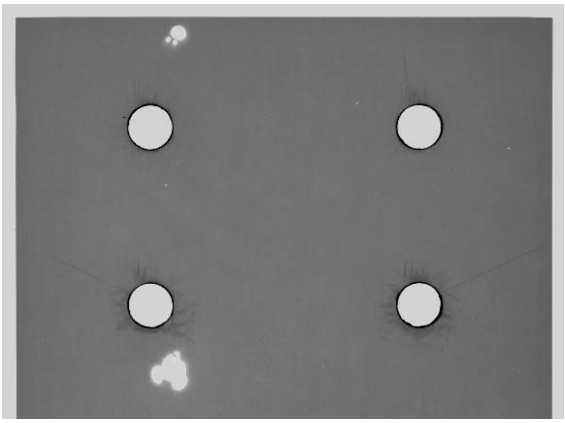

138 MPa (20 ksi) 50000 cycles

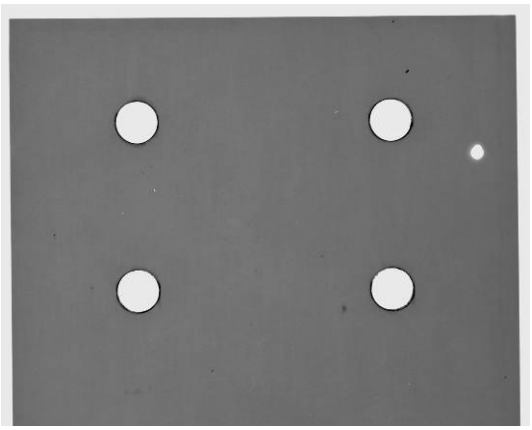

155 MPa (22.5 ksi) 50000 cycles

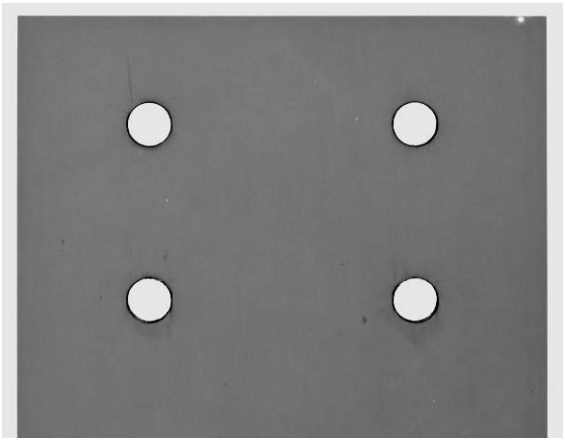

172 MPa (25 ksi) 50000 cycles

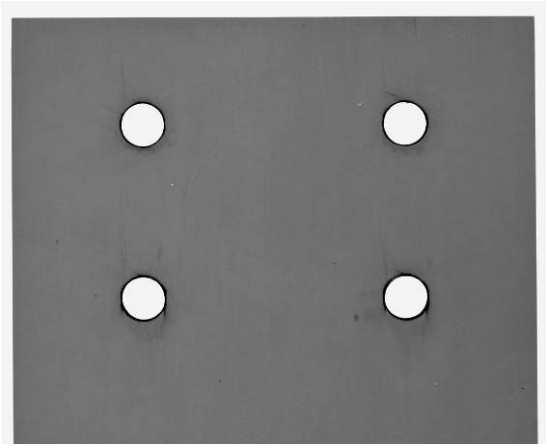

190 MPa (27.5 ksi) 50000 cycles

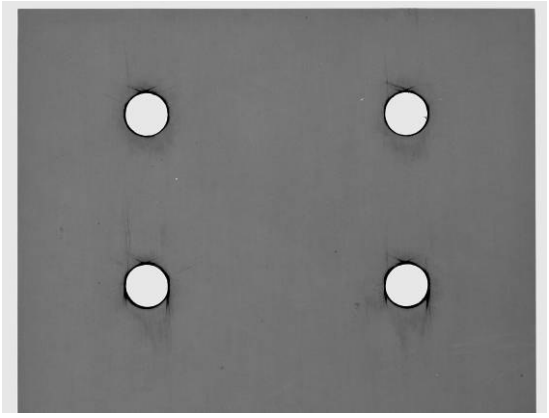

207 MPa (30 ksi) 50000 cycles

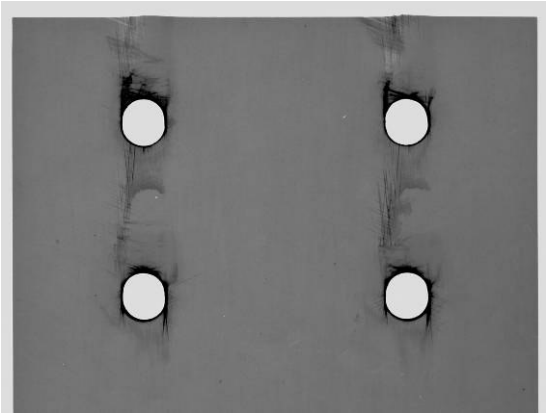

224 MPa (32.5 ksi) 11330 cycles
Critical Damage Achieved

50/40/10 Laminate

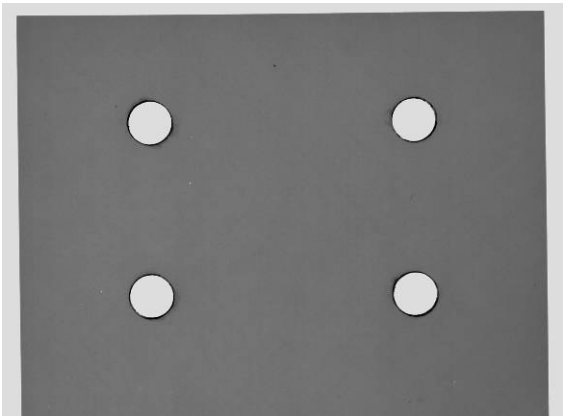

34.5 MPa (5 ksi) 50000 cycles

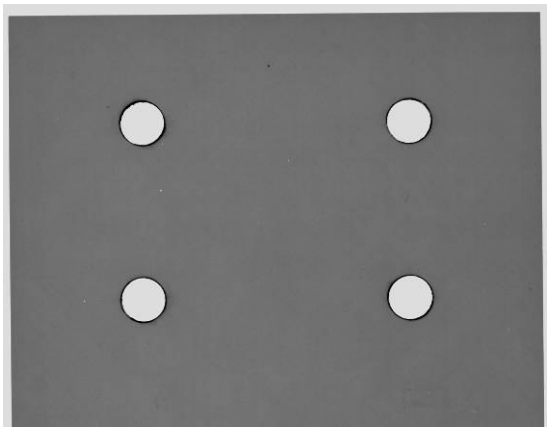

69 MPa (10 ksi) 50000 cycles

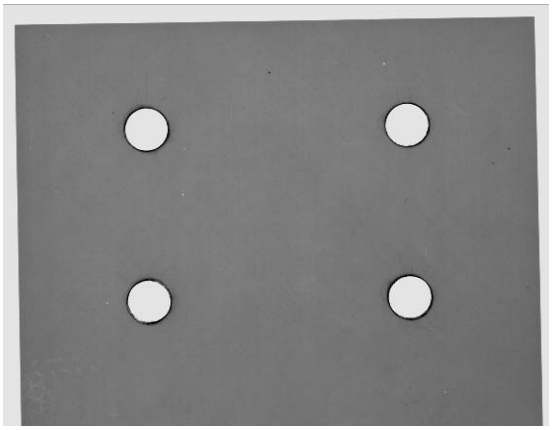

103 MPa (15 ksi) 50000 cycles

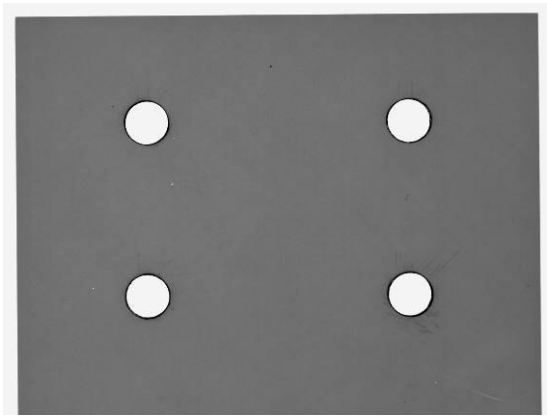

121 MPa (17.5 ksi) 50000 cycles

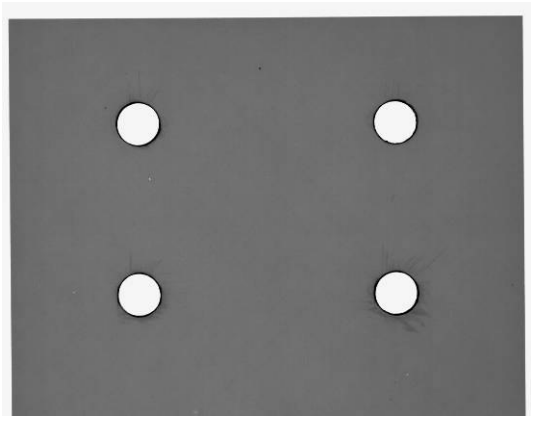

138 MPa (20 ksi) 50000 cycles

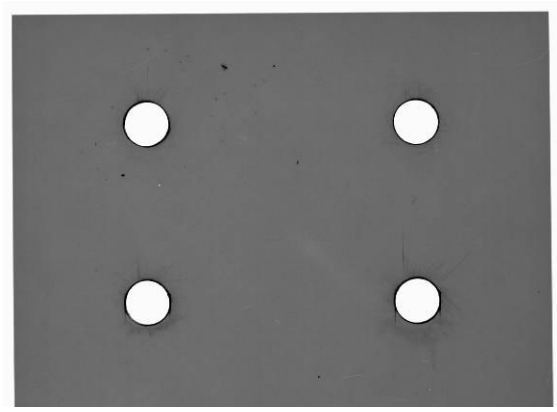

155 MPa (22.5 ksi) 50000 cycles

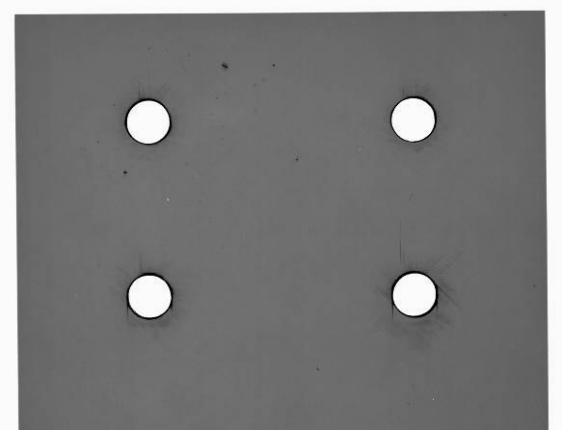

172 MPa (25 ksi) 50000 cycles

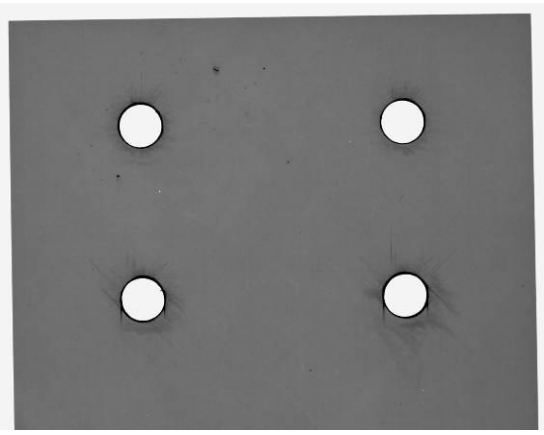

190 MPa (27.5 ksi) 50000 cycles

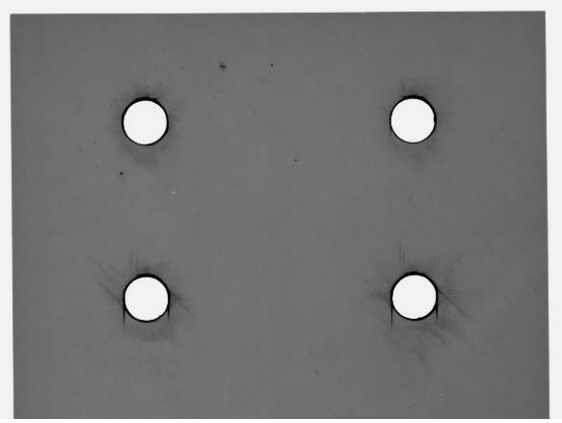

207 MPa (30 ksi) 50000 cycles

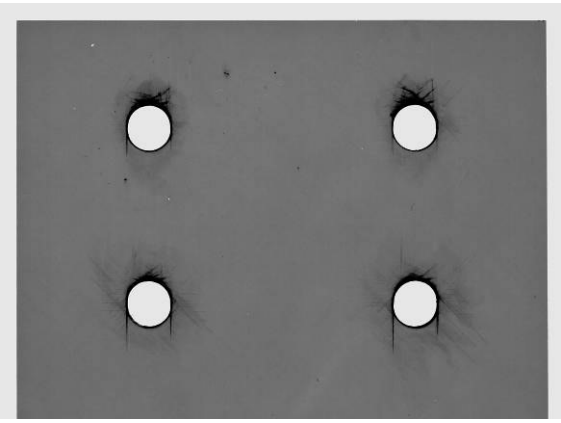

224 MPa (32.5 ksi) 50000 cycles

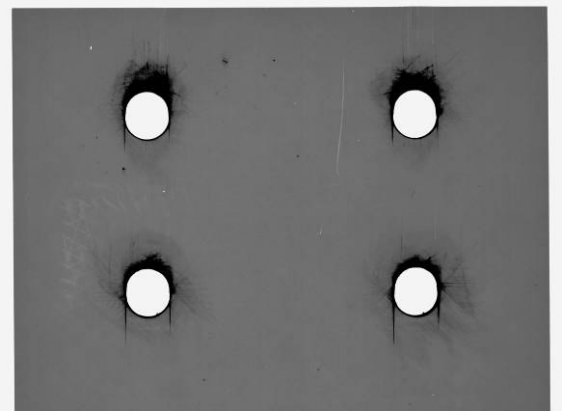

241 MPa (35 ksi) 1910 cycles
Critical Damage Achieved

Images of Laminates Tested at R = -0.35

80/10/10 Laminate

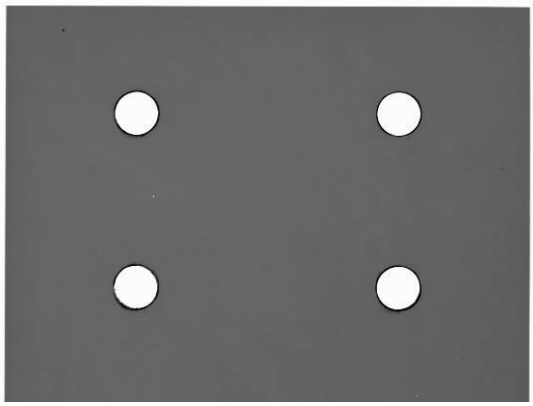

34.5 MPa (5 ksi) 50000 cycles

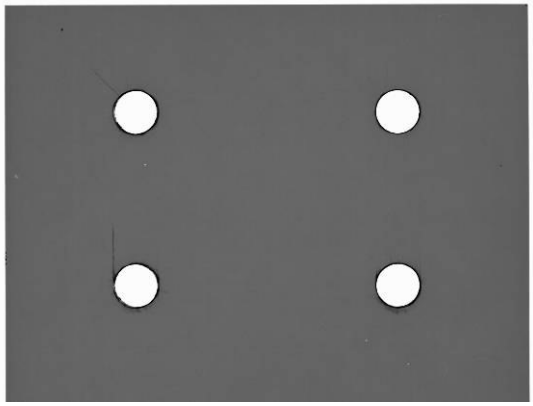

69 MPa (10 ksi) 50000 cycles

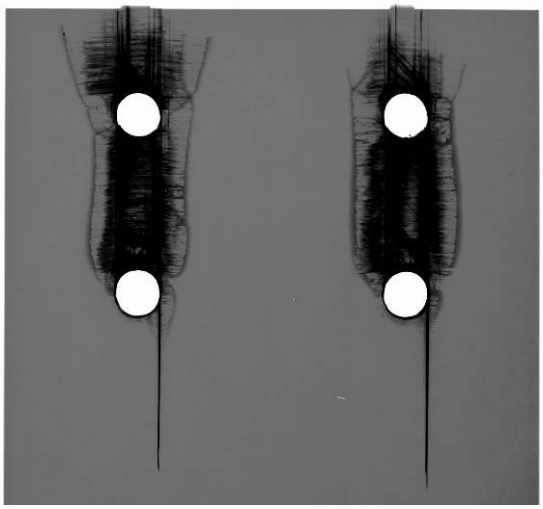

103 MPa (15 ksi) 11125 cycles
Critical Damage Achieved

80/20 Laminate

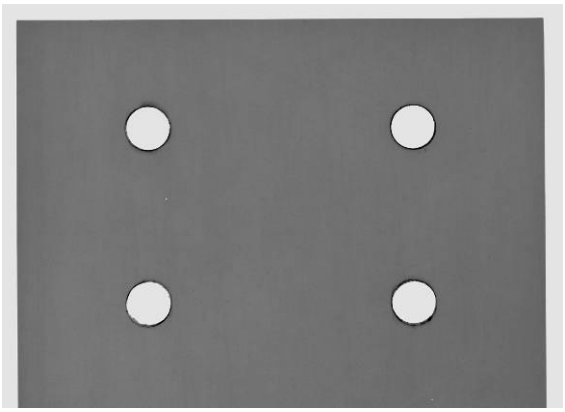

34.5 MPa (5 ksi) 50000 cycles

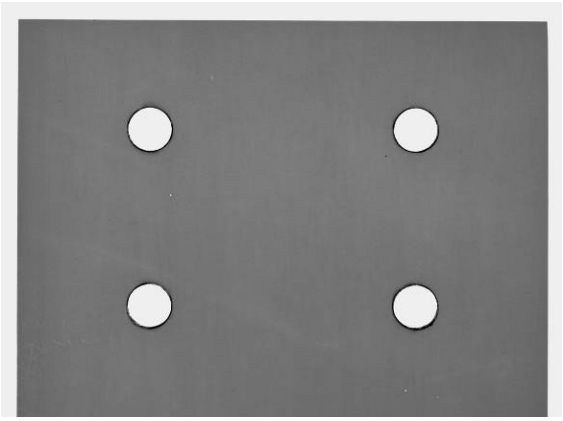

69 MPa (10 ksi) 50000 cycles

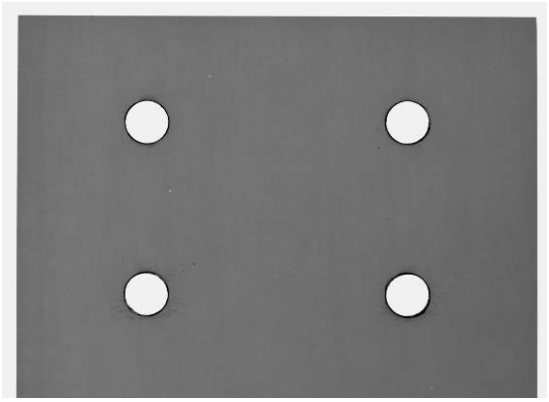

103 MPa (15 ksi) 50000 cycles

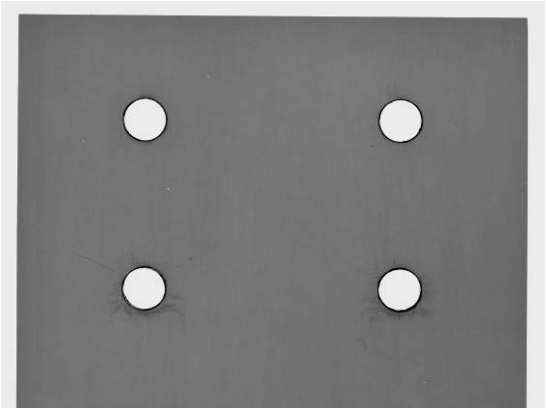

121 MPa (17.5 ksi) 50000 cycles

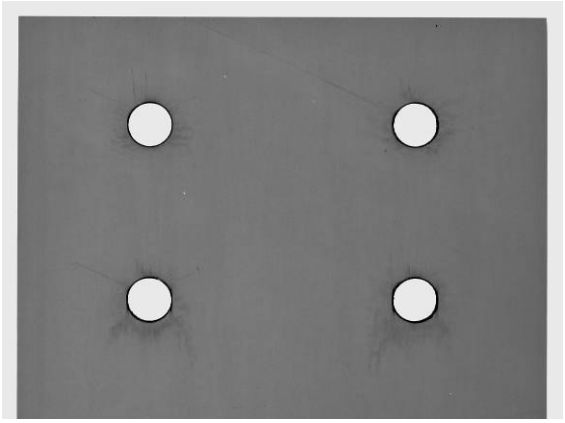

138 MPa (20 ksi) 50000 cycles

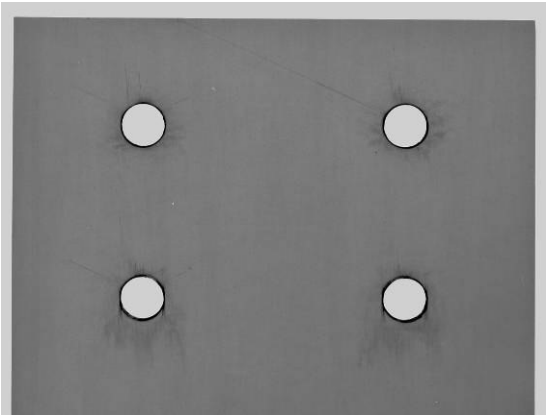

155 MPa (22.5 ksi) 50000 cycles

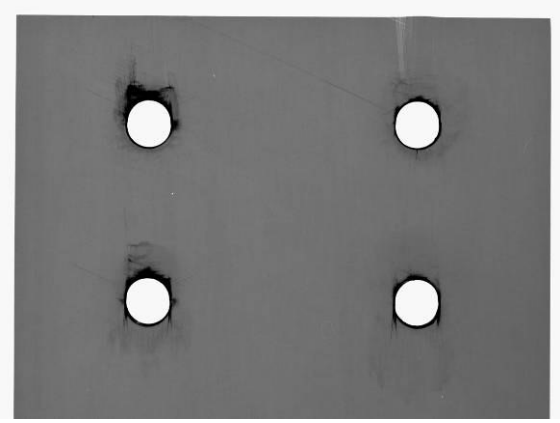

172 MPa (25 ksi) 2010 cycles
Critical Damage Achieved

70/30 Laminate

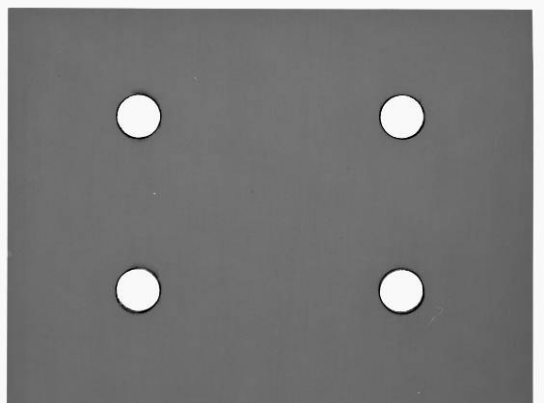

34.5 MPa (5 ksi) 50000 cycles

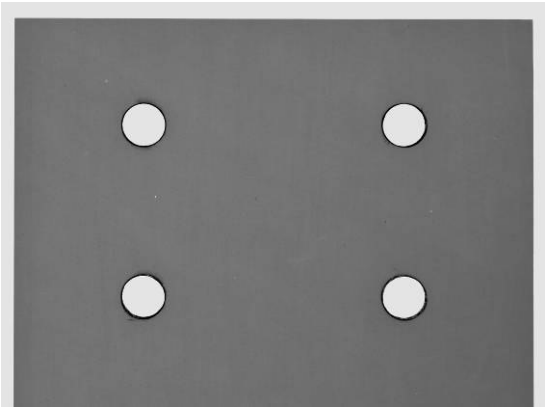

69 MPa (10 ksi) 50000 cycles

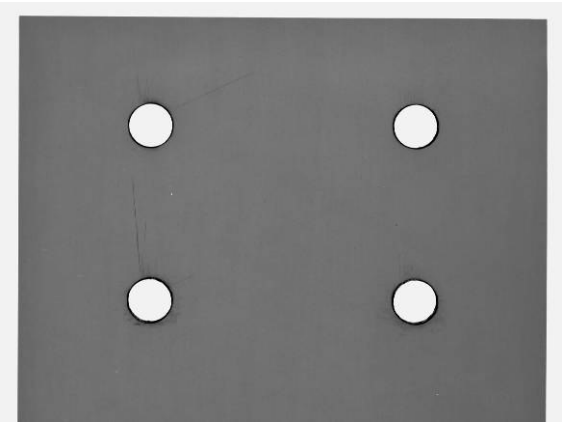

103 MPa (15 ksi) 50000 cycles

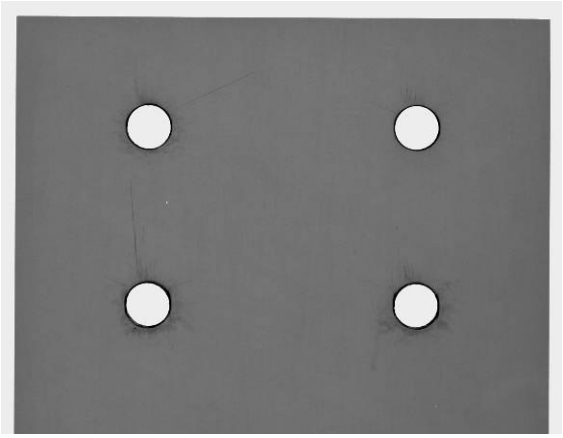

121 MPa (17.5 ksi) 50000 cycles

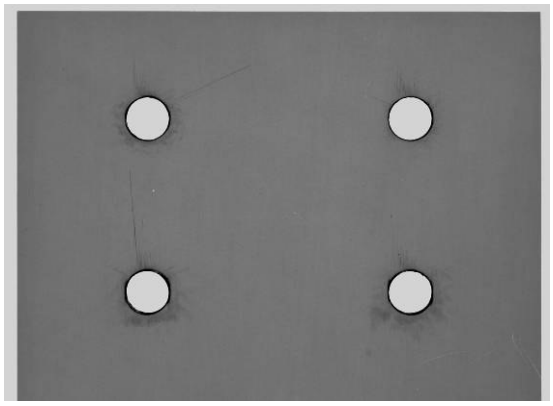

138 MPa (20 ksi) 50000 cycles

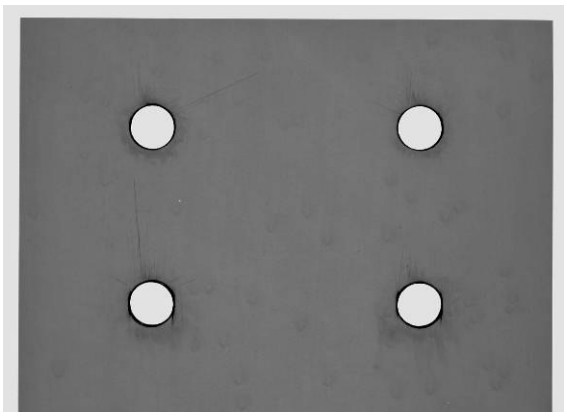

155 MPa (22.5 ksi) 50000 cycles

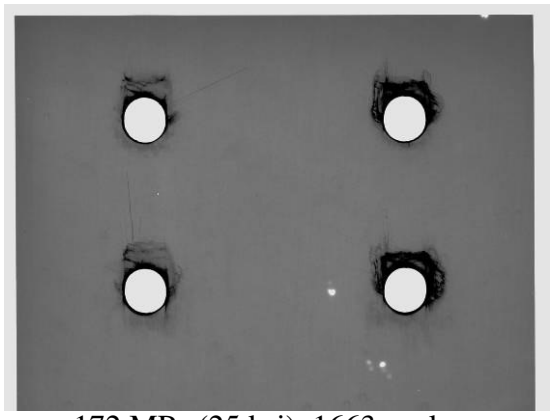

172 MPa (25 ksi) 1663 cycles
Critical Damage Achieved

50/40/10 Laminate

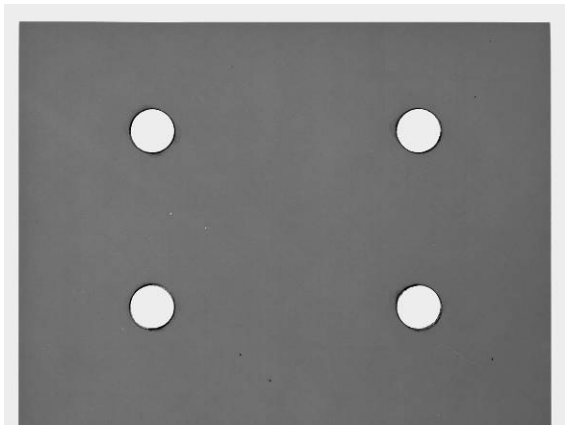

34.5 MPa (5 ksi) 50000 cycles

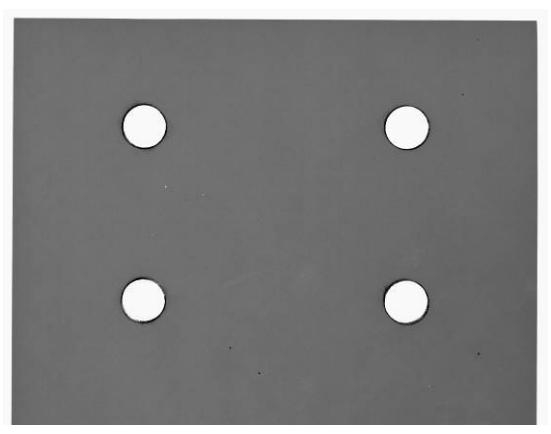

69 MPa (10 ksi) 50000 cycles

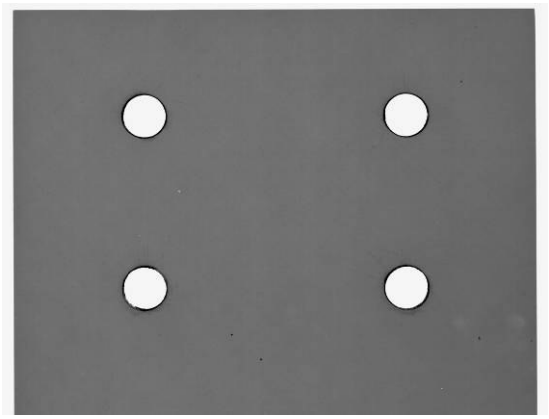

103 MPa (15 ksi) 50000 cycles

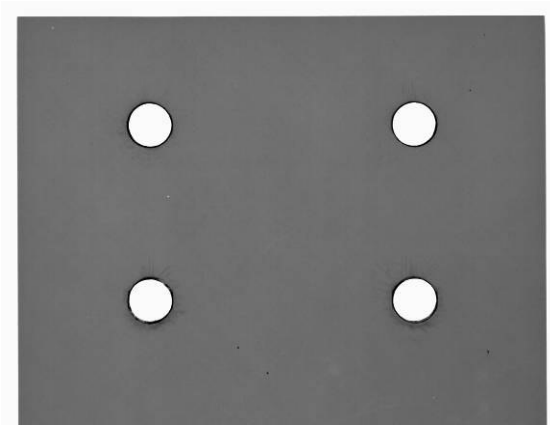

121 MPa (17.5 ksi) 50000 cycles

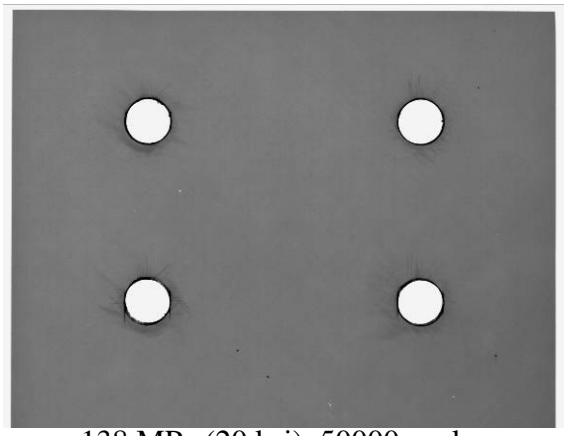

138 MPa (20 ksi) 50000 cycles

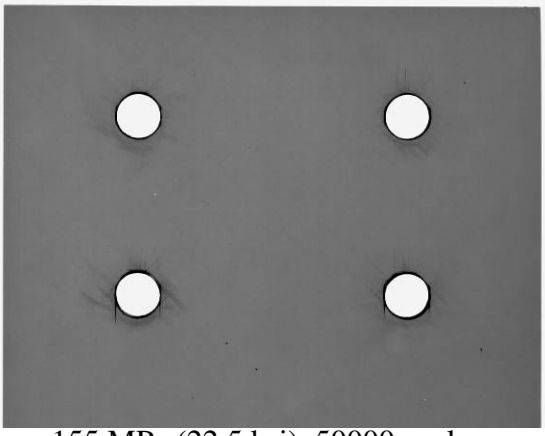

155 MPa (22.5 ksi) 50000 cycles

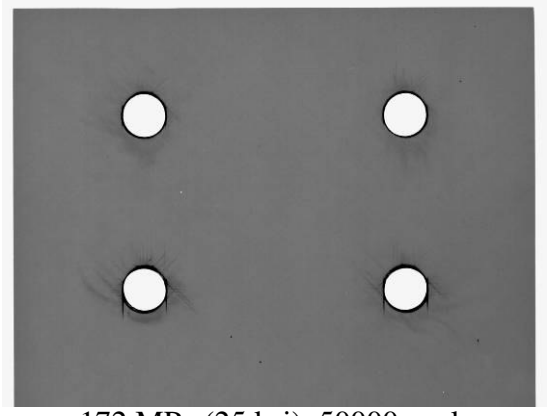

172 MPa (25 ksi) 50000 cycles

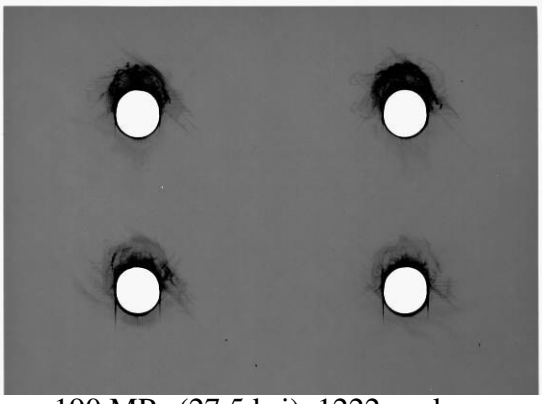

190 MPa (27.5 ksi) 1222 cycles
Critical Damage Achieved

Images of Laminates Tested at R = -10

80/10/10 Laminate

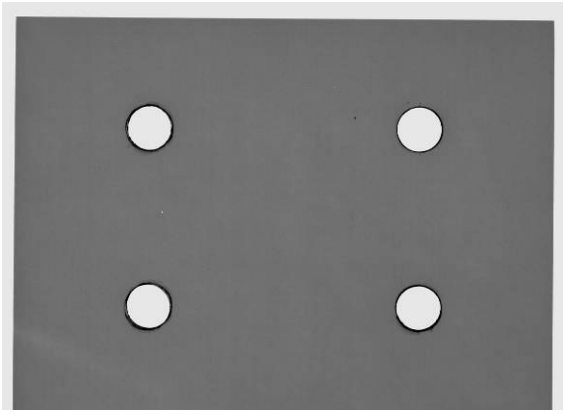

34.5 MPa (5 ksi) 50000 cycles

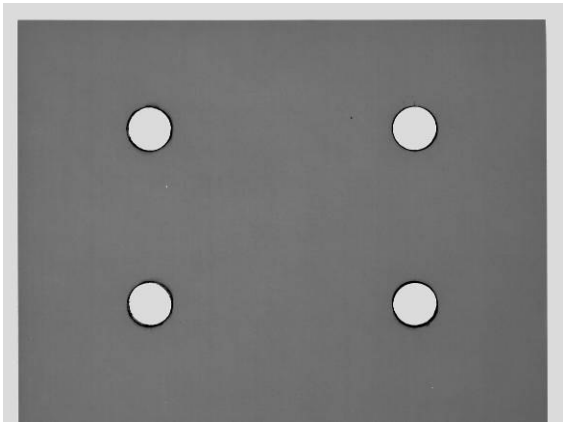

69 MPa (10 ksi) 50000 cycles

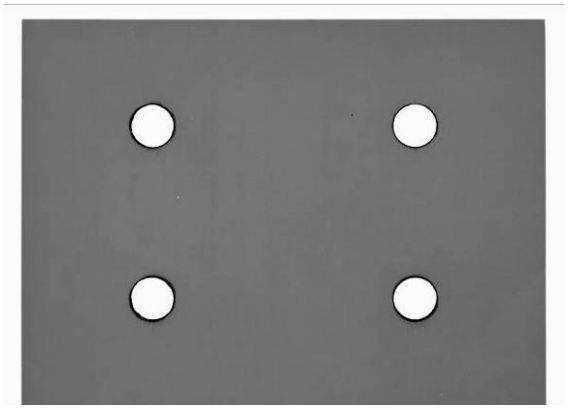

103 MPa (15 ksi) 50000 cycles

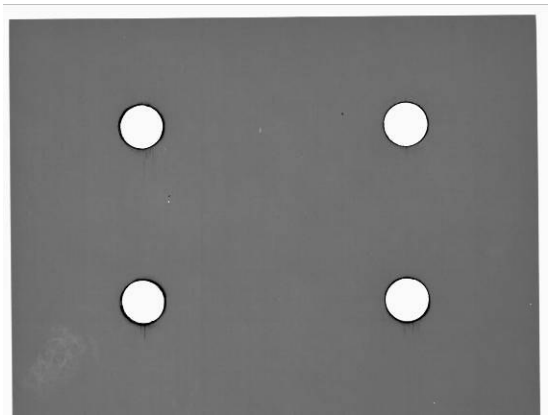

121 MPa (17.5 ksi) 50000 cycles

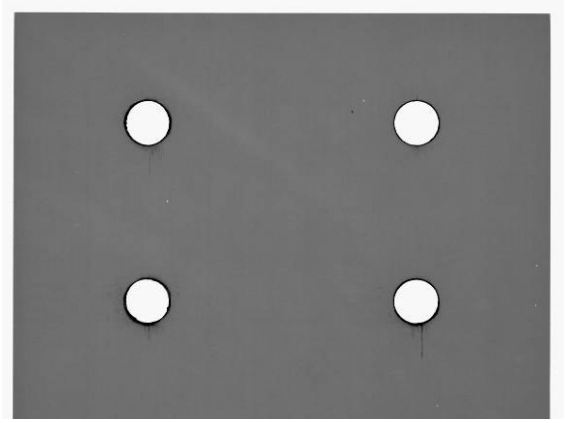

138 MPa (20 ksi) 50000 cycles

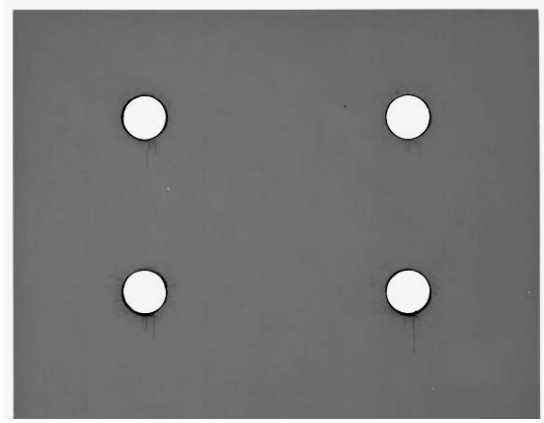

155 MPa (22.5 ksi) 50000 cycles

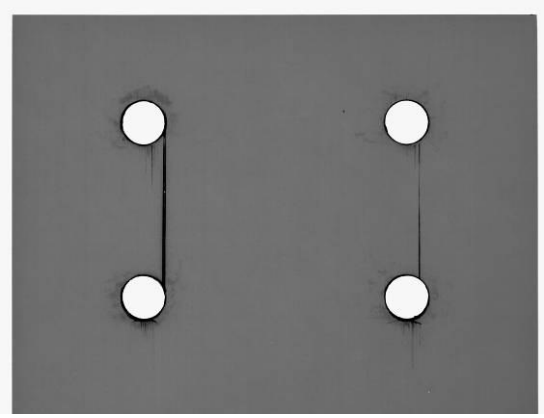

172 MPa (25 ksi) 50000 cycles

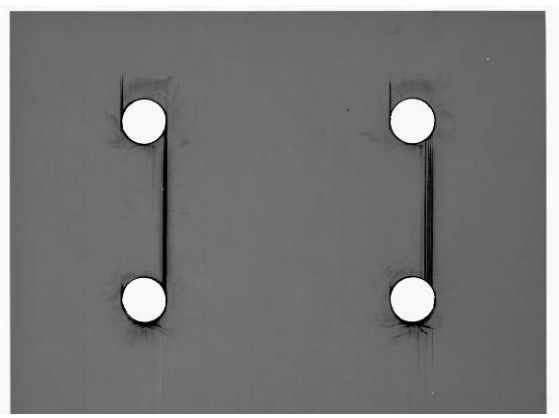

190 MPa (27.5 ksi) 50000 cycles

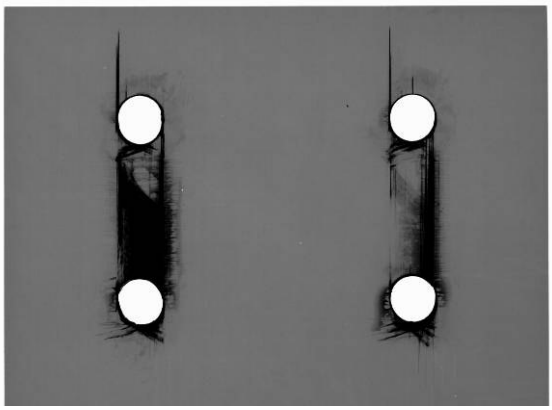

207 MPa (30 ksi) 31304 cycles
Critical Damage Achieved

80/20 Laminate

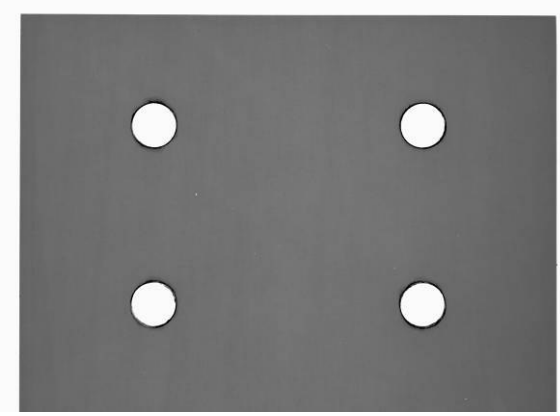

34.5 MPa (5 ksi) 50000 cycles

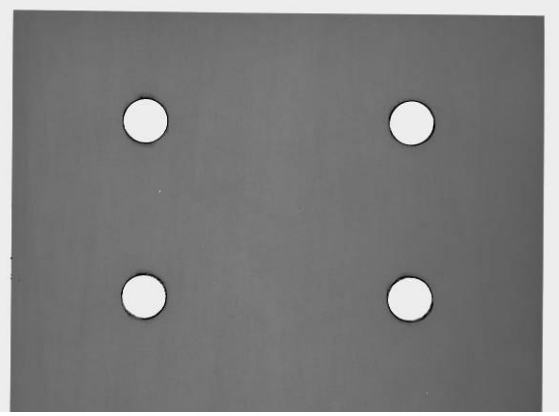

69 MPa (10 ksi) 50000 cycles

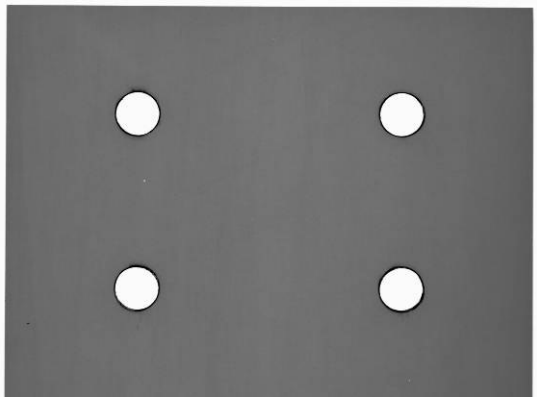

103 MPa (15 ksi) 50000 cycles

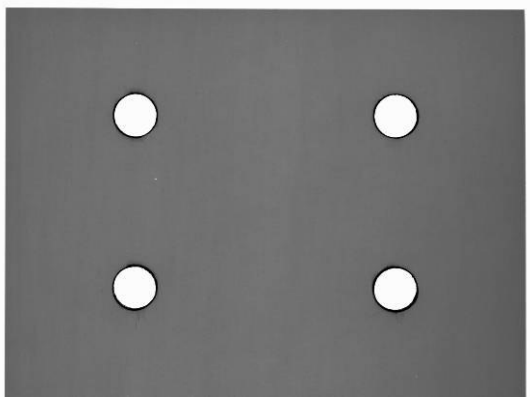

121 MPa (17.5 ksi) 50000 cycles

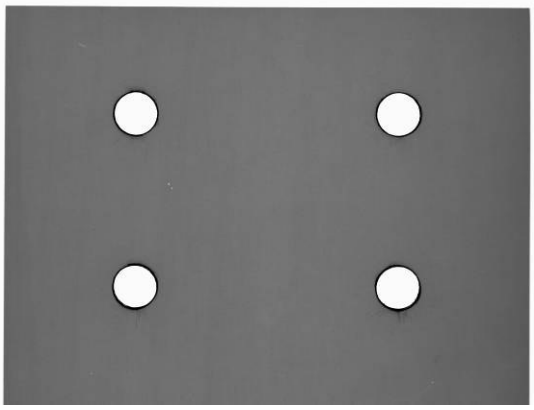

138 MPa (20 ksi) 50000 cycles

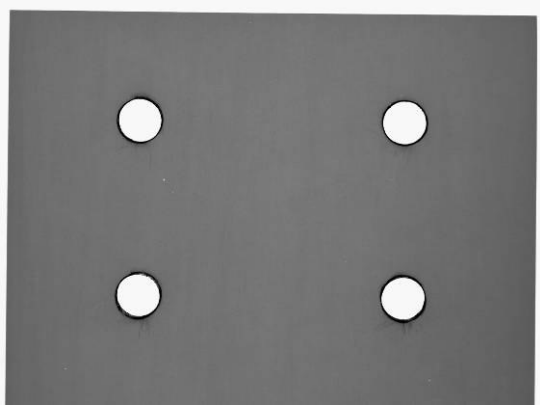

155 MPa (22.5 ksi) 50000 cycles

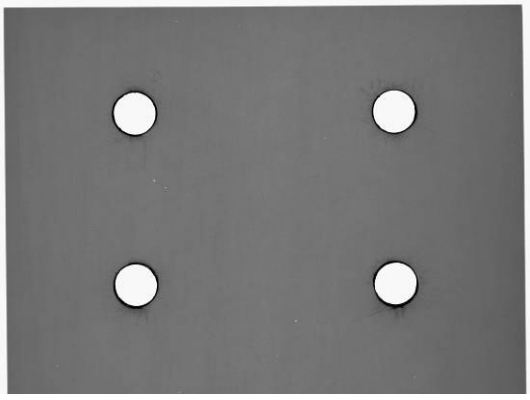

172 MPa (25 ksi) 50000 cycles

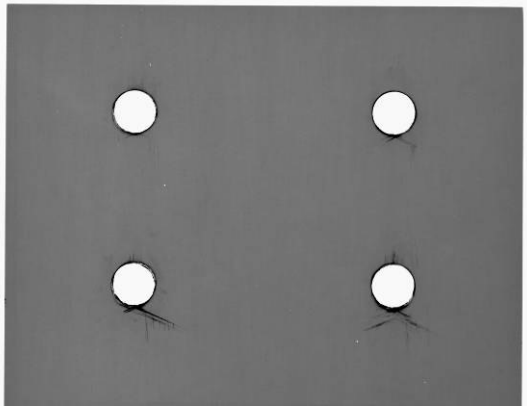

207 MPa (30 ksi) 50000 cycles

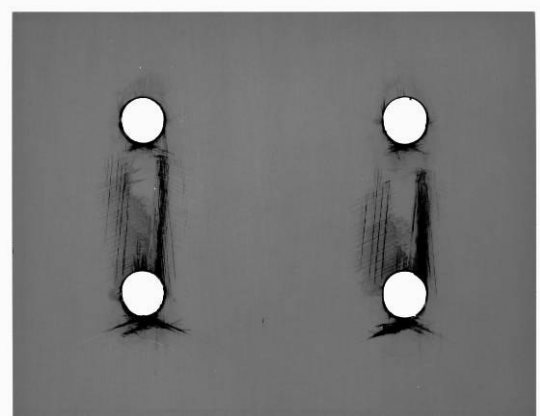

224 MPa (32.5 ksi) 50000 cycles
Critical Damage Achieved

70/30 Laminate

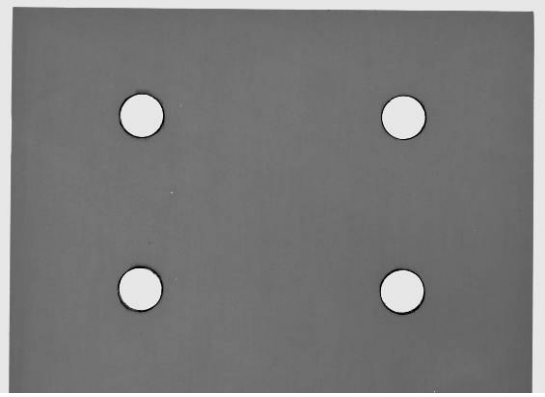

34.5 MPa (5 ksi) 50000 cycles

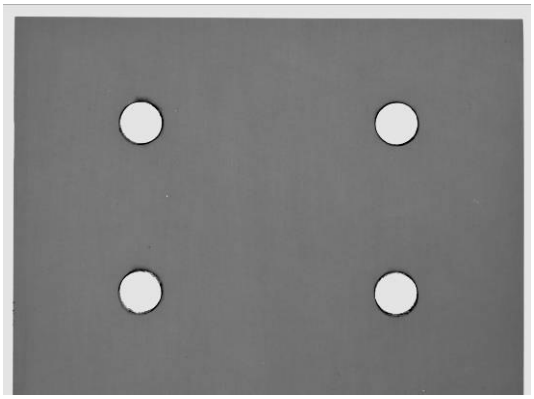

69 MPa (10 ksi) 50000 cycles

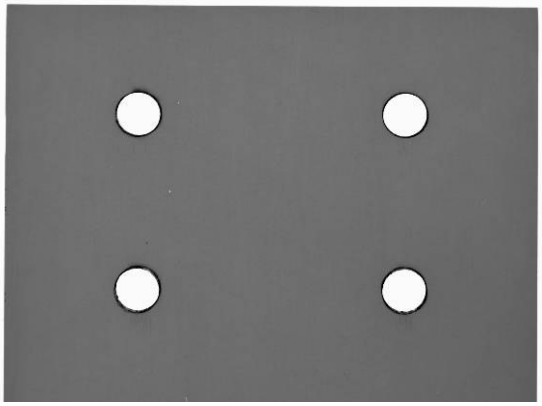

103 MPa (15 ksi) 50000 cycles

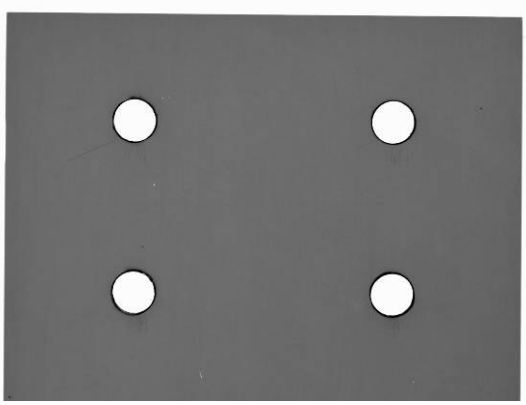

121 MPa (17.5 ksi) 50000 cycles

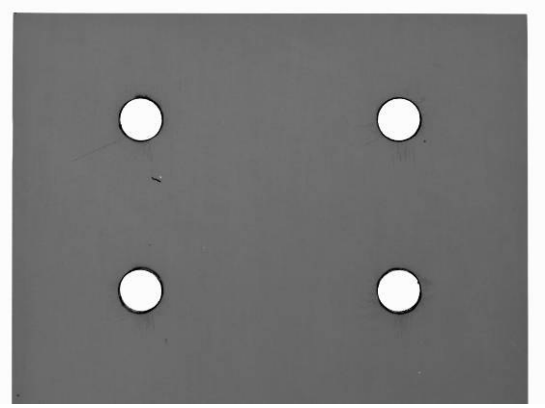

138 MPa (20 ksi) 50000 cycles

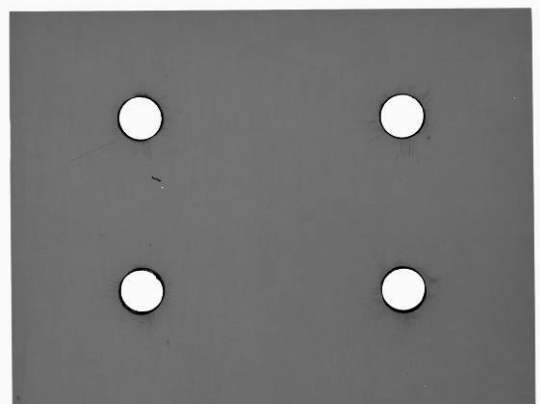

155 MPa (22.5 ksi) 50000 cycles

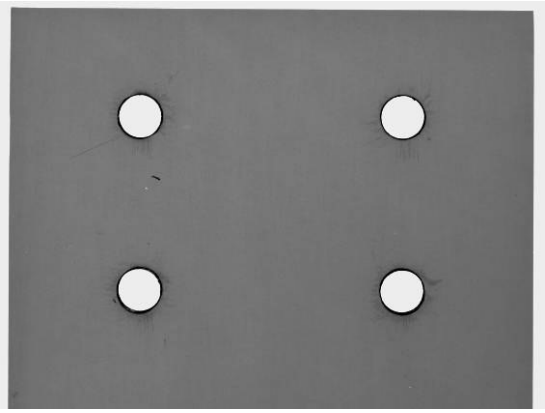

172 MPa (25 ksi) 50000 cycles

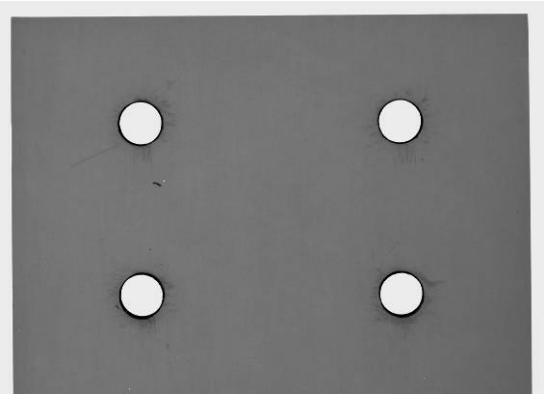

190 MPa (27.5 ksi) 50000 cycles

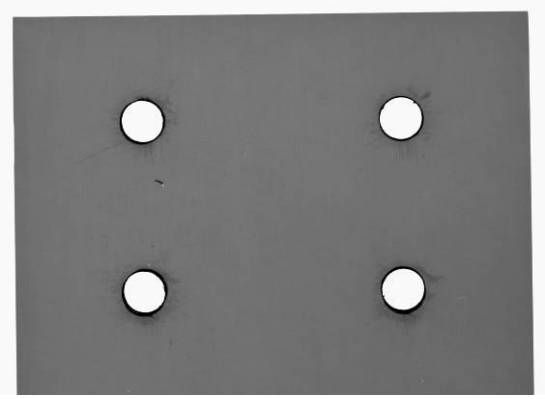

207 MPa (30 ksi) 50000 cycles

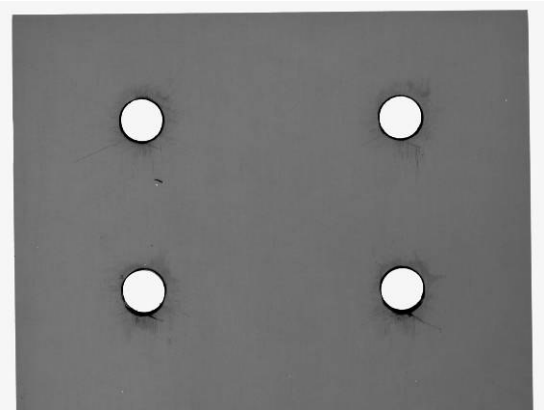

224 MPa (32.5 ksi) 50000 cycles

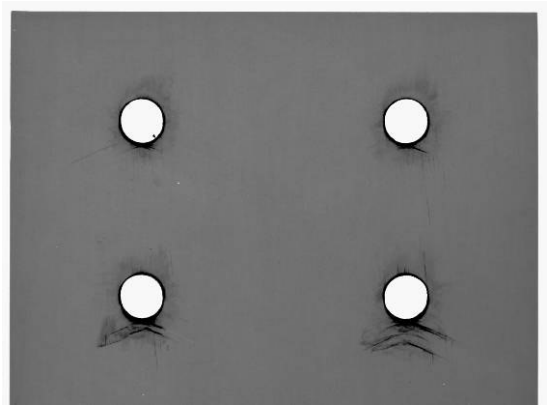

241 MPa (35 ksi) 50000 cycles

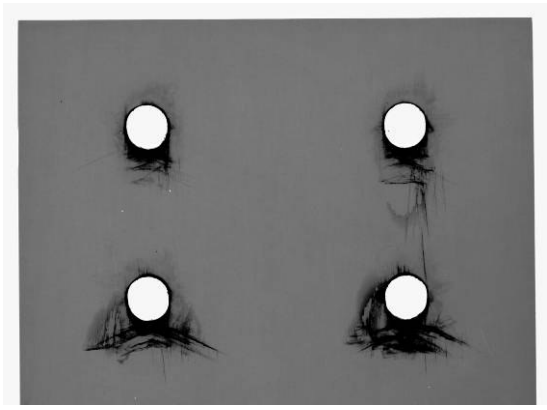

259 MPa (37.5 ksi) 7181 cycles
Critical Damage Achieved

50/40/10 Laminate

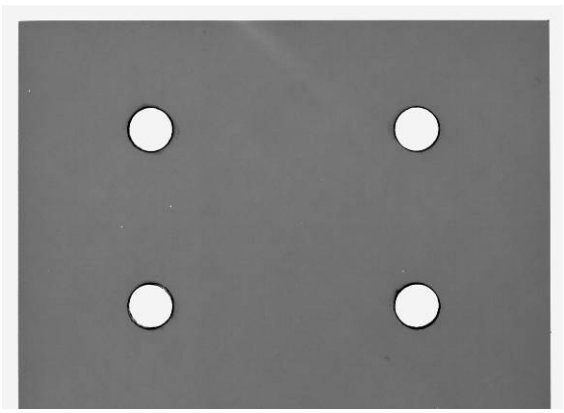

34.5 MPa (5 ksi) 50000 cycles

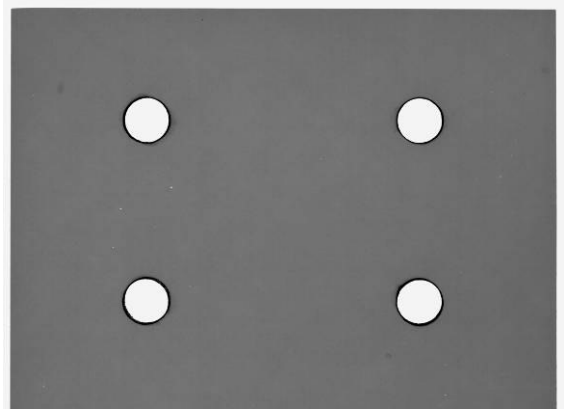

69 MPa (10 ksi) 50000 cycles

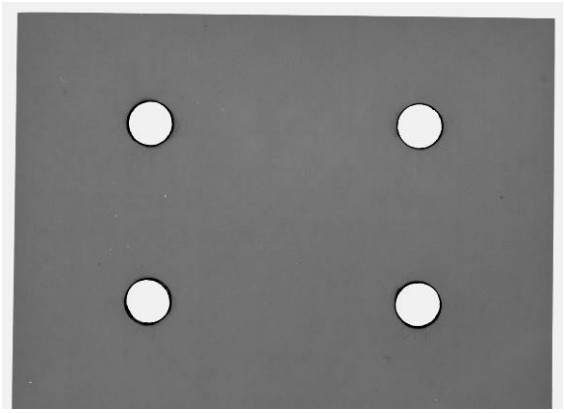

103 MPa (15 ksi) 50000 cycles

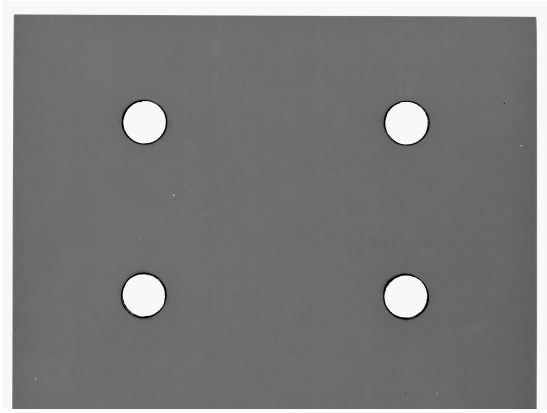

121 MPa (17.5 ksi) 50000 cycles

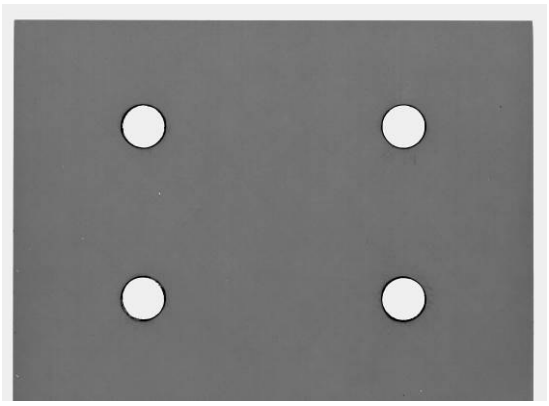

138 MPa (20 ksi) 50000 cycles

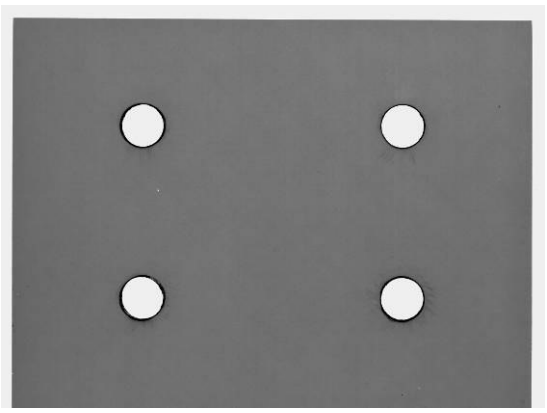

155 MPa (22.5 ksi) 50000 cycles

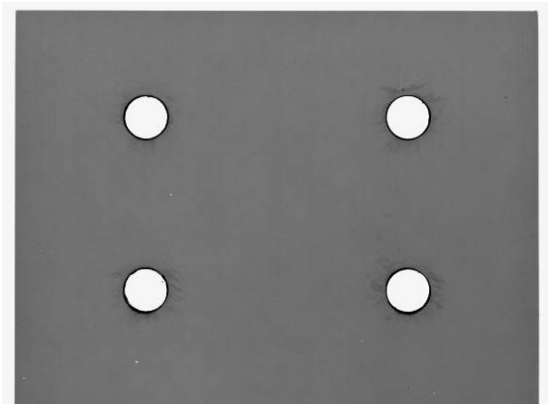

172 MPa (25 ksi) 50000 cycles

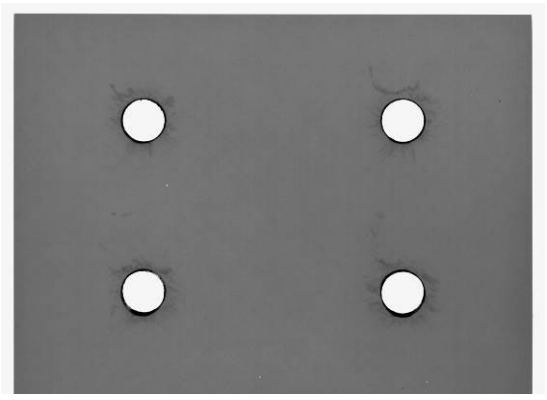

190 MPa (27.5 ksi) 50000 cycles

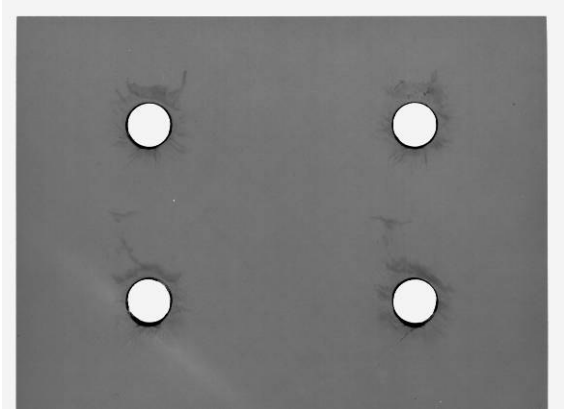

207 MPa (30 ksi) 50000 cycles

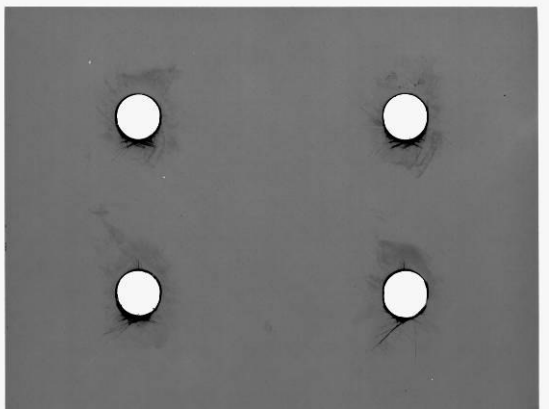

224 MPa (32.5 ksi) 50000 cycles

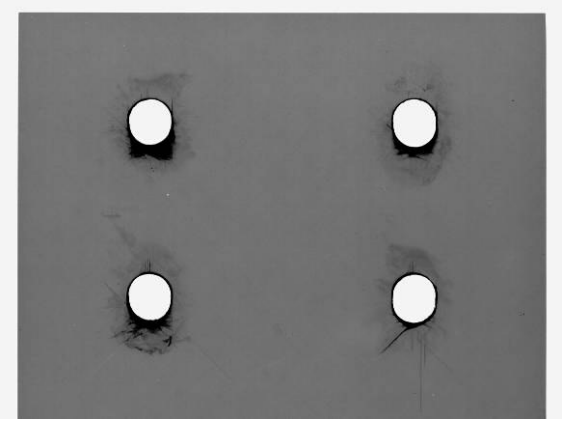

241 MPa (35 ksi) 8759 cycles
Critical Damage Achieved

REFERENCES

[1] Pawar, Prashant M., and Ranjan Ganguli. "On the effect of matrix cracks in composite helicopter rotor blade." Composites Science and Technology 65 (2005): 581-94.

[2] Johnson, W. S., and Paul Treasurer. "Radiographic investigation of the effects of ply modification on damage development in laminates containing circular holes." Journal of Composite Materials 42 (2008): 2143-161.

[3] Davis, J.W., McCarthy, J.A. and Schrub, J.N., "The fatigue resistance of reinforced plastics." Materials in Design Engineering, p. 87 (1964)

[4] Berbinau, P., "Effect of off-axis ply orientation of 0º fibre microbuckling." Composites – Part A: Applied Science and Manufacturing, 1999. 30: p. 1197-1207.

[5] Hong, C. S., and John H. Crews. Stress-Concentration Factors for Finite Orthotropic Laminates With a Circular Hole and Uniaxial Loading. Tech. no. 1469. Hampton, Virginia: NASA, 1979.

[6] Harn, Fung-En. "Approximate Finite-Width Stres Concentration Solutions." 45th International SAMPE Symposium 1 (2000): 1368-377.

[7] Pinnell, M. F. "An examination of the effect of composite constituent properties on the nothched-strength performance of composite materials." Composites Science and Technology 56 (1996): 1405-413.

[8] Yan, Y., W. D. Wen, F. K. Chang, and P. Shyprykevich. "Experimental study on clamping effects on the tensile strength of composite plates with a bolt-filled

hole." Composites: Part A applied science and manufacturing 30 (1999): 1215-229.

[9] Crews, John H., and C. S. Hong. Stress-Concentration Factors for Finite Orthotropic Laminates with a Pin-Loaded Hole. Tech. no. 1862. Hampton, Virginia: NASA, 1981.

[10] Rosner, Charles N., and Sami H. Rizkalla. "Bolted connections for fiber-reinforced composite structural members: Experimental program." Journal of Materials in civil Engineering 7 (1995): 223-31.

[11] Khashaba, U. A., H.E.M. Sallam, A. E. Al-Shorbagy, and M. A. Seif. "Effect of washer size and tightening torque on the performance of bolted joints in composite structures." Composite Structures 73 (2006): 310-17.

[12] Crews, John H. Bolt-bearing fatigue of a graphite/epoxy laminate. Tech. no. 81851. Hampton, Virginia: NASA, 1980.

[13] Marshall, I. H., W. S. Arnold, J. Wood, and R. F. Mousley. "Observations on bolted connections in composite structures." Composite Structures 13 (1989): 133-51.

[14] Cooper, C., and G. J. Turvey. "Effects of joint geometry and bolt torque on the structural performance of single bolt tension joints in pultruded GRP sheet material." Composite Structures 32 (1995): 217-26.

[15] Nassar, Sayed A., Vinayshankar L. Virupaksha, and Saravanan Ganeshmurthy. "Effect of bolt tightness on the behavior of composite joints." Journal of Pressure Vessel Technology 129 (2007): 43-51.

[16] Shivakumar, K. N., and John H. Crews. Bolt Clampup relaxation in a graphite/epoxy laminate. Tech. no. 83268. Hampton, Virginia: NASA, 1982.

[17] Rosner, Charles N. "Single-bolted connections for orthotropic fibre-reinforced composite structural members." Thesis. University of Manitoba, 1992.

[18] Lawlor, V. P., W. F. Stanley, and M. A. McCarthy. "Characterisation of damage development in single shear bolted composite joints." Plastics, Rubber and Composites 31 (2002): 126-33.

[19] Crews, John H., and Rajiv A. Naik. Effects of bolt-hole contact on bearing-bypass damage-onset strength. Tech. no. 30870. Hampton, Virginia: NASA, 1993.

[20] Mechanically Fastened Joint Tests. Composite Materials Handbook. Vol. 1. Department of Defense, 2002. 7-13--45.

[21] Lawlor, V. P., M. A. McCarthy, and W. F. Stanley. "Experimental study on effects of clearance on single bolt, single shear, composite bolted joints." Plastics, Rubber and Composites 31 (2002): 405-11.

[22] McCarthy, M. A., V. P. Lawlor, and W. F. Stanley. "An esperimental study of bolt-hole clearance effects in single-lap, multibolt composite joints." Composite Materials 39 (2005): 799-825.

[23] Stanley, W. F., M. A. McCarthy, and V. P. Lawlor. "Measurement of load distribution in multibolt composite joints, in presence of varying clearance." Plastics, Rubber and Composites 31 (2002): 412-18.

[24] Lawlor, V. P., M. A. McCarthy, and W. F. Stanley. "An experimental study of bolt-hole clearance effects in double-lap, multi-bolt composite joints." Composite Structures 71 (2005): 176-90.

[25] Vangrimde, B., and R. Boukhili. "Bearing stiffness of glass fibre-reinforced polyester: influence of coupon geometry and laminate properties." Composite Structures 58 (2002): 57-73.

[26] Crews, John H., and Rajiv A. Naik. "Combined bearing and bypass loading on a graphite/epoxy laminate." Composite Structures 6 (1986): 21-40.

[27] Garbo, Sam P. Effects of Bearing/Bypass load interaction on laminate strength. Rep. no. AFWAL-TR-81-3114. Wright-Patterson Air Force Base, Ohio: Airforce Systems Command, 1981.

[28] Naik, Rajiv A., and John H. Crews. Ply-level failure analysis of a graphite/epoxy laminate under bearing-bypass loading. Tech. no. 20372. Hampton, Virginia: NASA, 1988.

[29] Lim, Tae S., Byung C. Kim, and Dai G. Lee. "Fatigue characteristics of the bolted joints for unidirectional composite laminates." Composite Structures 72 (2006): 58-68.

[30] Kam, C. Y., “Bolt hole growth in graphite-epoxy laminates for clearance and interference fits when subjected to fatigue loads,” Fatigue of Fiberous Composite Materials, ASTM STP 723, American Society for Testing and Materials, 1981, 21-30.

[31] Ramkumar, R. L. and Tossavainen, E. W., “Strength and Lifetime of Bolted Laminates,” Fatigue in Mechanically Fastened Composite and Metallic Joints, ASTM STP 927, John M. Potter, Ed., American Society for Testing and Materials, Philadelphia, 1986, 251-273.

[32] Persson, E., and I. Eriksson. "Fatigue of multiple-row bolted joints in carbon/epoxy laminates: ranking of factors affecting strength and fatigue life." International Journal of Fatigue 21 (1999): 337-53.

[33] Herrington, P. D., and M. Sabbaghian. "Fatigue failure of composite bolted joints." Journal of Composite Materials 27 (1993): 491-512.

[34] Rast, Joshua. "Characterizing the fatigue damage in non-traditional laminates of carbon fiber composites using radiography." Thesis. Georgia Institute of Technology, 2009.

[35] Ethridge, A., "Investigation of progressive damage and failure in IM7 carbon fiber/5250-4 bismaleimide resin matrix composite laminates." Thesis. Georgia Institute of Technology, 1998.

[36] Etheridge, G. A., W. S. Johnson, and Scott Reeve. "Effect of lay-up and constraint on tensile notch strength." 13th Annual Technical Conference on Composite Materials. Baltimore. Baltimore: American Society for Composites, 1998. 489-504.

[37] Ludema, K. C., and R. G. Bayer. Tribological modeling for mechanical designers. Philadelphia, PA: ASTM, 1991.